UNIVERSITY OF CALIFORNIA, SAN DIEGO

Oscillating Hydrogel Based Bioreactors for Chondrogenic Differentiation of Mesenchymal Stem Cells

A Thesis submitted in partial satisfaction of the requirements

for the degree of Master of Science

in

Bioengineering

by

Veronica Juliet Neiman

Committee in charge:

Professor Shyni Varghese, Chair
Professor Michael Heller
Professor Xiaohua Huang

2010

The Thesis of Veronica Juliet Neiman is approved, and it is acceptable in quality and form for publication on microfilm and electronically:

Chair

University of California, San Diego

2010

DEDICATION

This thesis is dedicated to my family for their constant support, guidance, and love. Without their belief in me this work would not have come into fruition.

TABLE OF CONTENTS

LIST OF ABBREVIATIONS

3D	Three dimensional
AGN	Aggrecan
ANOVA	Analysis of variance
B/W	Black and white
BSA	Bovine serum albumin
Col II	Collagen type II
CS	Chondroitin sulfate
DAPI	4',6-diamidino-2-phenylindole
DEPC	Diethylpyrocarbonate
dH_2O	Deionized water
DMMB	Dimethylmethylene blue
EDTA	Ethylenediaminetetraacetic acid
EthD-1	Ethyidium homodimer
Ex/Em	Excitation/Emission
FBS	Fetal bovine serum
FPs	Fluorescent particles
GAG	Glycosaminoglycan
HCl	Hydrogen chloride
hMSC	Human mesenchymal stem cell
ID	Inner diameter
LCST	Lower critical solution temperature
LDPE	Low density polyethylene
Mw	Molecular weight
MO	P[MEO_2MA-OEGMA-EGDA]
NaOH	Sodium hydroxide
OH-pro	Hydroxyproline
PBE	Phosphate buffered saline
PBS	Phosphate-buffered solution
pDAB	p-Dimethylaminobenzaldehyde
PEGDA	Polyethylene glycol diacrylate
PI	Photoinitiator
SR	Swelling ratio
SS	Stainless steel
stdev	Standard deviation
TE	Thermoelectric
TGFβ-1	Transforming growth factor β-1

LIST OF FIGURES

LIST OF TABLES

ACKNOWLEDGEMENTS

I would like to thank Shyni Varghese for her support as chair of my committee. Her trust and faith in my abilities made failure impossible. I am fortunate to have had such a dedicated advisor who worked with me throughout this process, discussing results, and providing her invaluable guidance.

I would like to thank my committee members Dr. Michael Heller and Dr. Xiaohua Huang for their time and insightful comments on my thesis. I would like to thank Dr. Huang for letting me use his lab equipment without which I could not have built my device and completed my thesis.

I would like to acknowledge the Biomaterials and Tissue Engineering lab members who supported me, taught me, and shared their knowledge and experience with me, especially Joshua Hwang who proved to be the single most dependable and diligent researcher. He has been the most valuable, gracious, and unselfish teammate I have ever worked with. I would also like to thank Kris Barbee, who helped me design and build my bioreactor. This project would not have been possible without his amazing talents as an engineer. I could not have finished my work without both their help and guidance. It was a pleasure and an honor to work with each of them.

I would like to thank Ryan J. Bloom, Jerry P. George, Alfredo Caledon, Sean X. Sun, and Denis Wirtz, lab members in the Department of Chemical and Biomolecular and/or the Department of Mechanical Engineering at The Johns Hopkins University. Dr. Wirtz graciously shared their MATLAB code which I adapted for my analysis and is included in Appendix B.

Most importantly, I am blessed to have parents who have taught me the most fundamental values and lessons in life that have led me to success. They have guided me to finding intellectual and emotional happiness. I am forever grateful. I thank my sister, who is my confidante and has always been there to make me laugh, and my grandparents for helping raise me and making sure I never lose my culture. I would like to thank my amazing group of friends who have helped me along the way, cheering me on, and reminding me of my strengths. I could not have done this without the constant love from my best friend. I would like to thank Saleh Sayed Amirriazi for never faltering in his faith in me.

ABSTRACT OF THE THESIS

Oscillating Hydrogel Based Bioreactors for Chondrogenic Differentiation of Mesenchymal Stem Cells

by

Veronica Juliet Neiman

Master of Science in Bioengineering

University of California, San Diego, 2010

Professor Shyni Varghese, Chair

Harnessing the differentiative potential of stem cells for use in tissue repair could be a powerful therapy for debilitating diseases. However, one of the bottlenecks of stem cell based therapeutics and tissue engineering is inefficient and homogeneous stem cell differentiation. Various physico-chemical cues such as mechanical strain, chemical components, and soluble factors have been shown to direct stem cell differentiation. This study developed a multifunctional polymer-based artificial ECM replicating the multifunctional characteristics of native ECM to understand the physico-chemical cues

present in a 3D environment. Specifically, we have developed a synthetic hydrogel that acts as a scaffold and bioreactor providing dynamic mechanical cues and structural support to cells. A heating device was used to induce ~5% volume strain by applying temperature oscillations to thermoresponsive hydrogels. Human mesenchymal stem cells (hMSCs) were encapsulated in P[MEO_2MA-OEGMA-EGDA] (MO) (10 and 20% Mw PEG: 3400) and PEGDA(15% Mw PEG: 10000) hydrogels and cultured with and without TGFβ-1. Fluorescent particle tracking was used to measure realtime volume strains of acellular and cellular hydrogels under temperature oscillations and verified with swelling ratios. hMSCs produced cartilaginous ECM as evidenced from histological and biochemical analysis. Realtime PCR was used to characterize the expression of various chondrogenic markers, indicating optimal chondrogenic differentiation with 1 hour stimulated PEGDA (15% PEG) hydrogels and TGFβ-1. Due to static mechanical strains induced by high crosslinking density and confined heating chambers, enhanced chondrogenic differentiation was limited for all gels. Overall, this study demonstrated the potential use of polymer-based synthetic bioactuators for stem cell differentiation.

I. Introduction

Native articular cartilage plays a major role in dissipating mechanical loads applied in daily activity and covers diarthrodial joints providing almost frictionless surfaces for load bearing. However, due to its inability for self-healing, any damage imposed results in progressive deterioration. Initial studies in tissue engineering cartilage for reconstruction and augmentation surgeries have manipulated autologous chondrocytes isolated using invasive, painful biopsies, but with limited success [1]. It has been shown that tissue engineering of cartilage can be achieved via a biomimetic approach in which biomaterial scaffolds and bioreactors are used to mimic *in vivo* stem cell environments to direct stem cell growth and development into functional tissues. Consequently, recent studies have worked towards developing minimally invasive tissue engineered systems using hydrogels as scaffolds.

Chondrocytes, the main cell type in cartilage, have been shown to undergo dedifferentiation in culture without the proper signaling factors and mechanical stimuli. Large scale *in vitro* expansion of these cells has proven difficult due to changes in phenotype of chondrocytes in culture without appropriate signaling factors and mechanical stimuli in culture [2-5]. As such, chondrogenic differentiation dictates applying mechanical stimulation and biological cues to cell encapsulated hydrogels, which provide the structural support and enhanced transport properties for the delivery of nutrients and the removal of wastes necessary for chondrogenesis. Because hydrogels can be used to mimic the extracellular network of chondrocytes and are implantable using minimally invasive surgeries [6, 7], both non-stimuli responsive and stimuli-responsive hydrogels have been used as scaffolds for chondrogenesis. However, manipulating

thermoresponsive hydrogels to apply temperature-induced dynamic compressive strain has not been previously attempted.

The objective of this thesis is to develop a system *in vitro* to show thermoresponsive hydrogels are capable of producing 5% strains at a frequency within 0.001 and 1.0 Hz to enhance chondrogenic differentiation of hMSCs as a potential treatment for cartilage regeneration. The goal is to create a multi-functional, synthetic matrix that can emulate natural ECM, provide multiple dynamic mechanical and chemical cues, and provide structural support. We hypothesize that a tissue-specific environment under temperature induced mechanical strains can promote tissue specific stem cell differentiation. Such a system has promise as an *in vivo* treatment in which autologous hMSCs encapsulated in hydrogels can be implanted via a minimally invasive surgery directly to a damaged cartilage site, which can be exposed to daily temperature oscillations to stimulate *in vivo* chondrogenic differentiation.

1.1. Aims

The specific goals of this study are summarized below.

1) Develop a thermoresponsive hydrogel-based bioreactor system for stem cell culture and differentiation.
2) Engineer and optimize a fast-response heating device to apply sinusoidal temperatures with minimal overshoot to control the swelling behavior of cell-laden thermoresponsive hydrogels
3) Design a realtime imaging system to measure the induced volume strain of a hydrogel in response to temperature, frequency of temperature oscillations, and crosslinking density.

4) Measure equilibrium and realtime non-equilibrium swelling ratios of acellular and cellular hydrogels.
5) Calculate equilibrium and non-equilibrium, realtime 3D displacement and volume strains produced at various temperature points in acellular and cellular hydrogels using particle tracking
6) Test the synergistic or antagonistic effects of temperature, frequency, crosslinking density, and compressive strain on stem cell behavior such as proliferation, survival, and chondrogenesis in a 3D environment
7) Validate the thermoresponsive hydrogel-based bioreactor system for stem cell differentiation using chondrogenesis of hMSCs as a model system

1.2. Experimental Setup

hMSCs were encapsulated in thermoresponsive P[MEO_2MA-OEGMA-EGDA] (MO) and (polyethylene glycol diacrylate) (PEGDA) hydrogels cultured with transforming growth factor (TGFβ-1) and temperature oscillations. Chondrogenic differentiation was studied using four control and five experimental groups to characterize the effects of crosslinking density, duration and frequency of temperature oscillations, and temperature on the chondrogenic differentiation of hMSCs encapsulated in thermoresponsive hydrogels. The following sets of controls and experimental groups were used to study these:

1) ***Control A*:** MO hydrogel, with TGF-β1, no oscillation
2) ***Experimental* 1A**: MO hydrogel, with TGF-β1 and 1 hour oscillations
3) ***Experimental 2A***: MO hydrogel, with TGF-β1 and 3 hour oscillations

To determine the optimal number of oscillations per day and the optimal treatment duration, experimental groups 1 and 2 tested for one versus three hours of temperature oscillations with TGFβ-1, while control A isolated the effects of TGFβ-1 alone. TGF-β1 was chosen to induce early chondrogenic differentiation during incubation at 37^{o}C, but was not used during temperature oscillations to minimize nonhomogeneous diffusion of TGF-β1 due to changes in gel volume, which would have generated mass transfer gradients and added further variables to the experimental design [8-10].

To test the effects of temperature induced mechanical oscillations, TGF-β1 was used in combination with thermoresponsive MO hydrogels and PEGDA hydrogels on the chondrogenic differentiation of hMSCs. The duration of temperature oscillations was determined by the results of experimental groups 1 and 2. When present, TGF-β1 was used only during incubation as described above. The controls and experimental groups used were as follows:

1) ***Control B***: MO hydrogel, no TGF-β1, no oscillation
2) ***Control C***: MO hydrogel, no TGF-β1, with 1 hour oscillations
3) ***Control D***: PEGDA hydrogel, with TGF-β1, no oscillation
4) ***Experimental B****:* MO hydrogel, with TGF-β1, no oscillation
5) ***Experimental C***: MO hydrogel, with TGF-β1 and 1 hour oscillations
6) ***Experimental D***: PEGDA hydrogel, with TGF-β1 and 1 hour oscillations

Control B and C differed only in the treatment of temperature oscillations. Control D was used to show the effects of an alternate thermoresponsive hydrogel on chondrogenic differentiation. Experimental groups B-D showed the effects of TGF-β1 under various temperature and hydrogel conditions.

1.3. Summary of Results

1) 5% volume strains were successfully applied to encapsulated cells within a 0.001 to 0.0125 Hz frequency.
2) Cellular constructs showed a decrease in magnitude and frequency of volume strains overtime as compared to acellular gels, with PEGDA (15% PEG) having the shortest response time to applied temperature oscillations.
3) A 3:5 conversion ratio between swelling ratios and volume strain was characterized for the first time.
4) PEGDA (15% PEG) gels were shown to be temperature responsive within 31 to 37^{o}C using realtime particle tracking.
5) Temperature oscillations with periods within 120 s and 285 s provided the optimal frequencies for gel response.
6) A live-dead analysis of MO (10% PEG) hydrogels showed good cell viability with no significant difference among groups. Both aggrecan and collagen type II content were upregulated.
7) MO (20% PEG) showed upregulation of aggrecan, type II collagen, and Sox 9 with TGFβ-1 but no oscillations. TGFβ-1 alone enhanced aggrecan and collagen II expression, while temperature oscillations alone caused their downregulation.
8) PEGDA (15% PEG) constructs exhibited the best results for chondrogenic differentiation under 1 hour of stimulation and TGFβ-1, upregulating aggrecan, collagen type I, and Sox 9 over time under temperature oscillations and TGFβ-1.

9) MO (20% PEG) and PEGDA (15% PEG) crosslinking densities were too high, limiting the extent of cell proliferation and ECM production.
10) Static mechanical strains induced by high crosslinking density and confined heating chambers limited the degree of chondrogenic differentiation, and caused downregulation for MO (10% and 20% PEG).

II. Literature Review

2.1. Tissue Engineering Background

The overall goal of tissue engineering is to develop functional native tissue equivalents that can be implanted [11]. Due to aging, overuse, and loading of joints, damage to articular cartilage has increased the demand for tissue engineered solutions. In general, tissue engineering requires the application of biological cues to cells, manipulation of the cell microenvironment, and monitoring cell responses on many levels. In developing tissues, cells undergo various cycles of cell renewal, differentiation, and assembly in a constantly changing environment with temporal and spatial gradients of various biological cues. As such, tissue engineering requires modeling these environments by balancing the interaction between biology and engineering. This requires providing cues present *in vivo* during *in vitro* culture to guide cell differentiation and functionality. 3D organization of cells *in vitro* is manipulated via biomaterial scaffolds, while the conditions for cell development into a functional tissue are provided with bioreactors.

In general, biomaterial scaffolds provide the structure and support for cell attachment and growth, while bioreactors provide the environmental control during cell development in culture. Both provide the physical factors and regulatory signals determining the phenotype and function of the tissues formed. The focus of this study was to develop tissue engineered cartilage constructs by directing chondrogenic differentiation of hMSCs encapsulated in thermoresponsive hydrogels cultured in a temperature-controlled bioreactor system.

2.2. Cartilage Background

2.2.1. Cartilage Properties and Composition

Of the three main types of cartilage, hyaline articular cartilage was the targeted tissue engineered tissue. Hyaline articular cartilage is white, glassy, and avascular, and lines diarthrodial joints providing an almost frictionless surface for movement, structural support, and load bearing [12]. Chondrocytes, the only resident articular cartilage cell type, compose 1% of the volume of articular cartilage and are responsible for producing ECM proteins including type I and II collagen, chondroitin sulfate, and glycosaminoglycan (GAG)-bearing proteoglycans (aggrecan, biglycan decorin, and fibromodulin), hyaluronic acid, and non collagenous proteins that contribute to its tensile and compressive strength [13].

During embryo development, chondrocytes derived from mesenchymal stem cells within adult bone marrow form matrices which secrete the ECM proteins listed above and express a Sox-9 driven genetic program [14]. In culture, differentiated chondrocytes are characterized by the synthesis, deposition, and maintenance of cartilage-specific ECM molecules including type I and II collagen, aggrecan, and Sox-9 [15-17]. These differentiated chondrocytes have unstable phenotypes that become dedifferentiated after multiple passages by losing their spherical shape and forming into elongated fibroblast-like morphologies [2, 18]. However, when cultured in 3D scaffolds, chondrocytes maintain their chondrocytic phenotype, even after having dedifferentiated [18].

Overall, articular cartilage is composed of 65-85% water, 12-24% collagen (90 to 95% collagen type II), and 3-6% GAGs [13]. Physiological forces experienced by cartilage include not only compressive forces but shear force due to loading and fluid flow, and

changes in hydrostatic pressure. Under compression, cartilage is viscoelastic because of frictional drag due to interstitial fluid flow that provides lubrication and transport of nutrients to the tissue [19]. Although cartilage is physically strong, it is sensitive to biological degradation and cannot repair itself after significant injury precipitated by disease or trauma [20].

2.2.2. Anatomy of Articular Cartilage

Articular cartilage (0.5 – 5.0 mm thick) is organized as a function of distance from the surface and from the cells that lay down the ultrastructure and define the strength and tensile stiffness of each cartilage layer [20]. Consequently, it is divided into four zones: superficial, middle (transitional), deep (radial), and calcified cartilage zone [20-22] (Figure 1). Every zone contains chondrocytes with different sizes, shape and metabolic activity. The superficial zone, or outermost layer, is the thinnest and creates a frictionless joint surface composed of thin collagen fibrils that are parallel to the joint surface with elongated, inactive chondrocytes just below [23]. The middle zone is thicker, with spherical cells and larger collagen fibrils in a non-parallel arrangement. The deep zone is characterized as having spherical cells in a columnar orientation. The collagen fibrils are parallel to each other, but perpendicular to the superficial layer. The calcified cartilage zone contains collagen fibrils that provide a transitional mechanical support from and fixation between cartilage and bone.

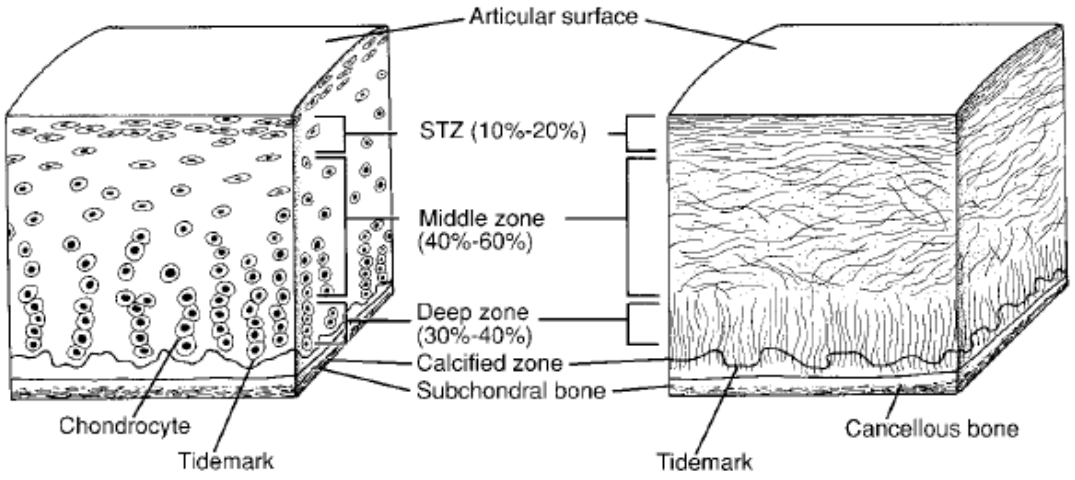

(A) **(B)**

Figure 1. Cartilage Microstructure. (A) Schematic of chondrocyte organization of the four zones: STZ = superficial tangential zone, the middle zone, deep zone, and the calcified zone. **(B)** Sagittal cross-sectional diagram of collagen fiber architecture. © 1994 American Academy of Orthopaedic Surgeons. Reprinted from the *Journal of the American Academy of Orthopaedic Surgeons*, Volume 2 (4), pp. 192-201 with permission [(24)].

2.3. Tissue Engineering and the Use of Human Mesenchymal Stem Cells for Chondrogenesis

2.3.1. Treatments for Articular Cartilage Defects

Surgical treatments used for severe cartilage damage are typically invasive and include osteochondral and autologous chondrocyte transplantation and artificial joint implantation for cartilage replacement. To repair damaged cartilage, tissue response techniques (e.g. microfracturing, abrasion, or drilling) [(25)] with or without the use of biomaterials have been used. For less severe damage, tissue grafts (autografts or allografts) are used to fill the damaged region; however, they induce an immune response and have a 95% survival rate of five years [(26)]. Instead of replacing damaged tissue, regeneration techniques have been developed to heal the tissues. Less invasive techniques

for cartilage repair include laser treatment, electrical stimulation, and injection of pharmacologics to stimulate chondrocyte growth [26] However, all of these techniques have had limited success and vary from patient to patient, which is due to the production of inferior cartilage tissue as a result of limited proliferation and differentiation of the repaired cells [27]. Attempts to achieve minimally invasive treatments have led to tissue engineering cartilage for repair and regeneration.

2.3.2. Cell Transplantation for Cartilage Damage

Direct transplantation of chondrocytes into damaged cartilage tissue has had a less than 40% success rate due to the inability to retain injected cells at the damaged site long enough to produce matrix [26]. Procedures in which chondrocytes are injected under a periosteal flap sutured over the defect have proven successful in the femoral condyle. However, they require donor periosteal flaps to perform the surgery and cannot be used to treat all cartilage damage. The most optimal design developed thus far has been the implantation of biomaterial scaffolds that provide the structural support and adhesion sites for proliferation of chondrocytes without causing dedifferentiation. While various polymer scaffolds have been developed, the focus of this study was the use of hydrogels for cell encapsulation.

2.3.3. Biomaterial Scaffolds for Tissue Engineering

Biomaterial scaffolds form the matrix in which chemical and biophysical cues are used to direct cell growth. In natural cartilage, this matrix is composed of proteoglycan content in a collagen matrix that provides tissues with mechanical strength to support physiological loads. The matrix shape and mechanical properties can be manipulated to direct cell differentiation by limiting cell shape and size. Various natural and synthetic

materials have been used to synthesize porous, fibrous, and hydrogel scaffolds [28]. Porous scaffolds allow migration and infiltration of cells into macroscopic voids, whereas fibrous scaffolds can be fabricated to mimic native ECM and direct cell alignment [29]. Hydrogels, on the other hand, are water-swollen polymers that can be synthesized from natural ECM components or synthetic materials to mimic native tissue properties.

2.3.3.1. Hydrogel Scaffolds

Various types of hydrogels have been used for cell tissue culture, including synthetic and natural polymers. Hydrogels provide structural support while having efficient transport properties required for delivering nutrients and removing cell waste. Their physical properties such as tensile modulus, crosslinking density, porosity, and topography can be easily tailored. As such, their mechanical properties and water content can be modified to imitate native tissue [14]. They have been used for mechanical loading of encapsulated cells by applying cyclic hydrostatic pressure, compressive loads, and low-intensity pulsed ultrasound to encapsulated cells [30].

In general, hydrogels consist of a three-dimensional crosslinked polymeric chain network that can swell and deswell through the diffusion of water and biological fluids. The network is either chemically or physically crosslinked, with covalent and ionic bonds forming the former, and entanglements, crystallites, and hydrogen bonds responsible for the latter. The elastic network holds absorbed solvents in the matrix via osmotic forces, while the liquid itself prevents polymer collapse. As such, the osmotic forces and elastic retractivity determine the hydrogel properties.

Natural hydrogels, such as Matrigel, collagen, agarose, and fibrin hydrogels, have been used for their ability to provide signaling to encapsulated cells [11], biocompatibility,

enzymatic degradability, and low immunogenicity. Under dynamic compressive strain at ~1 Hz frequency, agarose hydrogels were shown to promote an upregulation of proteoglycan synthesis [31, 32]. However, limited control over their polymerization and their overall gel mechanics has led to further development in synthetic hydrogel scaffolds, which have tailorable mechanics, chemistry, and degradation rates [11]. Specifically, their monomer molecular weight, functionality, and monomer concentration can be controlled, while their rate of enzymatic or hydrolytic degradation can be manipulated by altering the polymer backbone [33]. The most commonly used synthetic hydrogels include poly(glycolic acid) (PGA), poly(L-lactic acid) (PLLA), and poly(ethylene glycol) (PEG) hydrogels. Studies conducted using tissue engineered PGA constructs encapsulating bovine chondrocytes indicated static compression decreased sulfated glycosaminoglycans (S-GAG) and protein production, while dynamic compression at 5% amplitude and frequencies between 0.001 to 0.1 Hz enhanced S-GAG and protein production [34]. PEG hydrogels specifically are hydrophilic, preventing nonspecific material interactions [11]. They are typically modified with tethered groups to modify cellular interactions, with low molecular weights (Mw) being less responsive to temperature than higher Mw. Further studies showed hydrogel crosslinking density plays a role in chondrogenic differentiation in addition to dynamic compression.

Researchers have demonstrated hydrogels cross-linked with poly(ethylene glycol) (PEG) macromers provide matrix support for chondrocyte viability while promoting ECM deposition [35]. It has been shown that static compression inhibits proteoglycan and total protein synthesis [36]. Under dynamic compressive strains, increasing crosslinking density past a certain threshold has inhibited cell proliferation and proteoglycan synthesis

in PEG-based hydrogels due to increased production of nitrite [37]. Other studies have shown PEG-based hydrogels encapsulating bone marrow derived hMSCs and cultured in TGF-β1 have successfully upregulated Sox 9, aggrecan, type II collagen, and GAG content when gels were dynamically compressed daily at 10% strain in a bioreactor for 2.5 hours at 1 Hz [14]. Overall, PEG-based hydrogels were shown to promote cell viability under dynamic compressive strains ranging 10 to 15% and to enhance mechanotransduction as the gel compressive modulus increased, but within a limited range of crosslinking densities [38, 39].

Stimuli-responsive hydrogels have been developed as actuators for cell growth. They are characterized by their ability to undergo reversible, discontinuous, large volume changes under various stimuli including temperature, pH, chemical triggers, electric field, magnetic field, and light [40-45], which can be either external or internal. The stimuli-responsive behavior of hydrogels is mainly attributed to the various types of interactions between the polymer chains and the solvent. Most commonly used responsive hydrogels in cell culture have been used for artificial muscle development and are responsive to an electric field.

Among the various stimuli-responsive hydrogels, thermoresponsive hydrogels are one of the most extensively studied systems. One of the first accounts in which thermally responsive hydrogels were used to show viability of cell cultures *in vitro* used polyNIPAM gels as scaffolds for bovine chondrocytes [46]. Other studies designed thermoresponsive, partially biodegradable poly(N-isopropylacrylamide) cross-linked with poly(D,L-lactic acid) having dextran segments [47]. The gels were used to encapsulate embryonic chick chondrocytes and were cultured at a constant temperature, then lowered

to room temperature to harvest the cells from the gel. The chondrocytes maintained their phenotype and morphology during their four week *in vitro* culture suggesting thermoresponsive gels could be a promising scaffold for easy collection of encapsulated cells.

Despite all the studies conducted, the use of thermoresponsive hydrogels as scaffolds and *bioactuators* for cartilage regeneration under stimulation of a heating device for chondrogenic differentiation of hMSCs has not been attempted before. This study will present the techniques used to induce chondrogenic differentiation through temperature induced dynamic mechanical compression of hMSCs encapsulated in thermoresponsive hydrogels [30].

2.3.4. Cells for Cartilage Tissue Engineering

The three major cell types used for tissue engineering cartilage are committed chondrocytes, embryonic stem cells, and adult stem cells. However, due to limited differentiative capability of committed chondrocytes and tumorigenic potential, and legal and ethical issues surrounding embryonic stem cells, adult stem cells were the chosen cell source for this study. Human mesenchymal stem cells (hMSCs) have been used in autologous chondrocyte transplantation for regenerating cartilage due to their relatively easy isolation [48], regenerative potential [49], and pluripotency [50]. hMSCs have the ability *in vitro* and *in vivo* to differentiate into cartilage[8, 9, 51], bone[52, 53], adipose[53], and other tissues [49, 50] under specific environmental cues, and as such have been studied for their ability to form tissue constructs such as bone and cartilage implants.

2.3.5. Signaling Factors for Chondrogenesis

hMSCs under chondrogenic differentiation undergo phenotypes of transient chondrocytes residing in the growth plate of growing joints, which become hypertrophic and ossify during bone formation, whereas permanent chondrocytes are those with a fixed chondrocytic phenotype as in articular cartilage development [54]. Since chondrocytes control the synthesis of matrix components and their own distribution and incorporation into the ECM, they respond to various external factors. This includes the surrounding matrix composition and soluble mediators such as growth factors and cytokines, which can be manipulated when selecting parameters for cell culture. Similarly, mesenchymal stem cells require specific signals to differentiate into cartilage. More specifically, hMSCs have been shown to differentiate into chondrocytes *in vitro* in the presence of soluble signals such as bone morphogenic proteins 2 [55, 56] and 6 [57] and transformation growth factors 1 (TGF-β_1), 2 (TGF-β_2), and 3 (TGF-β_3) [8, 9]. TGF-β_1 has been shown to induce early chondrogenesis on hMSCs while inhibiting their late differentiation into hypertrophic chondrocytes once they become chondrocytes [58]. These signals have been successfully used to differentiate hMSCs in hydrogel scaffolds especially for use in tissue engineering applications.

2.3.6. Microenvironment Requirements for Chondrogenic Differentiation of hMSCs

While proper growth factors must be present, the local microenvironment must allow transport of these factors while providing delivery of nutrients and physical support. The scaffolding material used for tissue engineering must be tailored specifically to provide optimal biological conditions by controlling the architecture, surface roughness, and porosity (macro, micro, and interconnecting) [59]. Ideal scaffold properties for tissue

engineering include biocompatibility, biodegradability or bioresorbability, porosity, and mechanical stability [59]. The cells require proper surface chemistry to allow for cell attachment, proliferation, and differentiation by promoting cell permissivity and ECM production [60]. Ideally, the scaffold should have a controlled degradation rate that matches the tissue development with similar mechanical properties as that of native tissue.

Cell seeding densities also affect the efficiency of chondrogenesis. At low seeding densities (1-5 million cells/mL), an increased rate of matrix deposition per cell occurs [61] while at higher densities (20-60 million cells/mL) the matrix deposition per cell decreases [62] and mechanical properties are not improved with increasing MSC seeding density [63]. This phenomenon is due in part to negative feedback mechanisms and limited nutrient transport beyond a specific cell seeding density. However, this largely depends on the scaffold porosity and diffusion rates, and bioreactor properties.

2.3.7. Mechanobiological Conditioning

One of the most important factors enhancing MSC chondrogenesis is mechanical stimulation. It is well known that immobilization and overloading of joints causes cartilage wear and degradation [64-66] while normal daily activity is necessary to maintain tissue functionality. As mentioned before, studies performed *ex vivo* have shown that static, unconfined compressive strain inhibits proteoglycan and overall protein synthesis, while dynamic compression at frequencies greater than 0.001 Hz producing 10% strain (0.5 MPa) promotes chondrocyte biosynthesis [67]. However, dynamic strains have been shown to be frequency-dependent, where low frequencies ($\leq$ 0.001 Hz) have inhibited proteoglycan synthesis, while higher frequencies (0.01-1.0 Hz) have promoted it [68]. As such, mechanical stimulation has been shown to enhance MSC chondrogenesis, creating

greater collagen and proteoglycan content, upregulation of Sox-9, and increased gene expression of type II collagen and compressive strengths [69, 70].

Chondrocytes are known to respond to mechanical loading via changes in their surrounding environment including cell deformation, streaming potentials, and changes in fluid flow, hydrostatic pressure, pH, and osmolality [71, 72]. Various studies have been conducted to study these changes in native cartilage by encapsulating chondrocytes in hydrogels under mechanical stimulation. The conversion of mechanical stimuli to chemical activity known as mechanotransduction is described below.

2.3.8. Mechanotransduction

The process of mechanotransduction can be divided into four phases of cell response to mechanical forces: mechanocoupling, coupling, signal transmission, and ECM-coupling [73]. Mechanocoupling is the translation of forces from the macroscopic level to a local response at the surface of the sensor cell. Coupling requires the transduction of forces from the outside of the sensor cell to biochemical signals within the cell. Signal transmission transfers the signal from the signal cell to the effector cells. In the last response phase, ECM-coupling occurs when the altered ECM interacts with the effector and sensor cells and modifies their signal. These responses are either rapid or acute, occurring seconds to minutes or hours to months For cartilage, mechanocoupling is performed by the ECM surrounding the chondrocytes, where cartilage tensile strength is due to the ECM collagen fibril meshwork, while compressive resistance is provided by proteoglycans. The ECM matrix composition is highly dependent on the mechanical loads, with thicker matrices formed when exposed to greater loads. While the mechanisms and signaling pathways of mechanotransduction is still unknown, the

proposed transmembrane receptors responsible for this phenomenon include stretch activated ion channels, hyaluronan receptor CD44, anchorin II, and integrin receptors, with the latter having greater evidence as a mechanoreceptor regulating cell responses to ECM changes and mechanical stresses [73].

2.4. Background of Thermoresponsive Hydrogels

Thermoresponsive hydrogels undergo large, reversible volume changes in response to subtle temperature variations about the lower critical solution temperature (LCST). The volume phase transition (VPT) temperature is defined as the temperature at which a thermoresponsive gel undergoes a reversible phase transition between a swollen and deswollen state. The VPT is near the LCST, which is the transition temperature range of the corresponding linear polymers due to a sudden change in hydration and dehydration. The VPT is a result of a balance between the hydrophilic and hydrophobic moieties in the gel network [74], which are responsible for their thermoreversible behavior. The volume phase transition (VPT) observed at their LCST is attributed to the release of water molecules bound to the hydrophobic moiety of the polymer, followed by enhanced inter and intramolecular hydrophobic interactions.

The LCST can be manipulated by altering the polymer chemical composition and modify the hydrophilic-hydrophobic balance of the polymer chains. For instance, incorporation of hydrophobic comonomers decreases the transition temperature, while addition of hydrophilic comonomers increases the LCST [75]. This allows for the precise tuning of their transition temperature; thus, their swelling-deswelling kinetics are highly attractive for applications where temperature is an important consideration. The fundamental interactions that regulate this behavior and its kinetics are mainly covalent

bonds, ionic or hydrophobic interactions, secondary interactions such as hydrogen bonding, and Van der Waals forces [76]. A number of structures such as comb-like architecture with dangling chains have been adopted to overcome the diffusion limited swelling of hydrogels to improve their swelling-deswelling kinetics [76].

2.5. Bioreactors Used in Cartilage Tissue Engineering

3D culture systems require high mass-transport rates to develop uniform tissues and avoid necrosis in the central regions of the scaffold. This internal mass transfer is typically determined by the diffusion and convection of media contents in addition to cell density, scaffold structure [11]. As such the external mass transfer is determined by the hydrodynamics of a bioreactor. However, as mentioned above, successful synthesis of cartilage tissue requires application of dynamic mechanical strains of hMSCs during chondrogenesis. Typically, cell-laden hydrogels are grown in bioreactors that are combined with external mechanical systems that apply stresses for enhanced chondrogenesis. These bioreactors help direct differentiation by delivering regulated amounts of nutrients and regulating pH levels by providing uniform mixing and controlled mass transfer rates [26]. Overall requirements dictate fast and controlled cell expansion, high cell seeding density in 3D scaffolds, continuous exchange of oxygen, nutrients, and metabolites, and physiological stimuli [11]. Various types of bioreactors include spinner flasks in which a magnetic stir bar keeps media thoroughly mixed, a perfusion culture where a peristaltic pump delivers a constant flow of media to the culture, and rotating wall bioreactors in which centrifugal forces are balanced to keep polymer constructs in constant free-fall while mixing the media with the scaffold [26].

Mechanical loading can also be applied to induce shear, tensile, or compressive strains. For cartilage development and function, deformational loading and hydrostatic pressure are primary forces applied during tissue engineering cartilage [11]. Dynamic, unconfined, compressive loading has been most effective as shown above in hydrogel constructs, in addition to enhanced mass transport gradients provided by bioreactors. However, limitations of these bioreactors include anisotropic stress distribution in the construct, which can cause heterogeneous cell differentiation and constrain the construct size and shape, and cause cracking or buckling of the construct. These mechanical devices vary from perfusion systems that apply hydrostatic[77] pressure to pneumatic bioreactors with linear pistons [38]. As described above, enhanced chondrogenic differentiation is dependent upon the frequency of mechanical activation. As such, a custom made sterilizable device was needed to apply controlled heating cycles to cell-encapsulated hydrogels while allowing for optical imaging of the constructs. Temperatures ranged within physiological conditions and had a target actuation frequency greater than 0.01 Hz and produced 5% compressive strain.

2.6. Image Analysis

2.6.1. Methods of Deformation Tracking

Initial studies of the dimensions and structure of hydrogels was originally conducted using bright field microscopy. However, the internal dynamics could not be studied. Instead, techniques to image the static or dynamic scattering of light were developed for structural and bulk property analysis and diffusion coefficient determination of hydrogels including nuclear magnetic resonance [78] and electron-spin resonance [79, 80]. Current forms of tracking matrix deformation have been developed for

many applications including the study of matrix remodeling, of cell adhesion, of cell transport processes, and of cell contractility. These methods can be categorized as using (1) confocal microscopy to track beads embedded in the gel matrix [81-83] and (2) tracking of 2D projections of 3D matrix fiber movement using phase contrast imaging [84], differential interference contrast (DIC) microscopy [85, 86] or (3) fluorescent imaging [87]. Fluorescent microscopy has been used particularly for its ability to track 3D displacements of single particles and living cells in real time.

Typically, it is necessary to track all three dimensions of particle movement to fully track and study matrix and cell deformations, assuming both deform together. However, while fluorescent microscopy can be used to easily detect x and y displacement, it does not capture images in one focal plane, in contrast to confocal microscope, making z displacement tracking less straightforward. As such, images captured must be processed differently to track specific z location by analyzing the parallel illumination, or the size and pattern of diffraction rings surrounding the bead in out-of-focus images to detect the z position of tracked particles [88-90]. This method requires capturing images of one fluorescent particle embedded in a matrix at set increments in the z position from above to below the bead, which are used to create a set of calibration images from which the z position can be calculated as a function of the radial size and bead intensity. From this set, the z position of any image captured with the same fluorescent particle and matrix can be calculated. From a distance above and below the top and bottom planes of the bead, respectively, diffraction rings will appear due to light scattering from the bead. Imaging a bead from the top will appear as a diffraction ring with radius r, but as the focal plane moves downward towards the center of the bead, the intensity will be largest with radius

$r_o < r$, followed by a decrease in intensity as the plane moves towards the bottom of the bead.

Various methods have been used to locate the bead center. While calculating the point spread function of images has been performed, it does not allow for high precision due to optical parameters from the imaging system, which are difficult to characterize. Instead, cross-correlation techniques have been used to locate the center coordinates of each particle imaged for up to sub-nanometer precision in three dimensions [89]. Essentially, cross correlation compares two images as a function of time and is used to locate the max intensity in an image. It tracks the *x* and *y* coordinates by assuming a centro-symmetric image and averaging x and y profiles each in the opposite coordinate axis. As such, the mirror image of the averaged intensity profile $P(x+\delta x)$ should be equal to $P(-x-\delta x)$. To calculate δx, the offset from the centroid x coordinate (x_c) the cross correlation function R_{xy}, is defined as follows [91]

$$R_{xy}(m) = E\{x_{n+m} y^*_n\} = E\{x_n y^*_{n-m}\} \quad 1$$

where x_n and y_n are stationary random processes, $-\infty < n < \infty$, and $E\{\cdot\}$ is the expected value operator. The cross-correlation is defined

$$C_{xy}(m) = R_{xy}(m) - \mu_x * \mu_y \quad 2$$

Where μ_x and μ_y are the means for the *x* and *y* coordinates, respectively. However, because the images are finite segments and R_{xy} is defined as an infinite random process, an estimate must be used for *N* samples having coordinates x_n and y_n using a deterministic cross-correlation sequence, or time-independent function

$$\hat{R}_{xy}(m) = \begin{cases} \sum_{n=0}^{N-m-1} x_{n+m} y^*_n & m \geq 0 \\ \hat{R}^*_{yx}(-m) & m < 0 \end{cases} \quad 3$$

Where $\hat{R}_{xy}(m)$ ranges from -(N-1) to N-1, and x_n and y_n are indexed from 0 to N-1. MATLAB offers a built-in cross-correlation function $xcorr(x, y)$ in one dimension which calculates the summation for $\hat{R}_{xy}(m)$ using a fast Fourier transform (FFT) algorithm for inputs x_n and y_n, which are stored in vectors x and y with length N. In Fourier space, the summation of products in time space as shown in equation [3] becomes convolution according to the cross-correlation theorem, with one of the two subsequences reversed in time. For calculations in two-dimensions, the two dimensional cross-correlation function $xcorr2(X, Y)$ is used instead, where X and Y are matrices representing the original image and the image reflected about the y axis for calculating the x coordinates, and about the x axis for y coordinates. X has dimensions [M_X, N_X] and Y has dimensions [M_Y, N_Y]. The discrete cross-correlation in 2D is given by

$$C(i, j) = \sum_{m=0}^{(M_X-1)} \sum_{n=0}^{(N_X-1)} X(m, n) \bullet conj(Y(m+i, n+j)) \quad 4$$

where $0 \leq i < M_X + M_Y - 1$, $0 \leq j < N_X + N_Y - 1$, and $conj(Y(m+i, n+j))$ is the complex conjugate of Y defined as

$$conj(Y) = real(Y) - i \cdot imag(Y) \quad 5$$

The actual coordinates of the centroid (x_c,y_c) are calculated by subtracting a threshold value T from each point in the cross-correlation to locate the highest intensity coordinate. x and y are the coordinates of each pixel in the images X and Y examined [(92)].

$$x_c = \frac{\sum x\{C(i,j) - T\}}{\sum \{C(i,j) - T\}} \quad 6$$

$$y_c = \frac{\sum y\{C(i,j) - T\}}{\sum \{C(i,j) - T\}} \quad 7$$

The threshold value insures the centroid has the highest intensity in the analyzed image region. Similar to the one dimensional case, the $xcorr2(X,Y)$ calculates the double summation in equation [4] using a FFT algorithm, which results in convoluting X and the complex conjugate of Y twice. The function returns the x and y coordinates (equations 6 and 7) of each centroid of the chosen particle in each image.

2.6.2. Deformation and Volume Strain Calculation

The displacement of each particle was quantified as a ratio using the 3D centroid coordinates found using equations [6] and [7] as follows

$$R = \frac{d_i}{\sum_{i=1}^{n} D_i} \quad 8$$

where d_i is defined

$$d_i = \sqrt{(x_i - x_0)^2 + (y_i - y_0)^2 + (z_i - z_0)^2} \quad 9$$

with the initial centroid position (x_o, y_o, z_o). $\sum_{i=1}^{n} D_i$ is the total displacement in all n images of a stack, where D_i is defined

$$D_i = \sqrt{(x_{i+1} - x_i)^2 + (y_{i+1} - y_i)^2 + (z_{i+1} - z_i)^2} \quad 10$$

R is the ratio of the distance between the initial and current position of each bead to the total displacement of the bead.

Theoretical calculations of the volume strain have been calculated for various polymers using the deformation gradient tensor ***F*** of inhomogeneous polymer gels [93]**.** Assuming a homogeneous reference state followed by isotropic swelling, the volume fraction of a polymer in the reference state is ϕ_0 . Let the material coordinates of a marker fixed in the gel matrix (or the initial coordinates of a particle) be ***X*** while the position *x* of the material point represent the current configuration. The motion of the gel network is defined by the deformation gradient (***F***)

$$F = \frac{\partial x}{\partial X} \tag{11}$$

The volume ratio (*V*) between the current and reference (homogeneous) state is defined

$$V = \det(F) \tag{12}$$

The volume elements in the two states are related by

$$dx = \det(F)dX \tag{13}$$

Therefore, the volume fraction of the polymer in the current configuration ϕ to the reference state ϕ_0 is expressed

$$\frac{\phi_0}{\phi} = V = \det(F) \tag{14}$$

Equations [11] and [12] can be calculated by parameterize particle centroid coordinate raw data as a function of time (t) and spatial coordinates (*x,y,z*). The partial derivatives of the initial and final coordinate functions with respect to (*x,y,z*) are then calculated at each time point. Finally, the quotient of these two partial derivatives at each time is arranged into matrix F. The determinant of F(t) is calculated at each time point to arrive at the volume ratio V(t), which represents the change in volume at each time t.

III. Materials and Methods

3.1. Cell Expansion of Human Mesenchymal Stem Cells

Bone marrow derived human mesenchymal stem cells (hMSCs) were purchased from Tulane University (National Center for Research Resources (NCRR), Tulane University, New Orleans) at P1. They were passaged twice in T-175 flasks at a cell density of 1000 cells/cm^2 at 37^oC and 5% CO_2 in growth media (500 ml high glucose DMEM, containing 20% fetal bovine serum (FBS) (20% v/v premium select FBS (S11550, Atlanta Biologicals), 1% L-Glutamine, and 1% PenStrep (Gibco Invitrogen), which was changed initially every third day. P3 cells were expanded for 4 weeks and passaged 1:6 as follows: media was aspirated and the cells were washed with 20 mL of phosphate-buffered solution (PBS). After aspirating the PBS solution, the flasks were incubated with 7 ml of 0.25% trypsin-EDTA (cat # 25200-056, Invitrogen,) at 37^oC for 5 minutes. The cells were loosened with physical agitation for 1 minute then imaged using a bright field microscope (Axio Observer A1, Carl Zeiss) to verify all cells were detached from the flask. The trypsin was neutralized with hMSC growth media (Invitrogen) and the number of cells was counted with a Coulter counter (Z1^{TM} Series COULTER COUNTER ® Cell and Particle Counter, Beckman Coulter).

3.2. Synthesizing Oligomers

3.2.1 Synthesis of MO Oligomer

The MO oligomer was synthesized using reversible additional fragmentation chain transfer (RAFT) using di(ethylene glycol) methyl ether methacrylate (MEO_2MA) and oligo(ethyleneglycol) methyl ether methacrylate (OEGMA, Mw=475 g/mol) monomers. Azobisisobutylronitrile (AIBN) was used as an initiator along with the chain

transfer agent (CTA), S, S'-bis(α, α'-dimethyl-α"-acetic acid)-trithiocarbonate. Overall, an MO oligomer with a molecular weight of 8000 g/mol with a 4:1 ratio between MEO_2MA and OEGMA monomers with an LCST of ~37°C was synthesized as follows: 0.8 gram of OEGMA, 3.1704 grams of MEO_2MA, 105.6 mg of the CTA, and 6.48 mg of AIBN were charged in a Schlenk flask. The reaction mixture was purged with high purity nitrogen for 30 minutes and subjected to three freeze-thaw cycles, after which the flask was sealed and immersed in an oil bath at 80°C for 24 hours to ensure a complete conversion. The crude polymerization product was dissolved in tetrahydrofuran, precipitated in cold iso-propanol, and the precipitate was collected and dried in vacuum.

3.2.2. Synthesis of PEGDA Oligomers

PEGDA oligomers were synthesized as described elsewhere [94]. Briefly, 18.0g of PEG was refluxed for four hours in 300mL of toluene in a 500mL flask submerged in an oil bath at 150°C. Azeotropic distillation was used to remove any trace amounts of water. Upon cooling to room temperature, 1.093g (10.8mmol) of triethylamine was added to the solution and stirred vigorously. After stirring the flask for 30 minutes in an ice bath, 0.9775g (10.8mmol) of acryloyl chloride in 15mL of anhydrous dichloromethane was added drop wise to the reaction mixture for 30 minutes. The mixture was kept in an ice bath for another 30 minutes, then heated to 45°C overnight. After cooling the flask to room temperature, the quaternary ammonium salt was removed from the mixture by filtering through diatomaceous earth (2-3cm). A rotary evaporator was used to condense the filtrate, which was then precipitated in excess diethyl ether, and collected and vacuum dried at 40°C for 24 hours. The resultant PEGDA oligomer was purified by re-precipitation in diethyl ether followed by column chromatography on Sephadex® G-25

and dialyzed with dH_2O. The PEGDA was lyophilized prior to use to obtain a dried powder.

3.3. Characterization of Oligomers

The chemical structures of MO and PEGDA oligomers were characterized using proton nuclear magnetic resonance spectroscopy (^{1}H NMR). A Varian Mercury 400 spectrometer at 400 MHz frequency and deuterated chloroform ($CDCl_3$, Acros) solvent were used to record ^{1}H NMR spectra. The oligomers were dissolved in 0.5% (w/v) $CDCl_3$ before measurement.

3.4. Synthesis of MO and PEGDA Hydrogels

P[MEO_2MA-OEGMA-EGDA] (MO) (Figure A30) hydrogels were synthesized with 55% MEO2MA-OEGMA (10% w/v, Mw = 8000) with 45% PEGDA (10% w/v, Mw PEG: 3400 g/mol) crosslinker and 0.5% (w/v) photoinitiator (PI) (Irgacure 2959, Ciba, Switzerland) for experimental groups 1 and 2 (Table 1). The PI was prepared as a 10% (w/v) stock solution in 70% ethanol. For crosslinking density optimization, MO hydrogels were synthesized with 10, 15 and 20 % w/v PEGDA (Mw PEG: 3400 g/mol) (Table 1). PEGDA gels were similarly synthesized using a 99.5% PEGDA (Mw PEG: 10,000 g/mol, at 10, 15, and 20% w/v) and 0.5% PI solution. All monomers were filtered in a 0.22 μm filter (Millex GP filter unit). MO and PEGDA hydrogels were characterized to optimize cross-linking density for these experimental conditions. The closest matching MO and PEGDA swelling ratios were used for cell encapsulation in Exp B-D constructs. 150 μL of each polymer solution was transferred to 1.5 mL microcentrifuge tube caps (SealRite, USA Scientific Inc.), photopolymerized under UV light (365 nm) at 50

μW/cm^2 for 5 minutes, and removed using a spatula. See Figure A29 -Figure A30 for the chemical structures of MO and PEGDA.

Table 1. Various Crosslinking Densities of MO Hydrogels

Volume Percentage of Each Monomer		Overall 3400 PEG content	
MO (60 μL)	3400 PEG (10% w) (49.4 μL)	PEG Crosslinking Density	Mass of 3400 PEG (10% w) in 49.4 μL
55%	45%	10%	4.94 mg
45%	55%	15%	7.41 mg
38%	62%	20%	9.88 mg

3.5. Swelling Measurement Characterization of Hydrogels

The swelling ratios of MO (10% PEGDA) hydrogels were estimated at equilibrium by weighing the wet weights of 5 samples after 24 hours of incubation at different temperatures such as 4, 20, 30, 32, 34, 36, 38, 40, and 45^{o}C. They were subsequently dried at 37^{o}C for 24hrs each. The dry weights were measured and the swelling ratio (SR) was calculated as

$$SR = \frac{\text{wet weight}}{\text{dry weight}} \quad 15$$

For MO (10, 15, and 20% PEGDA (Mw PEG: 3400 g/mol)) and PEGDA (10, 15, and 20% PEGDA (Mw PEG: 10000 g/mol)), the swelling ratios of each gel type were first measured after equilibrating at 37^{o}C for 24 hours. These results were used to select MO and PEGDA gels with the most similar swelling ratios for hMSC cell encapsulation. PEGDA was used an alternate hydrogel with lower temperature response (magnitude and frequency of volume strain) than MO. After selecting the two most similar gels, a second measurement was made for nonequilibrium conditions. The two gels were allowed to equilibrate at room temperature (25^{o}C) for 24 hours, then immersed at 33^{o}C for 15

minutes. Their wet weights were immediately measured then immersed for five minutes in PBS pre-equilibrated at 35^{o}C. Their equilibrium swelling ratio was then measured at 37^{o}C after 24 hrs in a water bath.

3.6. Fluorescent Particle Encapsulation

Since it was necessary to determine optimal temperature conditions to induce about 5% volume strain, fluorescent particles (FPs) were encapsulated in MO (10% PEG 3400) hydrogels without cells to track gel displacement using image analysis. Once these temperatures were determined, fluorescent hydrogels were synthesized for each experimental group to measure volume strain in the presence of cells. All fluorescent hydrogels were synthesized with a 1% (w/v) fluorescent particle solution (Cat#FP-3056-2, 2.88 μm diameter polystyrene beads, Nile Red, 400-560 nm excitation, 535-650 emission nm, Spherotech, IL). 150 μL of each polymer solution with FPs and encapsulated hMSCs were transferred to autoclaved 1.5 mL microcentrifuge tube caps (SealRite, USA Scientific Inc.) and photopolymerized under UV light (365 nm) at 50 μW/cm^2 for 5 minutes. The hydrogels were removed from the mold with a spatula and cut into 4 equal pieces using a stainless steel surgical blade (No.10, Feather, Japan). Before cutting, the gels were cylindrical with a height of about 2 mm and 8.2 mm in diameter.

3.7. Cell Encapsulation

The swelling ratio results were used to determine the optimal crosslinking density of MO and PEGDA for experimental groups B through D. For all experimental groups, P4 hMSCs were resuspended in the prepared comonomer solution (MO and PEGDA) at a density of 20 million cells/mL and mixed gently to homogenize the suspension. The photoinitiator was then thoroughly mixed into the cell suspension. As before, 150 μL of

each polymer solution encapsulated with hMSCs was transferred to autoclaved 1.5 mL microcentrifuge tube caps and photopolymerized under the same UV light conditions for 5 minutes. The hydrogels were removed and cut into 4 equal pieces as in the FP tracking.

3.8. Engineering a Bioreactor Heating Device for Controlled Temperature Oscillations

3.8.1 Device Design and Fabrication

A bioreactor heating device was designed and built to apply temperature oscillations while capturing realtime images of gel constructs encapsulated with fluorescent particles. The device consists of four components: 8 gel compartment wells, a heating block, a peristaltic pump for circulating heated fluid, and a temperature regulated pump for circulating coolant fluid (Figure 2). The gel compartments in Figure A31 were constructed from 0.5 mm thick stainless steel (SS) tubes (ID = 5.84 mm, Type 316, McMaster-Carr) cut 6.22 mm tall that were inserted into 8 wells (9.35 mm) drilled out of a polycarbonate sheet (50 mm wide by 87.5 mm long and 9 mm tall) (McMaster-Carr). The SS tubes were sealed off from external fluid with a glass slide below held in place with a silicone rubber gasket, an aluminum plate, and rubber O-rings. The channel, well dimensions, and depth were designed to bifurcate heated fluid delivered upstream for equal distribution to the wells. The gel holder was connected upstream to a heating device that delivered temperature regulated water to the compartment. The heating component was made of two aluminum plates (alloy 6061, McMaster-Carr) sandwiching two thermoelectric (TE) modules (Table A5) (HP-199-1.4-0.8, TE Tech) connected in series (344 Watts). The TE modules were mounted with a thin film of thermal paste to fill any voids that could delay heat exchange due to air and other impurities. The TE modules

were connected to a TE controller (Figure A31)(TC-24-25, TE Tech, MI), which was controlled by LabVIEW software adapted from TE Tech (Figure A34). The water was circulated using a peristaltic pump at a constant flow rate of 1.47 ml/s (6.63 bar) (Table A5) (SVP4 H7, Stenner). The heating block was cooled with a secondary temperature controlled pump circulating water at 10 to 15^{o}C at 11 to 16 L/min (0.23 to 0.45 bars) (F12 MC Julabo, Labortechnik GmbH, Germany). To measure temperature, one thermistor (Sensor 1) (-20^{o}C to 100^{o}C measurement range, MP-244, TE Tech) was placed in one well compartment and another (Sensor 2) on the hot plate of the heating block. Sensor 1 was used to control the heating temperatures with LabVIEW, while Sensor 2 was used as an alarm sensor to ensure the heating block did not exceed 0 to 80^{o}C and destroy the TE modules. Tygon tubing was used for all tubing, except LDPE Polyethylene-NSF tubing (ID = 4.16 mm, OD = 6.54 mm) provided by the manufacturer for the peristaltic pump.

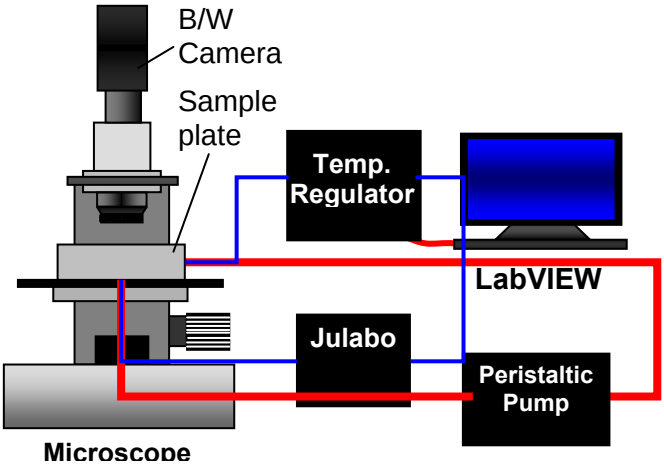

Figure 2. Device Setup. Temperature regulator (Temp. Regulator) represents the TE modules and TE controller. Sample plate holds constructs.

3.8.2. Component Specifications

The dimensions of the wells were chosen based on the constraints of the imaging system and to minimize fluid volume surrounding constructs to maximize heat exchange. The working distance of the 10x objective fluorescent microscope (Axio Observer A1, Zeiss) was 4.5 mm. This required the bottom thickness of the hydrogel compartment be small enough to fit within this region and allow imaging of hydrogel constructs, while providing structural support for the wells and prevent leaking. As such, the distance from the bottom of the hydrogel compartment (aluminum plate) to the top of the glass plate was < 2mm to allow 2.5 mm working distance for imaging the gels. The dimensions of the bottom aluminum plate and well were constrained by the cone diameter (∅10.5 mm), cone depth (8 mm), and outer diameter (∅24 mm) of the 10x objective.

The device was built using polycarbonate as the encasing hydrogel compartment due to its wide operating temperature range of -40^{O} to 93.3^{O}C, weather resistance, and low thermal conductivity (0.19 W/(mK) at 23^{O}C) making it an insulator for heat exchange. Tygon PVC tubing was selected due to its wide operating temperature range (-50 – 73.9^{O}C), low thermal conductivity (0.159 W/mK), autoclavability, and weather resistance. As such, heat loss was minimized during heating. Conversely, heat exchange between the heated fluid and constructs was maximized by using cylinders made of stainless steel alloy 316, which has a high thermal conductivity of 16 W/mK and high corrosion resistance up to 427^{O}C. The small thickness further enhanced the rate of heat exchange. While copper is an excellent thermal conductor (401 W/mK), it has a lower corrosion resistance than SS making its ionic toxicity a hazard for heated constructs. The aluminum alloy 6061 plates were used to sandwich the glass slide and gel holder because

of its yield strength (0.241 GPa), good corrosion resistance, and machinability. The high DTmax reduced power consumption while the high Qmax maximized the TE module coefficient of performance.

3.8.3. Device Characterization and Optimization

The heating device was controlled with a proportional-integral-derivative (PID) controller (TE controller) whose parameters were optimized for temperature precision and rate of heating. The proportional value (P) controlled the bandwidth or temperature range around a set point in which the controller could modulate power output. The higher the number, the smaller was the bandwidth. The integral gain (I) controlled the rate of power output calculating the difference between the set point and actual temperature and is measured in repeats/minute. The larger the I value, the faster the response and the less stable the oscillations. The derivative gain (D) measured the rate of change of temperature and anticipated the power needed, allowing the controller to compensate for fast temperature changes in the system. It enhanced the rate of response and was measured in units of cycles/minutes. PID values were located for the system such that the heating block produced critically damped temperature profiles.

3.9. 3D Fluorescent Particle Tracking

3.9.1. Particle Properties

The polystyrene fluorescent particles used were chosen for their size with a diameter of 2.88 μm, their hydrophobicity making them water insoluble, and their long fluorescent stability minimizing photobleaching effects. They were large enough to encapsulate within the crosslinked hydrogels and neglect spontaneous Brownian motion

during heat induced hydrogel deformations. Their charge and size allowed effective tethering to the matrix without significant particle loss during swelling and deswelling.

3.9.2. Image Acquisition

3.9.2.1. Calibration Images

An image stack of calibration images were captured at 10x using an inverted fluorescent microscope with an automated stage (Ix81, Olympus) and a mercury arc lamp for fluorescence excitation. MO (10% PEG) in PBS with encapsulated FPs were imaged to create a calibration profile with the diffraction radii of fluorescent beads as a function of their axial z position. A total of 329 images were captured at increments of 0.2 μm (total 65.5 μm distance) starting at the topmost focal plane through the bottom of the bead. This calibration set was used for all images captured to measure the z location of analyzed particles.

3.9.2.2. Hydrogel Imaging Under Controlled Temperature

Hydrogels with encapsulated fluorescent particles (FPs) were first imaged in PBS without cells to choose a target temperature range for oscillations and induce ~5% strain. Images were captured for the first and last 560s of a 1 hour oscillation treatment to measure the difference in volume strains over time and test for any hysteresis effects or decrease in magnitude.

Using these temperatures, the effects of cell presence on hydrogel volume strain were studied by imaging cell-free and cell-laden hydrogels at various time points under constant (room temperature) and oscillating temperature conditions. Cell-free hydrogels were imaged in PBS, while cell-laden hydrogels were imaged in chondrogenic media (500 mL DMEM (high glucose), 1 mL dexamethasone, 1 mL proline, 1 mL ascorbic

acid-2-phosphate, 4.5 mL sodium pyruvate, 5 mL ITS + Premix, 5 mL Pen/Strep, 5 mL TGFβ-1). The same focal plane and exposure settings were used for images within an image stack; however, they were changed for each construct imaged due to variations in dimensions, particle distribution, and cell density.

3.9.2.3. Hydrogel Oscillations and Response Time

Hydrogel response time and oscillations were measured by capturing images of cell and FP-laden MO (20% PEG) and PEGDA (15% PEG) hydrogels on day 17 after encapsulation. The images were acquired with the constructs at room temperature in 35 mm petridishes and chondrogenic media. Due to heat emitted by the fluorescent mercury vapor short-arc lamp, the construct temperature increased over 840s at a rate of 0.0016 ± 0.002 ^{o}C/s, allowing realtime measurement of the VPT under non-equilibrium conditions (from 25.9 to 27.6^{o}C for MO (20% PEGDA) and 27 to 28.5^{o}C for 15% PEGDA).

3.9.3. Data Processing

3.9.3.1 Coordinate Tracking

A cross correlation algorithm as described before was used to track the centroid coordinates of particles assuming centro-symmetry of the beads. To measure the bead displacement in the x direction, the x profiles were averaged over 200 lines centered in the y direction. Because correlation based methods are accurate when the window size is small and the translation of the image is minimal, a field of view was manually selected for tracking each particle in a stack of images [95]. MATLAB code from Johns Hopkins University [87] was adapted to locate the centroid coordinates of each particle. Assuming symmetry of the spherical particles, the averaged profile intensities $P(x+\delta x)$ was equal to its mirror image $P(-x-\delta x)$. The displacement δx was calculated with the 2D cross

correlation function *C(i,j)* equation [4] using the built-in MATLAB function *xcorr2()*. The coordinates of the centroid were calculated according to equations [6] and [7] [(94)].

3.9.3.2. Displacement and Volume Strain Calculation

The gel displacements (***R***) were calculated using equation [8] and the centroid coordinates found for the same 10 to 12 particles in a stack of images. The variation in the number of particles tracked was due to sudden changes in displacement, making the particles more difficult to track throughout the stack. If the hydrogel is perfectly elastic, this R ratio will be approximately 0, indicating recoil of the gel. If it is closer to 1, the gel does not exhibit relaxation. While the theoretical volume calculation was given in equation [12], the assumption of homogeneity and isotropic deformation could not be made. As such, the computationally intensive calculations were simplified by assuming linearity in all three coordinate axes as an estimate of volume strain. As such, the volume strain (%) was calculated as follows

$$V = \sqrt[3]{R \bullet 100} \qquad 16$$

3.10. Cell Temperature Oscillation Treatment

The hydrogel pieces were placed in 35 mm tissue culture dishes and incubated at 37^{o}C in 4 mL hMSC growth media for two days after encapsulation. They were placed inside PCR tubes (0.2 mL TempAssure PCR tube, USA Scientific) and exposed to daily temperature oscillations for 3, 7, 10, and 17 days for all experimental groups using the heating device in a tissue culture hood. The media was changed 3 days after encapsulation followed by every other day. For experimental groups 1 and 2, the thermoresponsive MO gels were exposed to 32 to 35^{o}C for one hour and three hours. For

experimental groups 3 through 5, the frequency of oscillation was increased due to the results from experimental groups 1 and 2. The MO and PEGDA constructs were exposed instead to temperature oscillations between 33 and 37^{o}C every day for one hour.

3.10.1. Volume Strains Induced by Temperature Oscillations

Cell-laden MO and PEGDA hydrogels with hMSCs and FPs were placed in the hydrogel wells directly with 180 μL of chondrogenic media and exposed to the same temperature oscillations as those in the hood for experimental groups 1 and 2 (34.5 to 37^{o}C) while imaging with a fluorescent microscope (Axio Observer. A1, Zeiss) on days 17 and 38 and days 7 and 17 for experimental groups 4-5 (31 to 37^{o}C). The images were analyzed to calculate displacement and volume strain as described above.

3.11. Cell Viability

A live-dead assay was conducted on 72 hour control A and experimental group 2A (3 hour treatment) to measure cell viability soon after encapsulation (Live-Dead Viability/Cytotoxicity Kit, Cat#: L-3224, Invitrogen). Live-dead assays were not conducted on experimental groups B to D due to limited cell number. The gel constructs were washed with PBS three times, cut into thin slices, and incubated with 1 ml Live-Dead solution composed of 1 mL Dulbecco's Modified Eagle Medium (DMEM) (Cat#. 11965, Invitrogen) 0.5 μL of calcein AM (green, Ex/Em = 494/517 nm) and 4 μL of ethyidium homodimer (EthD-1) (red, Ex/Em= 528/617 nm) [96]. EthD-1 penetrates the cell membrane and stains the nucleus, while calcein AM cannot penetrate and instead stains the cytoplasm. The gels were incubated at 37^{o}C for 30 minutes with 0.5 mL of Live-dead Assay solution, aspirated, then washed again with PBS. The gels were placed into a new petridish and imaged using a multichannel fluorescent microscope.

3.12. Real Time Quantitative PCR and Conventional PCR

RNA was extracted from samples using TRIzol then reverse transcribed to cDNA using SuperScript First-Strand Synthesis System (Invitrogen). Quantitative realtime and conventional PCR were performed.

3.12.1. RNA Isolation

The samples were washed twice with 1 mL PBS. RNA was extracted by adding a total of 1 mL TRIzol in parts to each sample in a 1.5 mL e-tube and crushing with a pestle. The samples were stored at -80^{o}C overnight. They were thawed the next day and thoroughly mixed with 250 μL chloroform per mL of TRIzol to extract the RNA. After storing the samples in room temperature for 10 minutes to allow separation of the two phases, they were vortexed and spun at 12,000g X 15min at 4^{o}C. The clear upper layer was removed and placed in a fresh tube, leaving the pinkish layer in the tube. 1 μL glycogen (20 μg) and 500 μL isopropanol were added, vortexed, and centrifuged at 12,000g X 10 min at 4^{o}C. The supernatant was poured out leaving behind the pellet. 1 mL of 75% ethanol made with DEPC water were added, mixed, and spun at 7,500g X 5 min at 4^{o}C. The supernatant was poured out once more. The samples were air dried for 10 minutes, mixed with 20 μL DEPC water, and dissolved by incubating at 60^{o}C for 10 minutes. The RNA solution was diluted with 10 mM Tris-Cl buffer solution at 1:100 and the concentration was measured using spectrophotometric absorbance at A260 nm/A280 nm.

3.12.2. cDNA Synthesis

BioRAD iScript™ cDNA synthesis kit (stored at -20°C, cat# 170-8891, BioRAD) was used to synthesize cDNA from RNA. The kit reagents and RNA samples were thawed on ice. 1 µL of RNA solution was mixed with 4 µL 5x iScript Reaction Mix, 1 µL iScript Reverse Transcriptase, and 14 µL nuclease-free water for a total 20 µL volume. The reaction mix was incubated at 25°C for 5 minutes, at 42°C for 30 minutes, and at 85°C for 5 minutes. The samples were stored at 4°C.

3.12.3. Real-Time PCR

The reagents and cDNA samples were thawed on ice. cDNA for each primer were run in triplicates in a 96 well plate using 29 µL of reaction mixture in each well. Aggrecan (AGN), collagen type II (Col II), and Sox 9 primers were the genes of interest chosen to quantify the degree of chondrogenic differentiation, while β-actin was used as the reference gene. 20 µL of each cDNA sample was diluted with 80 µL DEPC water (1:5 dilution). The reaction mixture was made using 0.5 µL each of the forward and reverse primers of each target gene, 11.5 µL DEPC water, 11.5 µL SYBR ® green PCR Master Mix (Part# 4367659, Applied Biosystems), and 5 µL of the diluted cDNA. The plate was sealed with parafilm and centrifuged at 1000 rpm for 30 seconds to make sure all liquid was at the bottom of the wells. The RT-PCR amplification was performed as follows: 3 minute step at 95°C, 40 cycles with a 10s step at 95°C, 45s at 65°C, and 20s at 78°C. The expression level of each gene was calculated using the $-2^{\Delta\Delta C_T}$ method described elsewhere by Livak and Schmittgen [97].

3.13. Electrophoresis Verification of PCR Results

A 2% agarose gel was prepared using 2g of agarose dissolved in 500 mL TAE buffer to verify PCR results. The gel was poured into a mold and allowed to solidify. 5 μL of the PCR product was combined with 0.5 μL 10X Blue Juice™ Loading Buffer dye (Cat# 10816-015, Invitrogen) on parafilm, then pipetted in separate wells of the agarose gel. For the β-actin standard, 0.5 μL 100bp DNA ladder was mixed into the 0.5 μL dye mixture, combined with 5 μL TAE buffer on the parafilm, and pipetted into separate wells of the agarose gel. After running the gel at 110V DC for 50 minutes, it was incubated in ethidium bromide (EtBr) solution (50 μL EtBr and 500 mL TAE buffer) for 20 minutes in the dark and imaged using UV light.

3.14. Biochemical Assays

3.14.1. Papain Digestion

Biochemical assays were conducted on hMSC laden MO and PEGDA hydrogels for samples collected on day 0 and 17. The wet weights of each sample were measured then lyophilized for 24 hours and their dry weights reweighed. They were digested with 1 mL of papainase solution (125 μg/ml papain) (Cat# LS003126, Worthington Biochemical Corp.), 10 mM $_{L}$-cysteine (Cat# 7352, Sigma Aldrich), 100 mM phosphate, and 10 mM EDTA, pH 6.3, crushed with a pestle in a 1.5 mL tube, and stored for 16 hours at 60^{o}C [(98)]. A 1 mL solution was isolated for DNA, GAG spectrophotometric assay, and collagen assay. The samples were stored at -20^{o}C until biochemical assays were conducted.

3.14.2. DNA Assay

DNA content was measured using a Quanti-iT™ PicoGreen® dsDNA Kit (Invitrogen) according to the manufacturer's protocol. Samples and standards were made

into biological duplicates and analyzed as technical duplicates due to a limited cell number. The kit included Quanti-iT^{TM} PicoGreen® dsDNA reagent, nucleic acid-free and DNase-free 20X TE buffer (200 mM Tris-HCL, 20 mM EDTA, pH 7.5), and Lambda DNA standard (100 μg/mL in TE).

3.14.2.1. Assay Buffer Preparation

The 20X TE buffer was diluted with diethylpyrocarbonate (DEPC)-treated water, making it sterile, distilled DNase-free water, to make a 1X TE buffer. 1X TE was used to dilute the PicoGreen® reagent, the DNA samples, and the assay as described below.

3.14.2.2. Reagent Preparation

The PicoGreen® reagent was prepared on the day of the experiment by diluting 200 fold with 1X TE buffer and wrapped in foil to protect from photobleaching.

3.14.2.3. DNA Standard Curve

The lambda DNA stock solution was diluted to 2 μg/mL followed by another dilution to 300 ng/mL in 1X TE buffer. A five point standard was made by diluting the DNA solution from 250 ng/mL to 0.25 pg/mL solution with 1X TE buffer and 1000 μL PicoGreen ® reagent as triplicates in a 96 well plate with the volumes shown in Table 2.

Table 2. Standard Curve Concentrations and Volumes [99].

Final DNA Concentration in PicoGreen®	Volume of 1X TE (µL)	Volume of 250 ng/mL DNA Stock (µL)
250 ng/mL Standard	0	350
25 ng/mL Standard	315	35
2.5 ng/mL Standard	346.5	3.5
.25 pg/mL Standard	349.7	0.35
Blank Standard	350	0

The plate was mixed thoroughly, covered with foil, incubated for 5 minutes at room temperature, and measured using a plate reader. The fluorescence value of the blank reagent was subtracted from all fluorescence values to correct the data. A standard curve of fluorescence versus DNA concentration was generated.

3.14.2.4. DNA Quantification

Using the Quant-iT PicoGreen dsDNA Kit, 1 µL of papain digested DNA solution was diluted 1:100 with 99 µL 1X TE and pipetted into a 96-well plate. Quant-iT™ PicoGreen® reagent was added to each well at a 1:2 ratio (100 µL of 1:100 diluted digested DNA solution to 100 µL of PicoGreen® reagent diluted in half) (overall dilution 1:200). The fluorescence was measured with a plate reader and the concentrations determined using the standard curve. The DNA concentration values were normalized to the dry weight measured after lypholizing the samples.

3.14.3. GAG Assay

Glycosaminoglycan (GAG) content was measured using a dimethylmethylene blue (DMMB) spectrophotometric assay at 525 nm. Chondroitin sulfate (CS), a sulfated GAG with a chain of alternating sugars, was used to create a standard curve using known concentrations of CS as before. CS is a major structural component of articular cartilage and provides compressive resistance in addition to joint mobility and flexibility [100].

3.14.3.1. Chondroitin Sulfate Standard Preparation

Stock CS 50 mg/ml was prepared by dissolving 0.105 g cysteine in 60 mL PBE and dissolving 50 mg CS in 1 mL PBE/cysteine solution. 100 µL of the CS stock solution was added to 49.9 mL PBE/cysteine to create a 100 µg/mL CS working solution.

3.14.3.2. PBE Buffer Preparation

7.1 g Na_2HPO_4 (143 g/mol) and 1.86 g Na_2EDTA (372 g/mol) were mixed with 500 mL of deionized H_2O (dH_2O). Concentrated HCL was used to adjust the pH to 6.5 and the buffer was stored at 4°C.

3.14.3.3. Dimethylmethylene Blue (DMMB) Dye Preparation

To prepare a 6 µg/mL stock solution in glycine/NaCl with pH 3.0, 3.04 g of glycine, 2.37 g NaCl, and 95 mL of 0.1M HCl were mixed with 905 mL of dH_2O. Using a magnetic stirrer, 16mg of DMMB were dissolved into this solution. The pH was adjusted to 3 using concentrated HCl with an absorbance (OD_{525}) between 0.31-0.34. The dye was stored in the dark at 4°C.

3.13.3.4. GAG Standard Curve: The spectrophotometer blank was set to 525 nm versus DMMB. Standard curves were generated using 0 to 100 µL of the CS working solution diluted with 100 to 50 µL dH_2O and 2.5 ml DMMB dye as shown in Table 3. 100 µL of

each 1 mL papain digested sample was mixed with 2.5 ml of DMMB and the light intensity read with a spectrophotometer. The standard curve was used to determine the CS (GAG) content for each sample.

Table 3. Chondroitin Sulfate Standard Curve Volumes. Blank reading and various CS concentrations used to build a linear standard curve.

Standards	µL CS working sol. (100 µg CS/mL)	Amount of CS (µg)	µL dH_2O	mL DMMB dye (16 µg/mL)
1	0	0	100	2.5
2	5	0.5	95	2.5
3	10	1	90	2.5
4	20	2	80	2.5
5	30	3	70	2.5
6	40	4	60	2.5
7	50	5	50	2.5

3.14.4. Collagen Assay

The collagen content was determined for MO (20%) hydrogels by measuring the hydroxyproline content of the samples after performing acid hydrolysis and reacting with *p*-dimethylaminobenzlhedhyde and chloramine-T as described below.

3.14.4.1. Reagent preparation

pH 6 buffer was prepared first to make Chloramine T solution. 250 mL of dH_2O was placed in a 500 mL beaker with a magnetic stir bar. While stirring, 17 g NaOH, 25 g citric acid monohydrate, 60 g sodium acetate trihydrate, and 6 mL of glacial acetic acid were added to the beaker. After fully dissolved, the solution was transferred to a 500 mL volumetric flask and filled to 500 mL. 150 mL isopropanol and 100 mL dH_2O were mixed into the solution. Concentrated HCl was used to adjust the pH to 6, after which 5 drops of toluene were added.

Hydroxyproline (OH-pro) standard stock solution (100 μg/mL) was prepared by placing 10 mg hydroxyproline with dH_2O in a 100 mL volumetric flask. Twenty-four hours before the assay, a Chloramine T solution (15.67 mg/mL) was prepared by dissolving 0.705 g Chloramine T in 40 mL of the prepared pH 6 buffer and 5 mL isopropanol. The solution was thoroughly mixed and stored at room temperature for 24 hours. p-Dimethylaminobenzaldehyde (pDAB) solution was prepared 24 hours before the assay in a 100 mL brown bottle. 7.5 g of pDAB were thoroughly dissolved in 30 mL isopropanol with a stir bar. The bottle was placed on ice and stirred in the fume hood. 13 mL of 60% perchloric acid were slowly added to the solution.

3.14.4.2. Sample Preparation and Assay

100 μL of each digested sample was hydrolyzed in 900 μL 6N HCl heated to 115^{o}C in an oven for 18 to 24 hours before the assay was performed.

3.14.4.3. Hydroxyproline Standard Curve

The hydroxyproline standard stock solution was diluted to 10 μg/mL. It was further diluted ten times with dH_2O to prepare a hydroxyproline standard curve with 7, 6, 5, 4, 3, 2, 0.5, 0.25, and 0 μg hydroxyproline. The hydrolyzed samples were allowed to cool to room temperature then titrated in 15 mL tubes to adjust the pH to 7. Two drops of methyl red were added to each sample and 2.5 M NaOH was added until the pink color disappeared. Two to three drops of 0.5M HCl were added to decrease the pH and return to pink, after which a few drops of 0.5M NaOH were added to obtain a yellowish color. Deionized water was added to fill to 15 mL. One mL was collected and placed in a new tube. 500 μL Chloramine T solution (15.67 mg/mL) was added to each standard curve and sample tube, vortexed, and incubated at room temperature for 20 minutes. 500 μL

pDAB was added to each tube while vortexing and incubated at 60^{o}C for 30 minutes in a water bath. The solutions were cooled and the absorbance measured with a spectrophotometer at 550 nm. The standard tubes were measured first to generate an standard calibration curved of absorbance versus concentration of OH-Pro (dilution factor = 150) to measure the collagen content of the samples.

3.15. Histology and Immunostaining

One sample from day 7 and 17 of control A and experimental group 1A was collected for histology. One sample of day 7 control B, and experimental B and C along with one sample from each day 17 experimental group and control B and C were collected. These samples were fixed on the day of collection in a 1.5 mL tube in 4% paraformaldehyde and stored overnight at 4^{o}C. The paraformaldehyde was replaced with 20% sucrose by immersing in PBS overnight at 4^{o}C. The sucrose solution was replaced with a 1:1 solution of 20% sucrose and optimal cutting temperature compound (OCT)(Tissue-Tek, Sakura Finetek, Tokyo) for 2 hours at room temperature. The sample was embedded with OCT in a cryo-mold. Isopentene was poured into a metal container which was placed within a dewar flask (Pope Scientific Inc) with liquid nitrogen to slow down the freezing rate of the mold placed inside the isopentene. The samples were stored at -80^{o}C until cryosectioned into 10 to 20 μm sections, transferred to silanized glass slides, and stored at -20^{o}C until all samples were stained together.

3.15.1. Hemotoxylin and Eosin Staining

The glass slides were rehydrated in distilled water for 5 to 10 minutes at room temperature. They were stained in hematoxylin to label basophilic structures indigo for 15 minutes, then washed under running tap water for 15 minutes. The slides were placed

in distilled water, followed by 80% ethanol for 2 minutes, and counterstained in eosin solution to label the eosinophilic structures pink. They were dehydrated twice for two minutes each time in 95% ethanol, 100% ethanol, and finally in xylene. Each slide was mounted with 150 μL Permount Mounting medium and covered with a coverslip. The slides were dried overnight and imaged using bright field microscopy then stored in -20^{o}C.

3.15.2. Safranin O Staining

Safranin O staining was used to label glycosaminoglycan (GAG), which is a major component of cartilage. Cryosectioned slides were rehydrated in distilled water for 5-10 minutes at room temperature. Staining jars were prepared as shown in Table 4 below with 100 mL in each jar. 0.1% Safranin O was composed of 0.1 g Safranin-O dissolved in 100 mL distilled water.

Table 4. Safranin O Staining Protocol

Jar	Contents
1	0.1% Safranin-O in distilled water
2	Distilled water
3	Distilled water
4	Distilled water
5	95% Ethanol
6	95% Ethanol
7	100% Ethanol
8	100% Ethanol
9	100% Ethanol
10	Xylene
11	Xylene
12	Xylene

The slides were placed in each jar in order for 5 minutes each as listed above. Each slide was mounted with 150 μL Permount Mounting medium after the last xylene

wash and covered with a coverslip. The mounting medium was allowed to dry overnight, imaged using a brightfield microscope, and stored at -20^{o}C.

3.15.3. Collagen Type II

Anti-Type II collagen immunofluorescent staining was performed on cryosectioned tissues. The slides were allowed to warm up to room temperature. A circle was drawn around each sample section using a PAP pen, a very strong hydrophobic agent that keeps reagents from falling off the slide. The slides were rehydrated at room temperature in PBS for 5-10 minutes. The Blocking Buffer (3% bovine serum albumin (BSA) and 0.1% Triton-X 100 (Invitrogen) in 1X PBS) was prepared for the blocking step and to dilute antibodies. Nonspecific binding was blocked by incubating the slides in 75 µL Blocking Buffer for 1 hour in a humidified chamber at room temperature. The type II collagen polyclonal antibody (70R-CR008X, Fitzgerald, MA) was diluted in Blocking Buffer at a 1:300 ratio. The sections were incubated for one hour with 50 µL each in the chamber at the same settings, drained and washed three times by immersing in 1X PBS at room temperature for 10 minutes each The secondary antibody (Alexa Fluor® 488 goat anti-rabbit IgG, Invitrogen) was diluted at 1:250 in Blocking Buffer. The sections were incubated in the dark with 50 µL of the diluted secondary antibody under the same conditions. They were drained and washed as before and covered to prevent photobleaching, and then mounted with 4',6-diamidino-2-phenylindole (DAPI) mounting medium, covered with a coverslip, and sealed with clear nail polish. The slides were imaged using fluorescent microscopy and stored at -20^{o}C in the dark.

3.16. Statistical Analysis:

Data were expressed as mean ± standard deviation (stdev). Analysis of variance (ANOVA) and a Tukey test was used to determine the statistical significance ($P < 0.05$) for all groups using GraphPad Prism.

IV. Results

4.1. Characterization of Oligomers

4.1.1. MO Oligomer

NMR results confirmed acrylate groups successfully conjugated to the ends of the MO oligomer showing peaks between 5.8-6.5 ppm (Figure 3). The degree of substitution (DS) of acrylate groups was calculated as 25% based on the relative peak integrals at 4.1 ppm and 5.8-6.5 ppm.

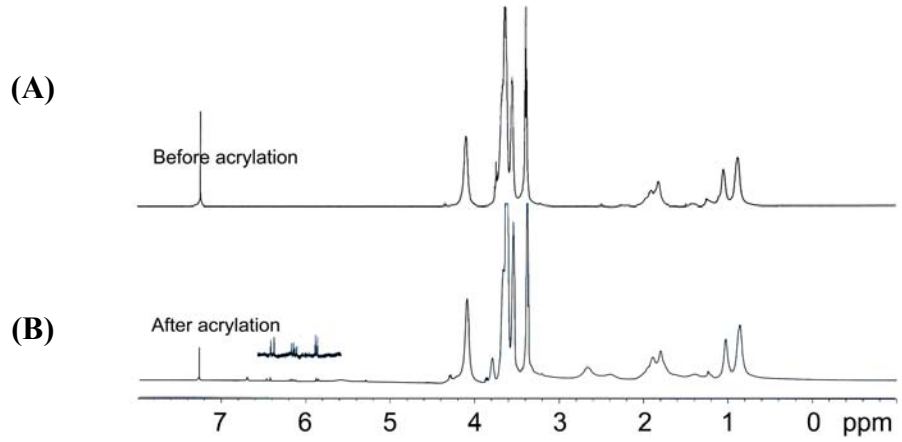

Figure 3. ^{1}H NMR spectra of oligo(OEGMA-*co*-MEO$_2$MA) before and after acrylation. (A) ^{1}H NMR results of oligo(OEGMA-co-MEO$_2$MA): ^{1}HNMR (400MHz, $CDCl_3$, δ, ppm): 0.7-1.5 (-$CH_2C(CH_3)$COO-), 1.6-2.0 (-$CH_2C(CH_3)$COO-), 3.4 (-OCH_3), 3.5-3.8 (-OCH_2CH_2O-), 4.1 (-$COOCH_2CH_2O$-). **(B)** ^{1}H NMR results of oligo(OEGMA-co-MEO$_2$MA) diacrylate: ^{1}HNMR (400MHz, $CDCl_3$, δ, ppm): 0.7-1.5 (-$CH_2C(CH_3)$COO-), 1.6-2.0 (-$CH_2C(CH_3)$COO-), 3.4 (-OCH_3), 3.5-3.8 (-OCH_2CH_2O-), 4.1 (-$COOCH_2CH_2O$-), 5.8-6.5 (CH_2=CHCOO-).

4.1.2. PEGDA Oligomer

The ^{1}H NMR results for PEGDA 3400 and PEGDA 10000 are shown in Figure 4. The DS of acrylate groups was determined by the relative integrals of peaks

corresponding to acrylate groups and ethylene oxide repeating units. The DS of acrylate groups in PEGDA 3400 and PEGDA 10000 was 85.4% and 43.3%, respectively.

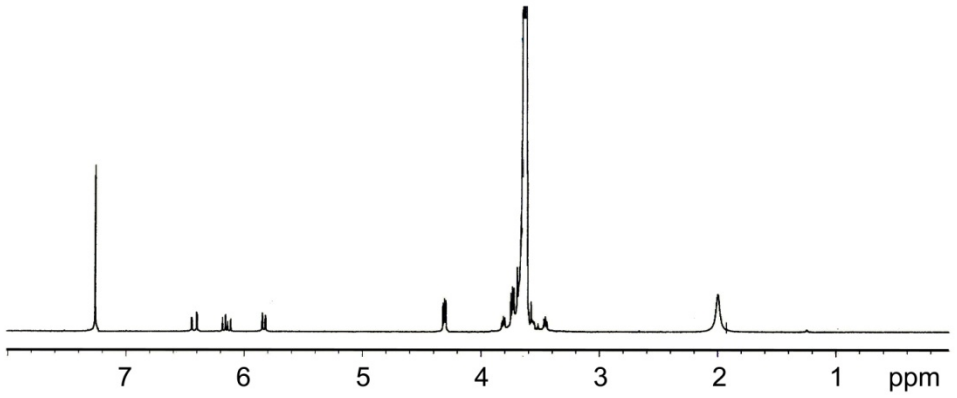

Figure 4. ^{1}H NMR spectra of PEGDA 3400. PEGDA 3400 and PEGDA 10000 have similar ^{1}H NMR spectra. ^{1}HNMR (400MHz, $CDCl_3$, δ, ppm): 3.65 (-OCH_2CH_2O-), 4.3 (-COOCH_2CH_2O-), 5.8-6.5 (CH_2=CHCOO-).

4.2. Device Characterization

Temperature precision and rate of heating were inversely proportional. Initial device settings used PID values of 90; 1.29; 0, which provided better precision but slow heating rates (precision $T_{set} \pm 1.5^{o}C$). To increase the period of oscillation, the PID values were changed to 15; 15; 10. Decreasing the P value allowed delivering a greater bandwidth of power to the heating block, increasing the integral value enhanced the rate of power delivery, and increasing the derivative value improved the system's ability to respond to temperature changes. As such, the second settings allowed larger fluctuations about the set point $T \pm 2^{o}C$.

4.3. 3D Hydrogel Deformation and Volume Strains Induced by Temperature Oscillations

Three dimensional hydrogel movement was tracked using multiple-particle tracking to locate the time-dependent x, y, and z coordinates of each centroid. The volume strains (***V***) were calculated by tracking the intensity-weighted center of mass of each bead. The z location was calculated for all image sets by analyzing the radius of ring diffraction and correlating with the calibration curve (Figure A37).

4.3.1. Cell Temperature Oscillation Treatment

For MO (10% PEG) (Exp. 1A and 2A), the heating device was set to oscillate between 35 and 36^{o}C with PID settings of 90, 1.29, and 0. Overshoot and undershoot was minimal (± 1.5), but the temperature oscillation frequency averaged 0.0024 Hz (about 8.52 ± 1.09 cycles/hr) (Figure A36). The frequency was sacrificed for temperature precision to prevent cell exposure to extreme temperatures (above 37^{o}C and below 30^{o}C). However, this frequency was too slow as indicated by PCR, biochemical, and histology assays below, since it was just above the low frequency range (0.001 Hz), which has been shown to inhibit proteoglycan synthesis as described before [(34)]. MO (10%) Exp. 2A constructs became progressively softer over cultivation time and began to fall apart on day 11, indicating the crosslinking density was too low for these experiments under three hours of oscillation.

The image analysis results for acellular MO (10%) indicated the overall volume strains produced between this temperature range were ~4%, but at a low frequency (Figure 7). As such, the heating device was optimized for faster heating within a larger temperature range. For MO (20% PEG) and PEGDA (15% PEG) hydrogels, the device

PID settings were set to 15 ;15 ;10 to with temperature set points changed to 33 and 35^{o}C to increase the percentage of strain imposed on the constructs. The gels were exposed to one hour daily temperature oscillations between 31 and 37^{o}C due to over and undershoot, at a frequency of 0.0033 Hz (12.0 ± 5.7 cycles/hr) which was 1.4 times greater than the previous PID settings (Figure A36). The large standard deviation was due to a failing TE module, which was replaced midway through the experiments and caused delayed cooling rates. Heating data from day 17 was not included due to a failing thermistor, which produced faulty readings from overuse and introduced larger oscillations than desired, decreasing the heating frequency on day 17. Chondrogenic differentiation of hMSCs induced by temperature-induced mechanical strains was characterized by swelling ratio measurement (equilibrium and non-equilibrium), non-equilibrium volume strains, PCR, biochemical assays, and histology analysis.

4.3.2. Volume Strain and Fluorescent Particle Tracking Results

Acellular MO (10% 3400 PEGDA) hydrogels encapsulated with 1% FPs imaged at 0, 1, 2, 5, and 10 minutes each at 27, 30, 33, 34, 35, 36, and 37^{o}C indicated the gels responded within 120 s (See Figure 5 for a sample volume strain graph at 27^{o}C). The gels averaged 285 ± 22s to equilibrate below 30^{o}C and 2.25 min from 30 to 37^{o}C. This required the heating device induce temperature oscillations with a period between 120s and 285s to allow the gel to respond to the change in temperature but prevent them from equilibrating to maintain dynamic volume strains.

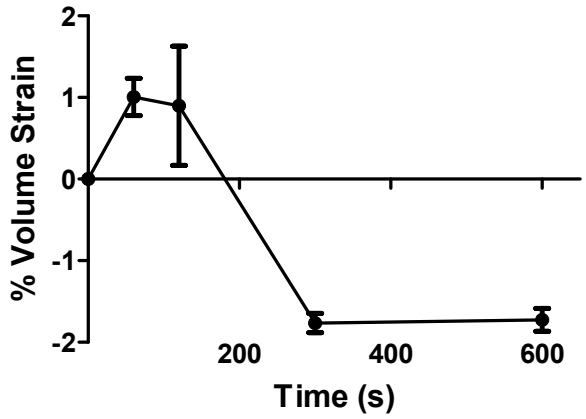

Figure 5. Acellular MO (10% PEG) Response to Temperature. Gel was equilibrated at 27.24 ± 0.18°C for 10 minutes and then imaged at 0, 1, 2, 5, and 10 minutes.

4.4. Hydrogel Characterization

4.4.1. Acellular MO (10% PEG) Equilibrium Swelling Ratios

Equilibrium swelling ratios for acellular MO (10% Mw PEG: 3400) hydrogels were measured with five samples incubated at various temperatures for 24 hours as indicated in Figure 6. MO (10% PEG) gels induced a 25% change in SR between 4 to 45°C.

The swelling ratio at 35°C and 36°C set points produced a 1.14 % change in swelling ratio (Figure 6). However, accounting for heating device precision, which at PID 90;1.29;1 allowed a temperature fluctuation ±1.5°C about the set points, the actual temperature range became 33.5 and 37.5°C inducing a 3.87% strain using linear interpolation. While the target strain magnitude was 5%, the delayed device response required this small heating range to increase oscillation frequency. As such, the device setpoints were set to 35 and 36°C, while sacrificing applied strain. FP tracking was not

used to verify these results since it was not feasible to maintain a constant temperature for 24 hours.

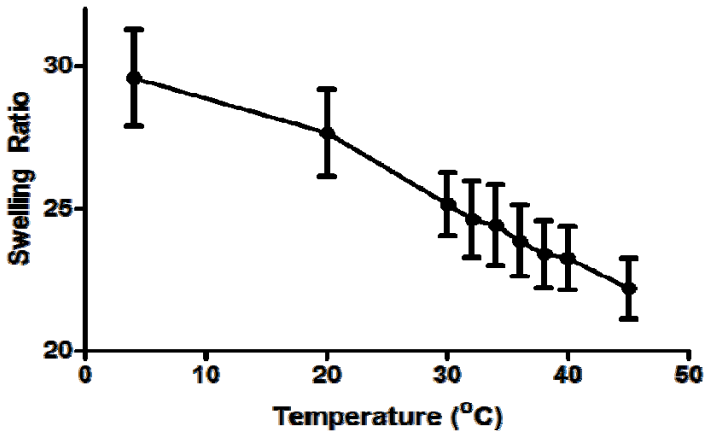

A

Figure 6. Acellular MO (10% PEG) Hydrogel Swelling Ratios. Gels kept at equilibrium for 24 hours at each temperature point before measuring wet weights. LCST ~22°C.

4.4.2. Acellular MO (10% PEG) Volume Strain Characterization

The first and last 560s of a 1 hour temperature oscillation experiment were imaged to test the time dependency of volume strains independent of crosslinking density. A repeated measures ANOVA with a Tukey post test was conducted for each time point between 12 particles tracked for the first (Figure 7A) and last cycles (Figure 7B) of the hour, indicating volume strain did not vary significantly ($P < 0.05$) over the course of 1 hour. As such, it was assumed images captured during the first cycles of the hour were representative of the entire 1 hour cycle.

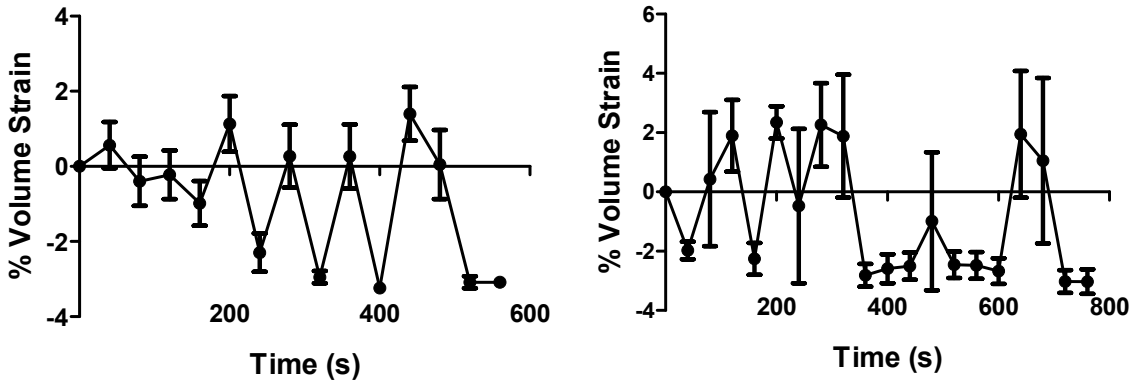

(A) **(B)**

Figure 7. Acellular MO (10% PEG) Volume Strains. (A) First 560s of 1 hr temperature oscillations between 32.8 and 34.4^{o}C at a frequency of 0.01 Hz. Values were graphed as average ± stdev. **(B)** Last 560s of 1 Hr oscillations. Temperature oscillated between 32.6 and 34.3^{o}C at a frequency of 0.0125 Hz. Values were graphed as average ± stdev.

4.4.3 Cellularized MO (10% PEG) Volume Strain Characterization

Cellularized MO (10% PEG) hydrogels (Figure 8) exhibited a decrease in volume strain frequency in comparison to acellular constructs (Figure 7). Both day 16 and 38 constructs indicated a significant decrease in frequency of gel oscillations, which was independent of applied temperature oscillation frequency since day 38 and acellular gels were oscillated at the same frequencies. However, day 16 exhibited a 3 fold faster gel oscillation frequency even though the period of temperature oscillations was 6 times longer. These results indicate cell matrix penetrated throughout the gel matrix over time since it caused a delay in mechanical oscillations. Interestingly, even though the temperature frequency of day 16 was lower than day 38, the magnitude of strain was greater for day 38, implying the higher temperature frequency created an additive volume strain that culminated as peaks followed by periods of collapse. However, beginning day

14 the frequency decreased to 4.5 cyles/hr (0.0013 Hz), causing downregulation of chondrogenic differentiation shown on day 17 qRT PCR and biochemical analysis.

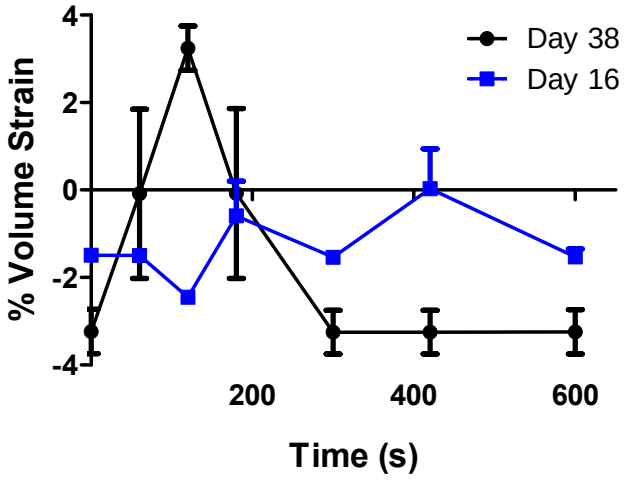

(A)

Figure 8. Cellular MO (10% PEG) Volume Strains. **(A)** Temperature oscillated between 34.5 to 37°C at a frequency of 0.002 Hz on day 16, and between 35.7 and 36.4°C at 0.012 Hz for day 38. Both day 16 and 38 oscillating profiles shown above repeated over a 1 hour duration. See Table A6 for the number of average heating oscillations per day.

4.5. Crosslinking Density Optimization

MO and PEGDA gels with various crosslinking densities were equilibrated at 37°C for 24 hours and their swelling ratios were measured (Figure 9). The two most similar swelling ratios were those for MO (20% PEG) at 11.18 ± 0.30% and 15% PEGDA at 10.75 ± 0.80%. These two gels were used for cell encapsulation (Exp. groups B-D). Acellular and cellular constructs were shown together for comparison in Figure 9, indicating swelling ratios were enhanced by 18.7% for MO (20%) and 26.3% for PEGDA (15% PEG) gels after cell culture for 17 days. This implies cell presence and matrix

deposition increased swelling profiles by absorbing more aqueous solution. However, this data alone cannot be used to imply the gel elasticity increased.

4.5.1. Acellular Constructs Swelling Ratios

Cell free MO (20% PEG) and MO (15% PEG) hydrogels exhibited similar swelling ratio profiles in non-equilibrium conditions; however, the magnitude of SR was lower for 20% crosslinking density (Figure 10). This correlated with the non-equilibrium swelling ratios measured using particle tracking where MO (15%) showed larger volume strains than MO (20%), but no significant difference in volume strain frequency (Figure 11). Within the 32 and 37.8^{o}C temperature range applied to MO (15%) the expected change in swelling ratios was 3.16 A/U (19.4% change) (Figure 10), which correlated with a 5.22% change in volume strain (Figure 11). For MO (20 %), the SR measured between 31.6 and 36.2^{o}C was 2.25 A/U (16.7% change) or 3.8% volume strain. Both these results consistently indicated a 3:5 ratio between SR and volume strain.

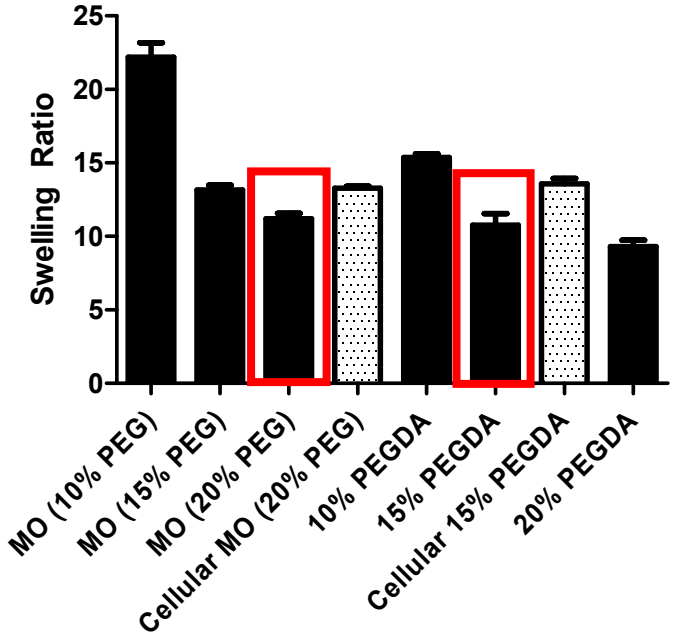

Figure 9. Swelling Ratios of Various Crosslinked Densities of MEO_2MA-OEGMA and PEGDA Gels. Hydrogels were equilibrated at 37°C for 24 hours. Swelling ratios for cellular constructs were measured on day 17 of culture.

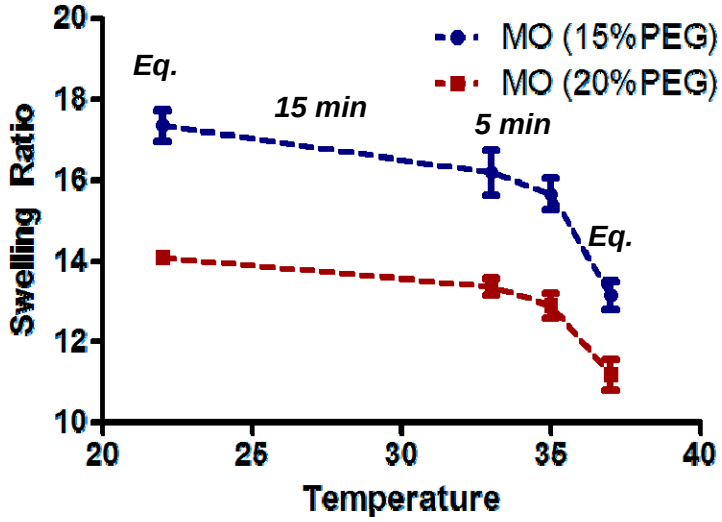

Figure 10. Non-Equilibrium Swelling Ratios for Acellular MO (15 and 20% PEG) at 33 and 35°C. Wet weights were measured after gels were equilibrated at 23°C for 24hrs, then immersed at 33°C for 15 mins, followed by 5 mins at 35°C, and finally 24 hrs at 37°C. Both exhibit an LCST ~ 35°C.

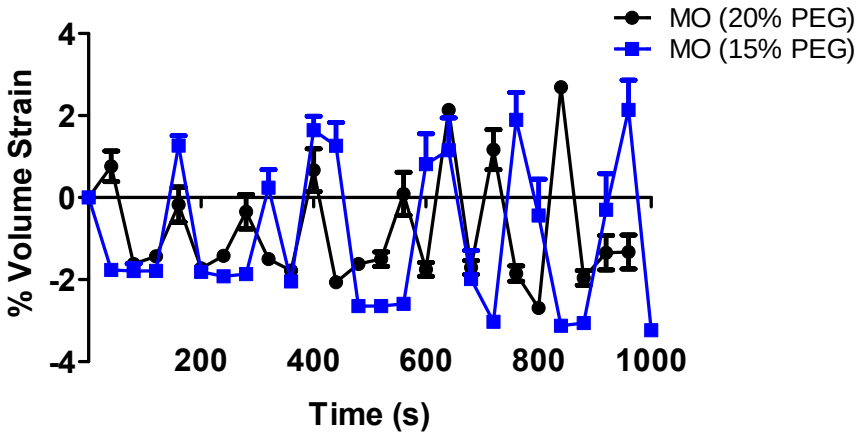

Figure 11. Non-equilibrium Acellular MO Hydrogel Volume Strain. MO (15% PEG) gels were oscillated between 32 and 37.8°C at a frequency of 0.006 Hz, while MO (20% PEG) gels were oscillated between 31.6 and 36.2°C at a frequency of 0.0045 Hz.

4.5.2. Cellularized MO (20% PEG) and PEGDA (15% PEG)

4.5.2.1. Non-Equilibrium Volume Strains

Day 7 cellular MO (20 % PEG) gels indicated smaller volume strains than acellular gels. However, cellularized gels indicated an increase in compressive volume strain magnitude over time at 0.012 Hz (Figure 12). PEGDA (15% PEG) hydrogels did respond to temperature although they have been characterized as thermoresponsive gels. Unlike the MO gel, its compressive volume strain magnitude decreased over time occurring as sudden peaks lasting about 80 s, with delayed peaks every 133.3 ±122.2 s. The large standard deviation was attributed to recovery time of the PEGDA hydrogel after bulk deformation due to crosslinking density and chemical composition.

Day 17 cell encapsulated hydrogels indicated an almost linear decrease in swelling ratio of 15.4% for MO (20% PEG) versus a mere 3.8% drop in swelling ratio for PEGDA (15% PEG) (Figure 13). The swelling ratios for cellular MO (20% PEG)

hydrogels increased in comparison to acellular gels by 10.66 ± 5.93%, with the greatest change exhibited at 37°C.

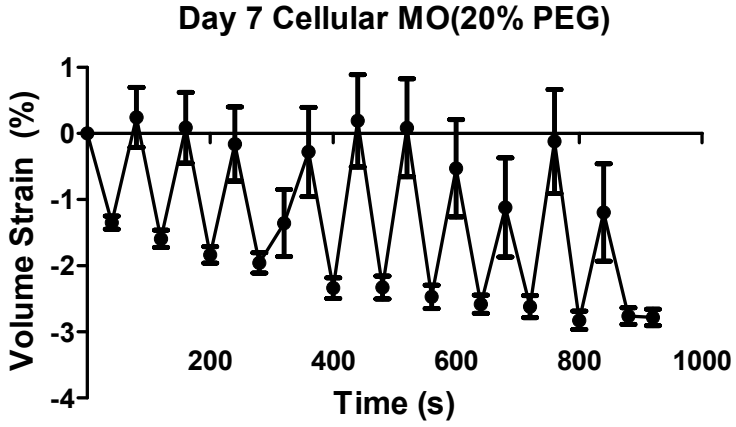

(A)

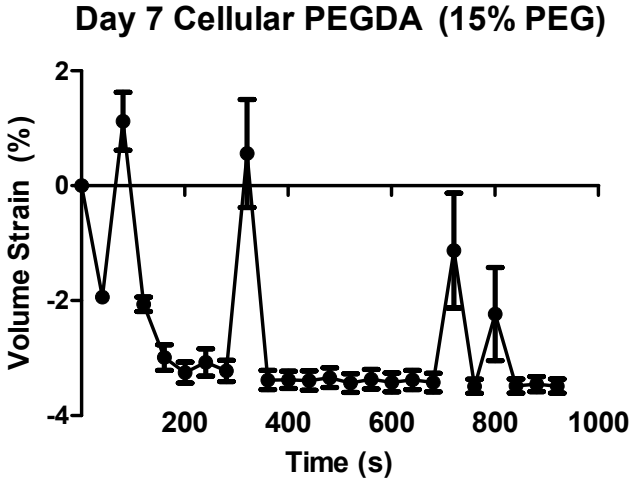

(B)

Figure 12. Day 7 Volume Strain for Cellular Hydrogels Using FP Tracking. (A) MO (20% PEG) oscillations between 32.2 and 35.8°C at 0.010 Hz. **(B)** PEGDA (15% PEG) oscillations between 32.3 and 36.5°C at 0.011 Hz.

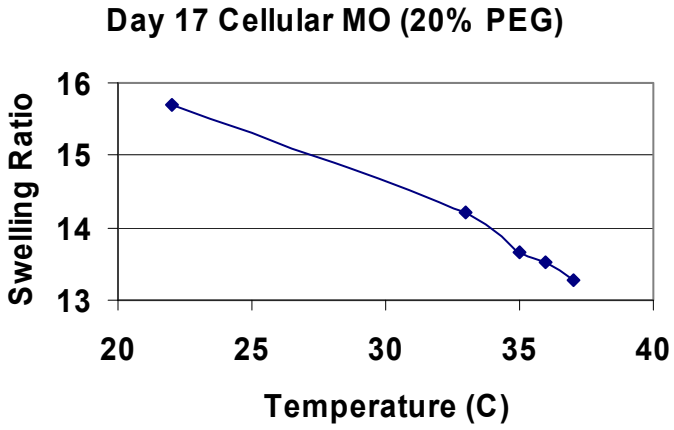

(A)

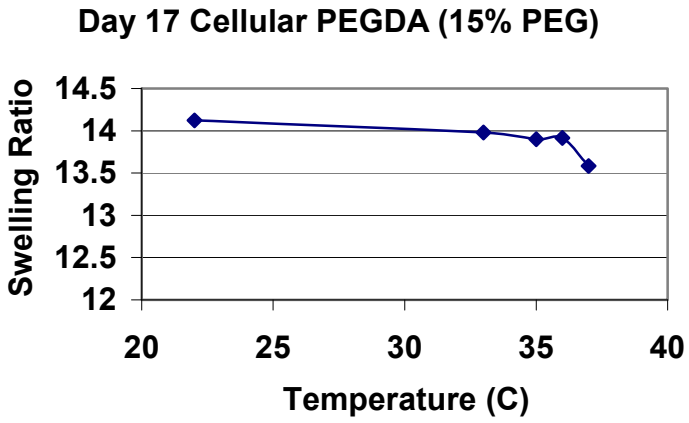

(B)

Figure 13. Equilibrium Swelling Ratios for Cellular Hydrogels. (A) MO (20% PEG) and **(B)** PEGDA (15% PEG) Hydrogels. Day 17 gels were equilibrated at each temperature for 24 hours. See Table A7 for the average number of heating oscillations per day.

4.5.2.2. Equilibrium Volume Strains and Hydrogel Response Time

Constant temperature volume strain measurements on day 17 indicated MO (20% PEG) and PEGDA (15%) exhibited gel responses even under small temperature oscillations (Figure 14). A graph of the z coordinates indicated the response time for MO

(20% PEG) was 120s and 80s for PEGDA (15% PEG), introducing a 17% change in z position for MO and 9.5% for PEGDA (15%). Due to heating effects from the fluorescent arc lamp, the temperature changed at a rate of 0.0016 ± 0.002 ^{o}C/s over 840s. A possible explanation for this gel sensitivity is photobleaching effects which would have caused a sudden drop in particle intensity that would have been reported as a change in volume strain. This data confirmed PEGDA was thermoresponsive, although its volume strain response was not as large as MO (20%).

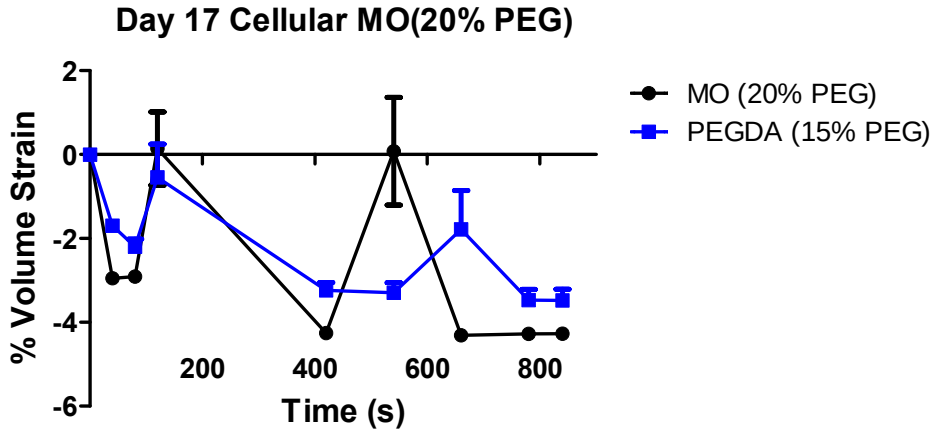

Figure 14. Constant Temperature Volume Strain of Day 17 Cellularized Hydrogels. MO (20% PEG) gels were held at 27.0 ± 0.68^{o}C while PEG (15% PEG) gels were held at 27.9 ± 0.59^{o}C.

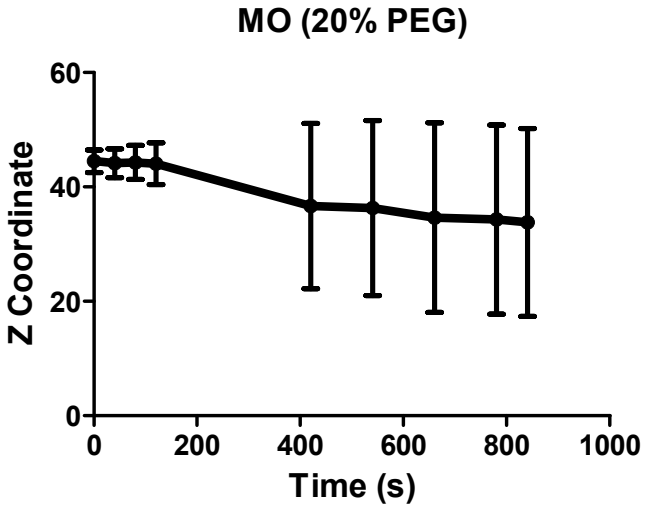

(A)

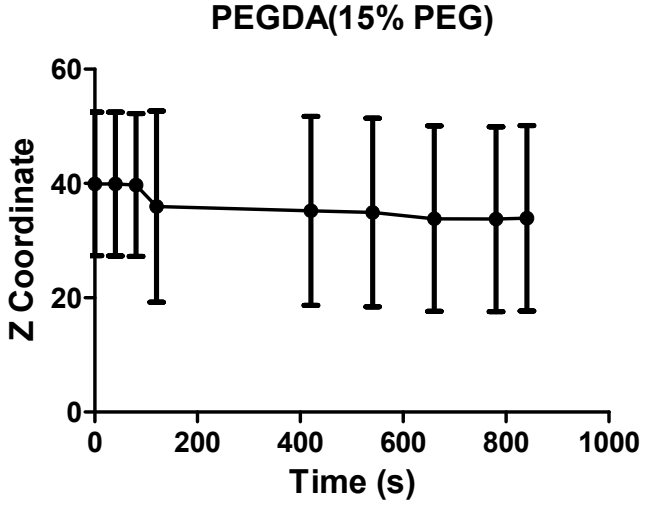

(B)

Figure 15. Averaged Z Position for Day 17 Cellular Gels.
(A) MO (20% PEG). **(B)** PEGDA (15% PEG).

At non-constant temperature conditions, day 17 cellular MO (20%) showed no volume strain oscillations, but instead decreased in magnitude towards a collapsed equilibrium state (-3.6 ± 0.51% volume strain) within 600s (Figure 16A). PEGDA (15%) showed gel collapse followed by small volume fluctuations with a delayed peak swelling at 520s (Figure 16B). These results indicated cell matrix deposition caused a severe

decrease in gel response causing the gel to reach equilibrium within 800 s of temperature oscillations. However, at an almost constant temperature (Figure 14), the day 17 gels showed a better response rate and magnitude, implying the frequency of temperature oscillations in Figure 16 was too fast to allow the gels to respond.

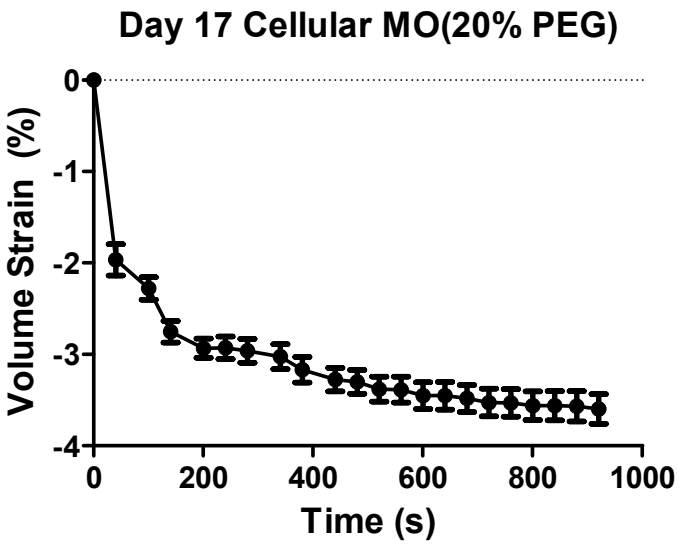

(A)

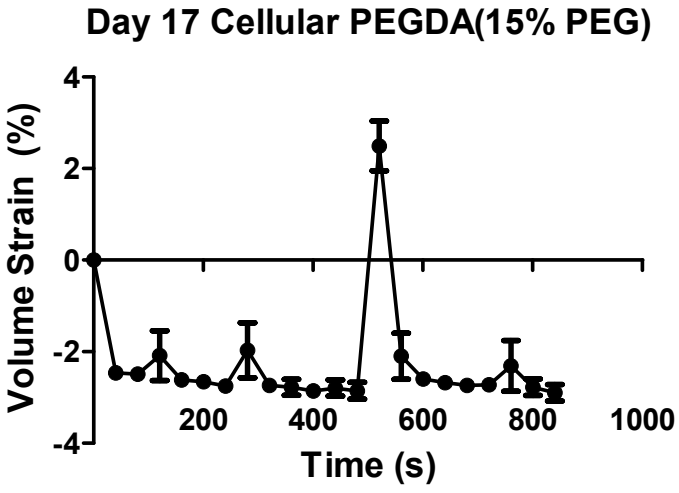

(B)

Figure 16. Day 17 Cellular Hydrogels. (A) MO (20%) was exposed to 33.89 ± 1.17°C at 0.011 Hz. **(B)** PEG (15%) was exposed to 33.88 ± 0.98°C at 0.011 Hz.

4.6. Effect of Temperature Oscillations on Chondrogenic Differentiation

4.6.1. Cell Viability

The Live-dead assay conducted on 72 hour control A and experimental group 2A (3 hour oscillations) (Figure 17) showed high cell viability (live cells stained with Calcein AM, dead cells stained with EthD-1) and almost no difference between the two groups. This indicated 3 hours of temperature oscillations did not induce cell death after 72 hours of *in vitro* cultivation. Experimental group 1A was not tested since it was the less extreme temperature treatment (1 hour oscillations), so its effect on cell viability was less severe than experimental group 2A.

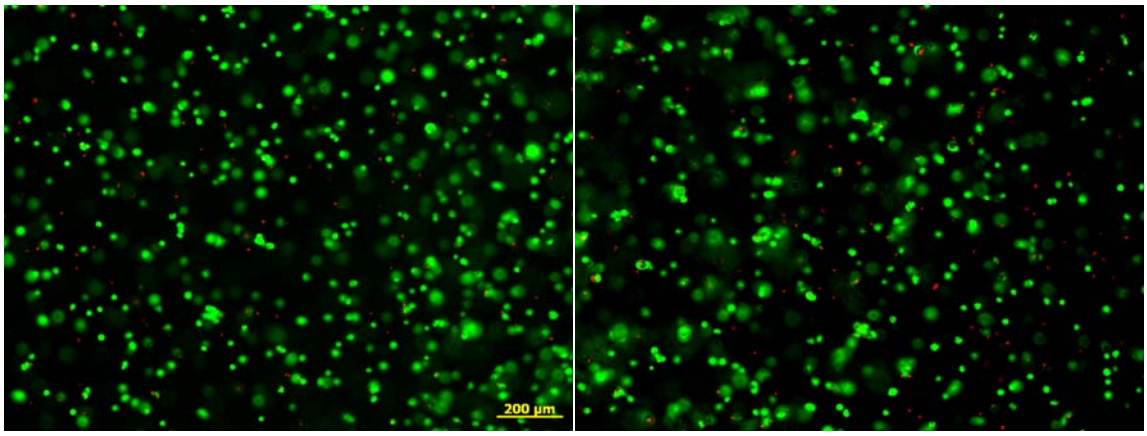

(A) **(B)**

Figure 17. Live-dead Assay of hMSC-laden MO (10% PEG) Hydrogels After 72 Hours of *in vitro* Culture. (**A**) Constructs without oscillation (Control A). (**B**) Constructs with oscillation (Exp. 2A).

4.6.2. Real Time Quantitative PCR and Biochemical Assay

Realtime qPCR results of MO (10% PEG) (Figure 18) were normalized to day 7 control values. The results indicated the largest upregulation of aggrecan content occurred on day 10 with a 2.85 ± 0.07 fold increase for Exp. 1A and 1.9 ± 0.5 fold for Exp. 2A. Day 17 showed downregulation, in part due to a decrease in the frequency of

temperature oscillations. Control values for type II collagen content steadily increased over time reaching a peak on day 17 (6.9 ± 0.6). Biochemical analysis did not show any significant increase in DNA or GAG content throughout the study for control A and Exp. 1A & 2A (Figure 19). This was most likely attributed to cell loss due to low crosslinking density, which allowed approximately 20% of encapsulated cells to diffuse out during day 0 through 3 in addition to mechanical disruption observed on day 11.

These results correlated with the decrease in mechanical strains over time as indicated by the volume strain results. Overall, Exp. 1A consistently expressed greater chondrogenic differentiation on day 10 than Exp. 2A, indicating that 1 hour of temperature oscillations was optimum for an MO hydrogel with crosslinking density of 10% PEG for that duration. Since greater chondrogenic expression was desired without gel breakage, the crosslinking density was increased in the following experimental groups to increase the magnitude of compressive strains on encapsulated cells.

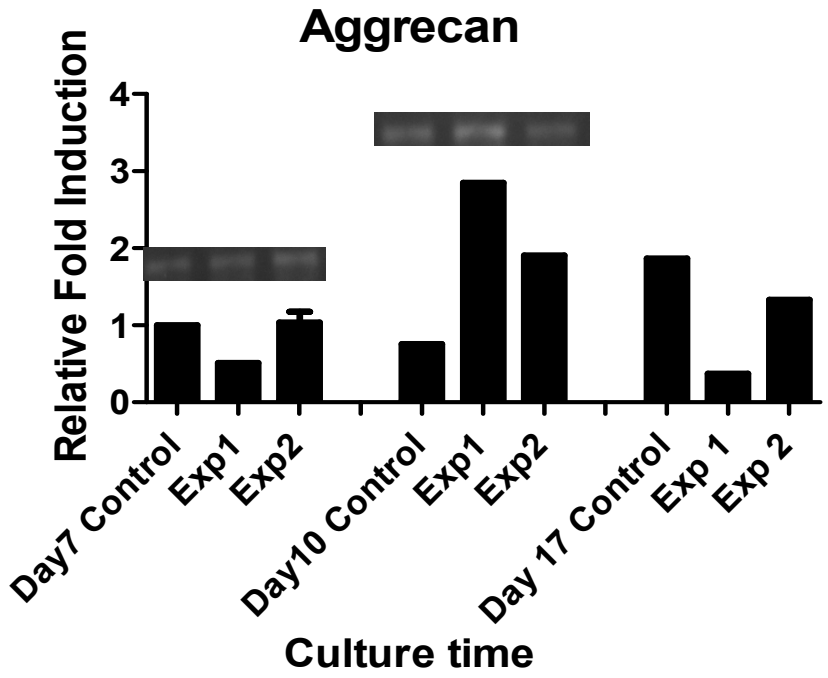

(A)

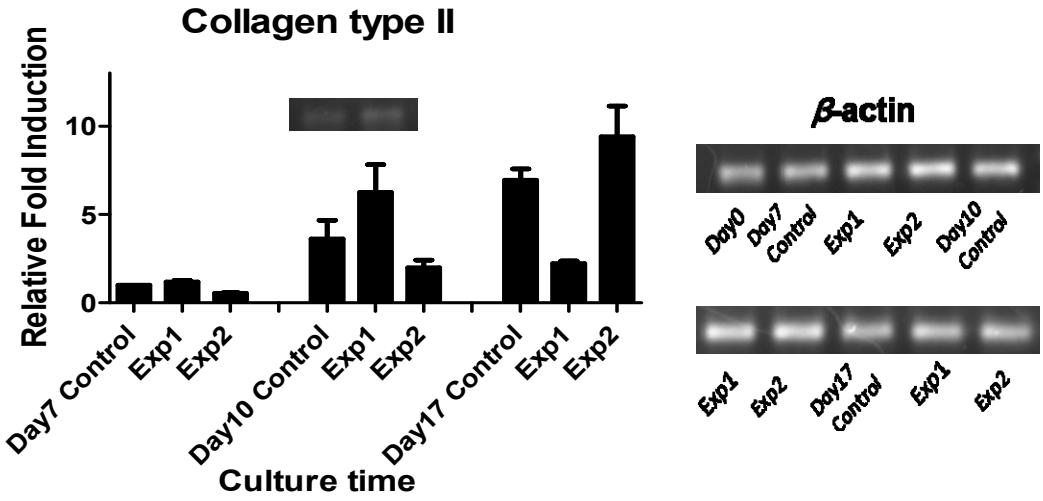

(B) **(C)**

Figure 18. Gene Expression for MO (10% PEG). qPCR results for Control A and Exp. 1A & 2A. **(A)** Aggrecan content. **(B)** Type II collagen content. **(C)** β-actin standard electrophoresis gel. All values were normalized to day 7 control.

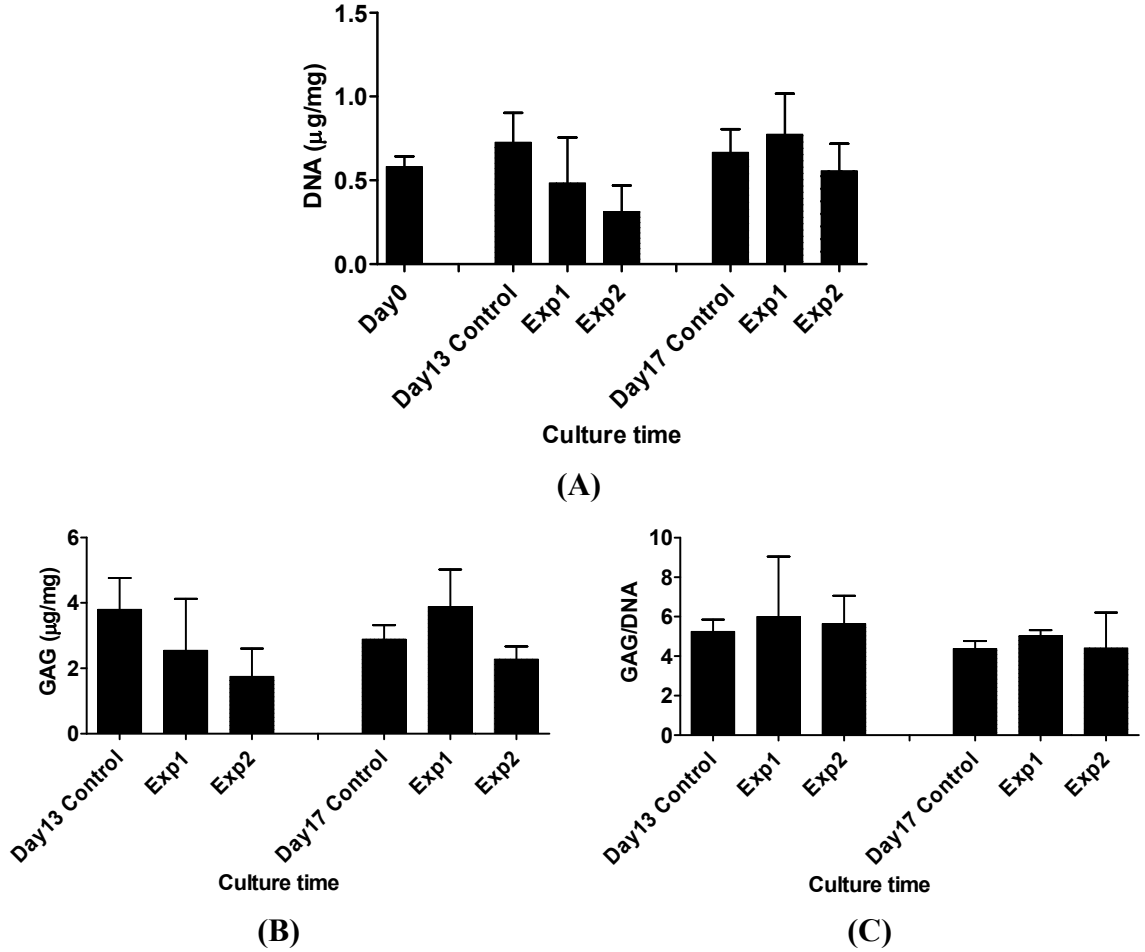

Figure 19. Biochemical Assay for MO (10% PEG). (A) DNA content. **(B)** GAG content. **(C)** GAG/DNA content.

Realtime qPCR results for Exp. B (MO (20% PEG), +TGFβ-1, no oscillation) was the only group indicating a significant change over culture time reaching a maximum aggrecan content on day 17 (10.24 ± 1.43) (Figure 20 A). Conversely, type I collagen content was greatest on day 0 for MO (20% PEG) control and exhibited a sudden drop on day 3 (Figure 20A). Again, Exp. B increased overtime reaching a maximum of 0.59 ± 0.05 on day 17. Except day 17 Exp. B and C, all other experimental groups did not change significantly ($P<0.05$) past day 3. Collagen type II content reached its highest content on day 17 Exp.B at 0.96 ± 0.32.and 1.53 ± 0.56 fold increase for Exp. C (TGFβ-1,

with oscillations). Oscillations showed a significant difference ($P<0.05$) between Exp. C and B causing a 1.6 fold upregulation of collagen type II, indicating temperature fluctuations did enhance chondrogenic differentiation. Meanwhile, collagen type II content for Exp. B and C showed a significant difference ($P < 0.05$) from control groups without TGFβ-1 starting day 10, indicating the growth factor did affect collagen type II upregulation but was time dependent. Sox 9 content upregulation reached its highest amount on day 17 for control B (no TGFβ-1) and Exp. B (TGFβ-1) both with no oscillation. Temperature oscillations actually caused a decrease in Sox 9 expression over time as evidenced by Exp.C.

Biochemical results could not be used to verify qPCR results since the data for day 0 and day 17 (Figure 21) showed no significant difference between GAG/DNA content for all control and experimental groups. However, there was a significant difference ($P<0.05$) between Day 17 control C and Exp. C, and Exp. B and Exp. C, indicating a slight increase in GAG content with oscillations but these differences disappeared when calculating GAG/DNA. Overall, the data suggests the longer the culture time, the more upregulation expressed for aggrecan, type II collagen, and Sox 9, with Exp. B having the most consistent increase. However, the trend from one gene to the next was not consistent, indicating there was an underlying variable causing this phenomenon including crosslinking density and compressive strains induced.

During the experiment, MO (20%) and PEGDA constructs were tightly fit into the PCR tubes because they were initially at a swollen state ($27^{o}C$) with larger volumes than MO (10%) due to their higher crosslinking density. During temperature oscillations (31 to $37^{o}C$), even though the compressive strains caused sustained gel collapse they were

still tightly fit. Initially, the gels responded to temperature, but since they were compressed by the PCR walls, they underwent static compressive strains, rather than dynamic. Collagen assay results were inconclusive for MO (20%) and were not reported. This was consistent with the low gene expression observed past day 0.

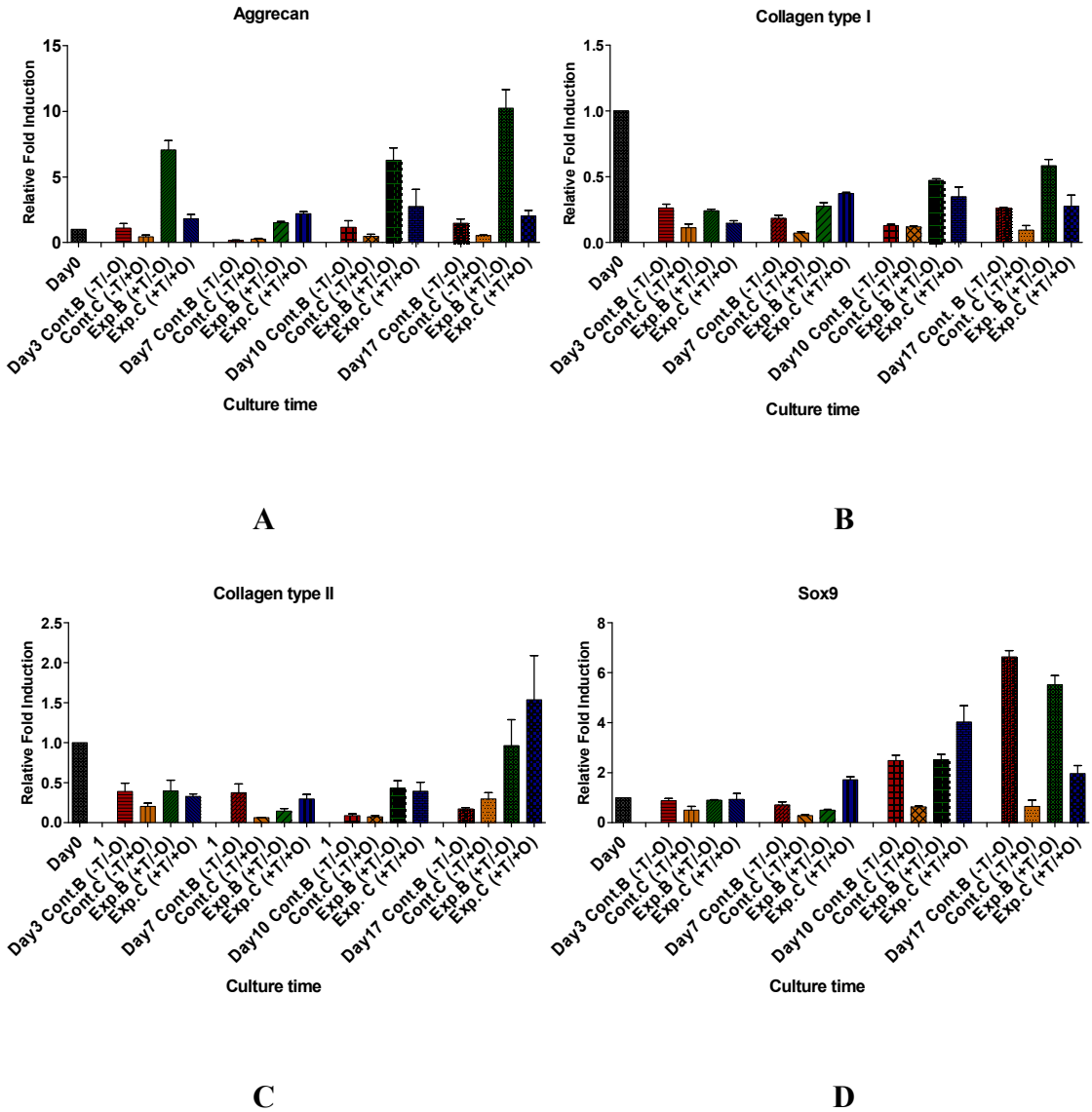

Figure 20. Gene Expression for MO (20% PEG). qPCR results for **(A)** Aggrecan, **(B)** Collagen type I, **(C)** Collagen Type II, **(D)** Sox 9. All values were normalized to day 0 control B.

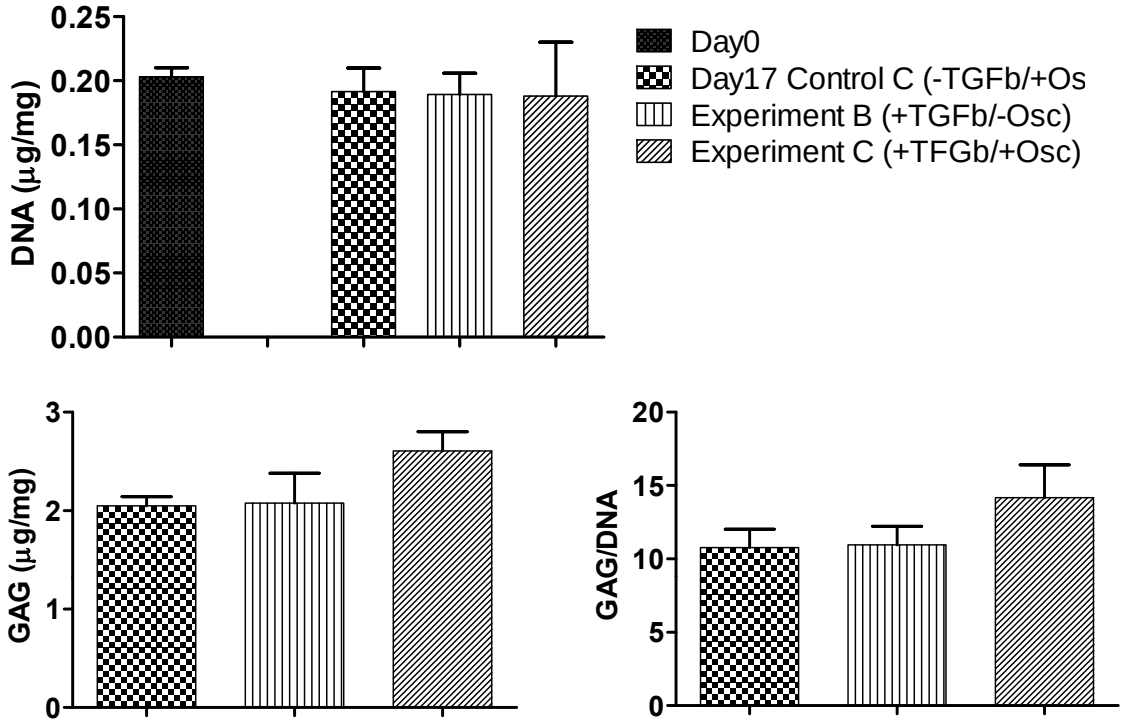

Figure 21. Biochemical Results for MO (20% PEG) Hydrogel. Day 0 and 17 samples were measured.

The results for PEGDA (15% PEG) showed greater upregulation of chondrogenic markers than MO (10 and 20% PEG). Aggrecan and Sox 9 content had similar profiles, with maximum values on day 7 for Exp. D (TGFβ-1 with oscillations), while collagen type I peaked on day 17 for Exp. D. However, the biochemical assay did not show any significant difference between groups ($P < 0.05$) making it difficult to correlate with qPCR results. PEGDA exhibited periodic volume strains showing the best results in the presence of temperature oscillations and TGFβ-1 with increasing time. This suggests temperature itself enhanced hMSC chondrogenic differentiation in addition to periodic volume strains.

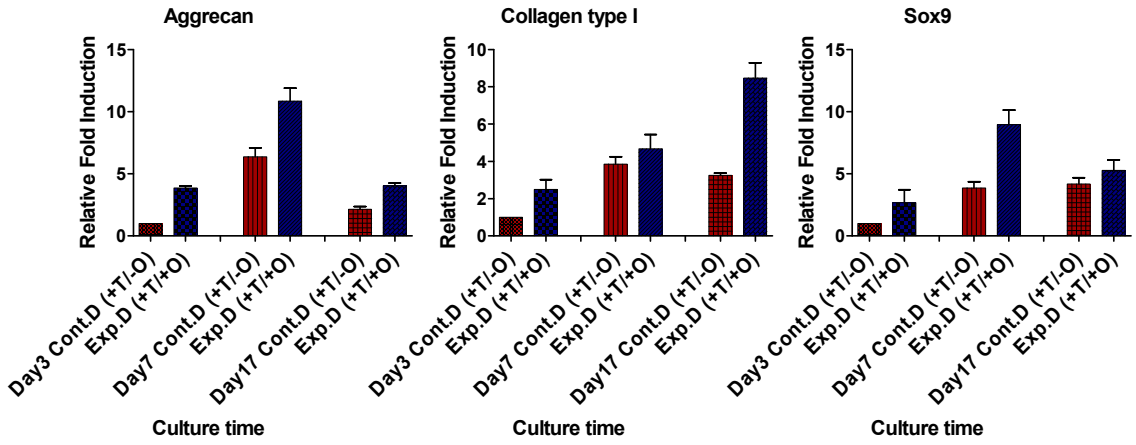

(A) **(B)** **(C)**

Figure 22. Gene Expression for PEGDA (15% PEG). qPCR results for **(A)** Aggrecan, **(B)** Collagen type I, and **(C)** Sox 9. All values were normalized to day 3 control D.

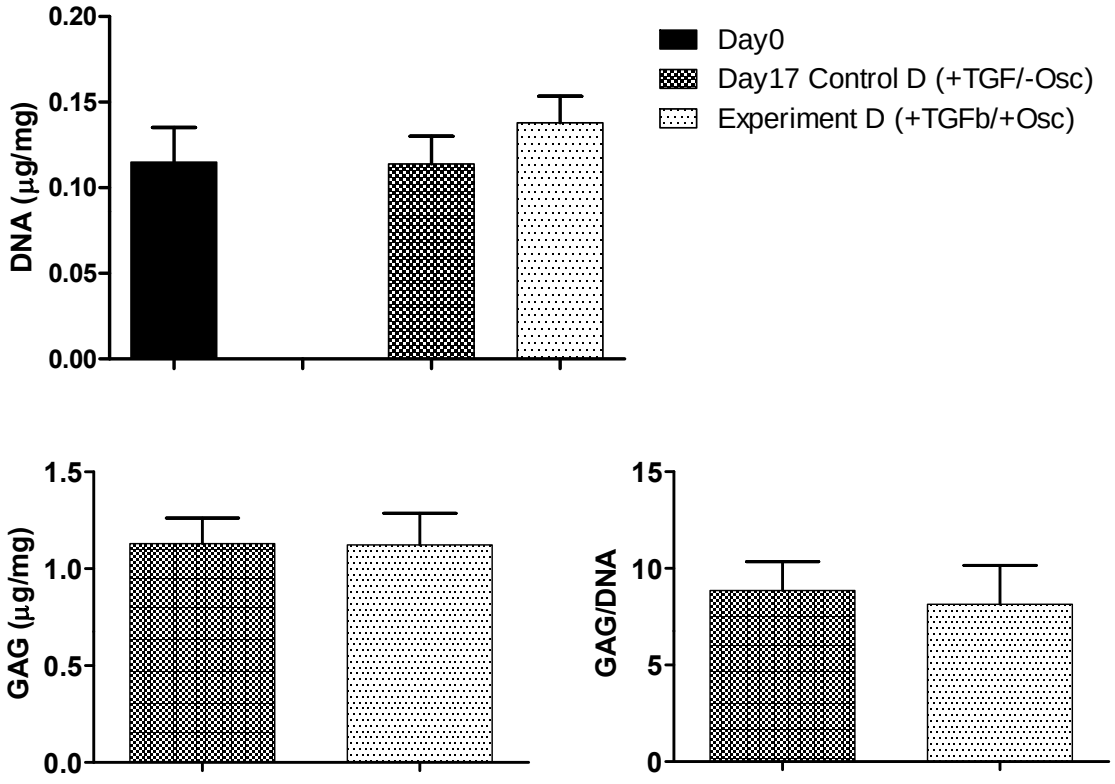

Figure 23. Biochemical Results for PEGDA (15% PEG) Hydrogels.

4.6.3. Histology and Immunostaining

Safranin O staining for MO (10% PEG) day 7 and 17 indicated greater proteoglycan content for 1 hour heating than control A (Figure 24 A & B). Exp. 2A (3 hour) samples were not available for staining due to gel disruption. This data supported the use of 1 hour oscillations for the remaining control and experimental groups, even though the crosslinking density was increased to prevent the gel from breaking apart over time.

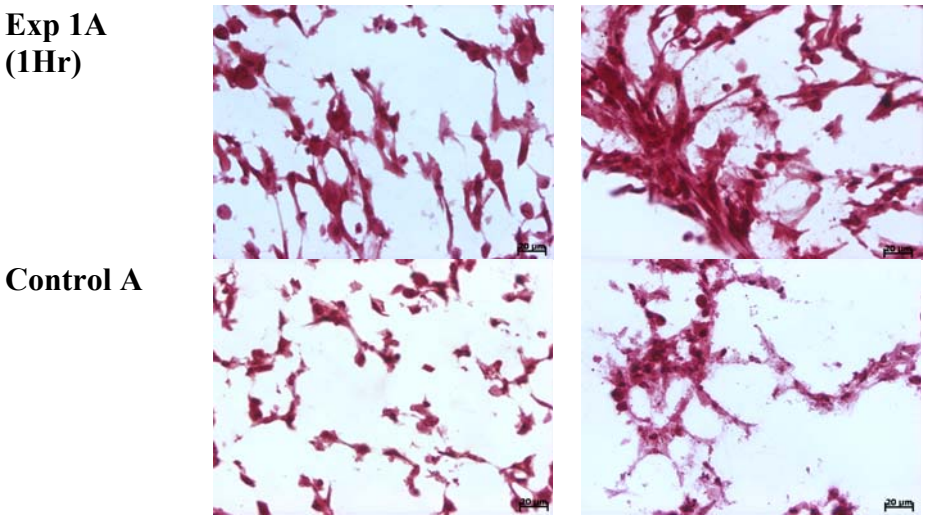

Figure 24. Safranin O staining for MO (10% PEG) constructs. Labels GAG content for **(A)** day 7 and **(B)** day 17. (20 μm scale bar for all images).

H&E staining for MO (20% PEG) showed little to no eosinophilic structures (Figure 25 and Figure 27), which is supported by low GAG composition (Figure 21). However, cell concentration and GAG content was greater for Day 7 control B (-TGFβ-1, with oscillation) than other day 7 samples (Figure 25). Day 17 MO (20% PEG) slides indicated constructs exposed to temperature oscillations had increased cell concentrations and GAG content independent of the presence of TGFβ-1 (Figure 27). Day 17 MO (20%)

histology slides indicated higher cell concentration and GAG content from day 7 constructs. PEGDA (15% PEG) indicated lower cell concentration due to larger pores, but higher GAG content (Figure 26).

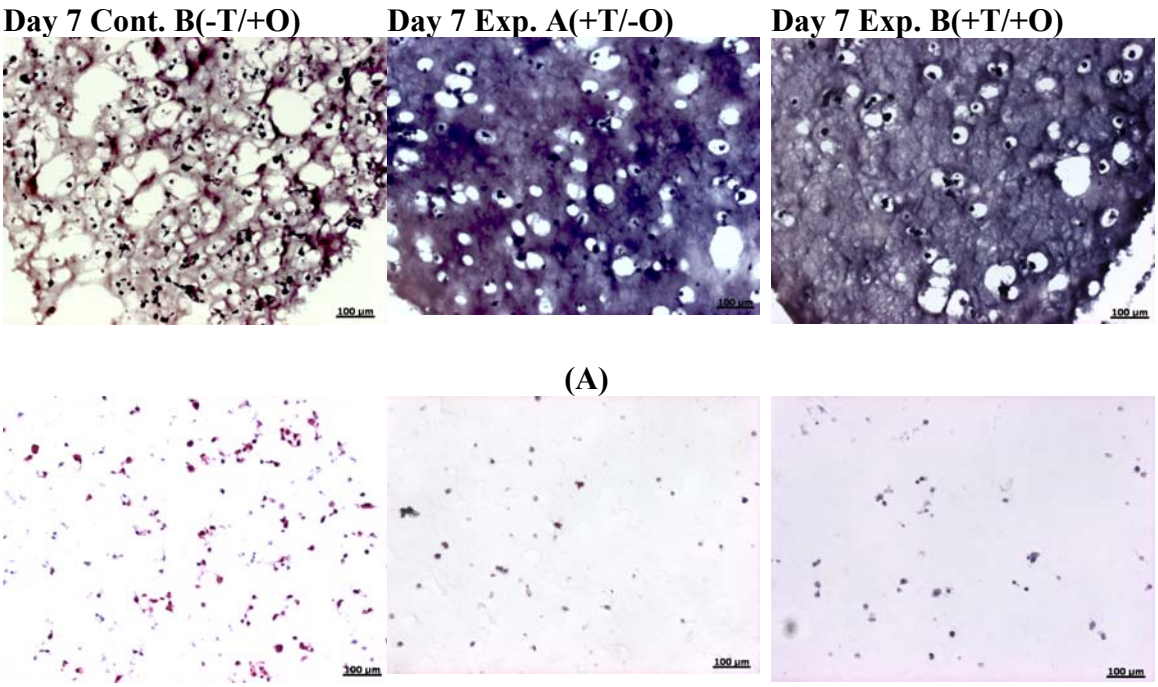

Figure 25. Histology and Immunostaining for Day 7 MO (20% PEG) Hydrogels. (A) H&E and **(B)** Safranin O staining at 10x magnification.

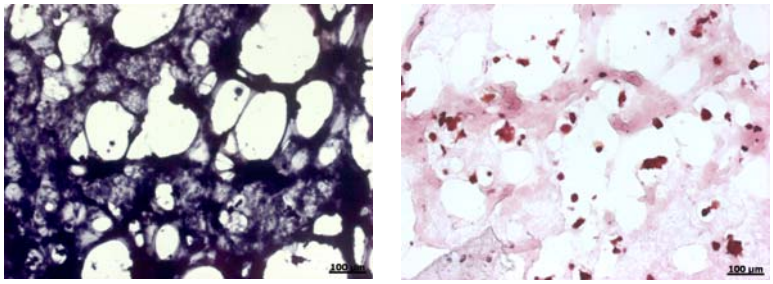

Figure 26. Histology and Immunostaining for Day 17 PEGDA (15% PEG). (**A**) H&E and (**B**) Safranin O Staining at 10x of Exp. D (TGFβ-1 with oscillations).

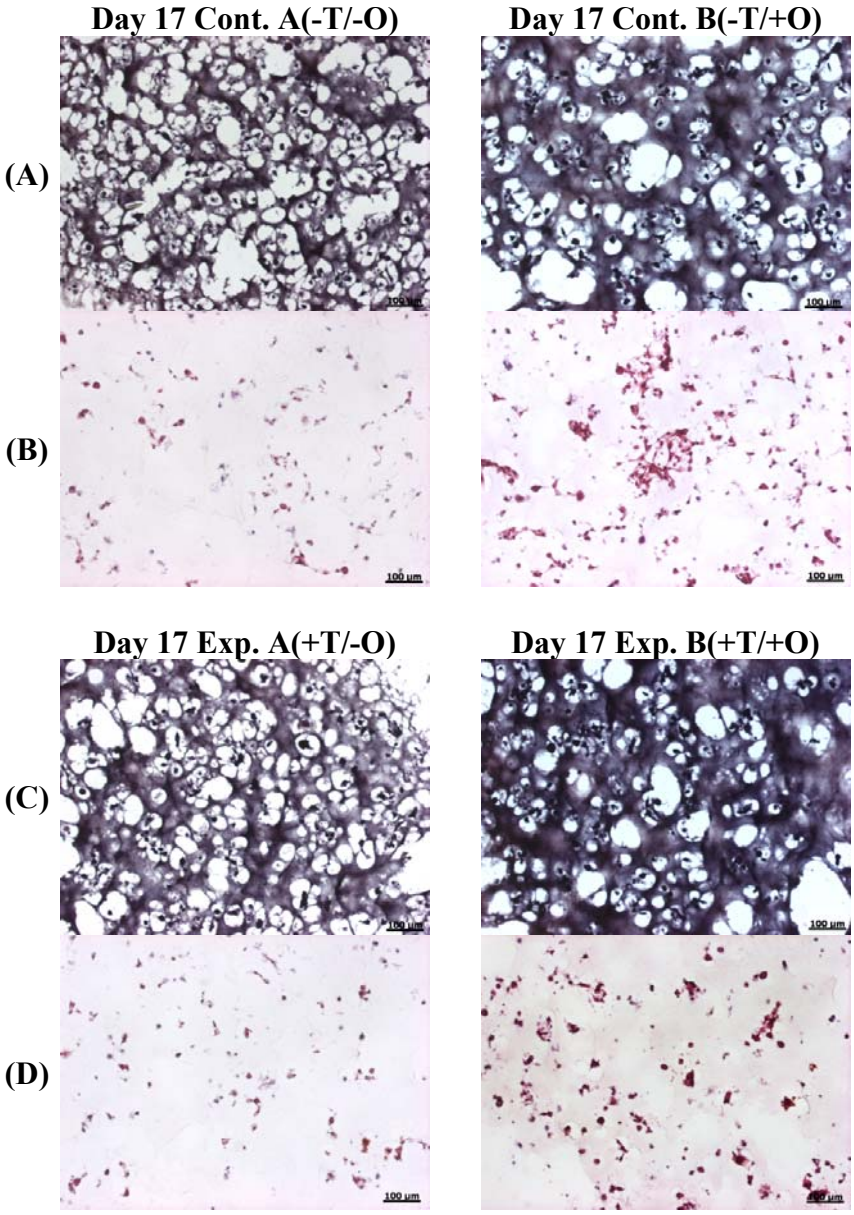

Figure 27. Histology and Immunostaining for Day 17 MO (20% PEG) Hydrogels. (A) & **(C)** H&E and **(B)** & **(D)** Safranin O Staining at 10x.

V. Discussion

Chondrocytes in developing articular cartilage are known to respond to mechanical compression, which induces extracellular matrix remodeling, and alters their composition, structure, and biomechanical properties. Understanding the effects of mechanical stimuli on cartilage development is essential to developing functional cartilage tissue. This study investigated the effect of temperature-induced cyclic mechanical compression using approximately 5% strain at various frequencies on the chondrogenic differentiation of hMSCs. A novel heating device for manipulating temperature profiles of thermoresponsive, hydrogel based bioreactors was developed to produce mechanical strains on encapsulated hMSCs. PID settings of 15;15;10 resulted in the fastest temperature oscillation profiles with 2^{o}C overshoot at a frequency of 0.0033 Hz.

Hydrogel crosslinking densities were optimized in addition to fluorescent particle tracking techniques to track realtime deformation of hydrogels. Volume strains quantified using MATLAB developed software indicated all cellular hydrogels showed a decreased response time to temperature stimuli, with cellular MO (20% PEG) exhibiting the fastest volume strain frequencies. A correlation ratio of 3:5 between swelling ratios and volume strain was characterized for the first time, which allowed verification of hydrogel deformation.

The qPCR results confirmed that static compression in conjunction with high crosslinking density caused a down regulation of chondrogenic differentiation, which was apparent in the inconsistencies in gene expression for all gels. However, a lower crosslinking density as used in MO (10%) dictated lower oscillation durations to prevent

gel deterioration. As such, one hour of mechanical stimulation was the optimal duration found for inducing an upregulation in aggrecan, collagen type I and II, Sox 9, and GAG content.

The live-dead analysis of oscillating cell-laden MO (10% PEG) hydrogels showed that most of the encapsulated cells were viable and found no significant difference in cell viability in comparison with their non-oscillating counterparts. They exhibited increased chondrogenic gene expression on day 10 under the presence of TGFβ-1 and one hour of temperature oscillations between 34.5 and 37^{o}C. Interestingly, even though MO (10% PEG) gels under three hours of stimulation were mechanically compromised, they expressed greater collagen type II content on day 17 than the one hour group.

MO (20% PEG) hydrogels showed an overall upregulation of aggrecan, type II collagen, and Sox 9 in the presence of TGFβ-1 but no oscillations. MO (20%) gels showed a downregulation of aggrecan and collagen type I when oscillations were applied between 31 and 37^{o}C at 0.0033 Hz with or without TGFβ-1, whereas TGFβ-1 alone enhanced both of these gene expressions.

Realtime PCR results and volume strain analysis showed 15% PEGDA hydrogels did respond to the same temperature oscillations as MO (20%), and overall provided a better cell scaffold than all other gels for chondrogenic differentiation in the presence of TGFβ-1 and temperature oscillations. PEGDA gels showed oscillations enhanced aggrecan and Sox 9 content up through day 7 then dropped, while it increased collagen type I over time. The only consistency between MO (20%) and PEGDA (15%) gels was an increase of collagen type I and Sox 9 on day 7, and a downregulation of Sox 9 on day 17 in the presence of oscillations. Low GAG content in MO (10%) indicated the matrix

either diffused out, or the gels did not undergo sufficient mechanical strains. For MO (20% PEG) and PEGDA (15% PEG), poor GAG accumulation confirmed that the application of static mechanical strains instead of dynamic ones in addition to high crosslinking density inhibited cell matrix deposition.

It has been shown that hydrogels can support chondrogenic differentiation in the presence of TGFβ-1 and mechanical stimulation [32]. However, because all qPCR control values for MO (20%) and PEGDA over time showed very low expression of all genes and poor proliferation (low DNA content), the hydrogels themselves need to be optimized by lowering their crosslinking densities to around 10% for MO and PEGDA while enhancing oscillation regimes. The inconsistencies in gene expression indicated underlying variables contributed to the differences observed. In addition to crosslinking density and static mechanical strains, the uncontrolled frequency of compressive strains could have played a major factor. Temperature oscillation frequencies were affected by changes in ambient temperature, ventilation, drafts, trapped air bubbles, and TE module, thermistor, and pump performance. These variables combined made the system less controllable, and require device improvement to establish precise control over temperature cycles.

VI. Conclusion and Future Work

This study developed a heating device and real-time particle tracking system, demonstrating thermoresponsive hydrogels can serve both as a *scaffold* and *bioreactor* without applying direct physical mechanical loads for enhancing chondrogenic differentiation of hMSCs. We demonstrated custom-tailored LCST hydrogels with reversible swelling/deswelling ability can be used to provide dynamic mechanical cues to encapsulated cells. Production of cartilage-ECM was dependent on the crosslinking density and thermoresponsiveness of the hydrogel to temperature oscillations in addition to the presence of TGFβ-1. The following is future work that could be performed to improve the chondrogenic differentiation of encapsulated hMSCs:

- Optimize the physical properties of MO and PEGDA (crosslinking densities, swelling ratio, response time, etc.) to produce volume strains of ~10% with frequencies between 0.01 – 1.0 Hz.
- Characterize the mechanical properties of the hydrogels (tensile, elastic, compressive moduli, tensile strength, etc.).
- Modify the device with an enclosure to limit the effects of environmental factors on heating performance.
- Increase heat oscillation frequency and enhance heat transfer to the constructs by combining the heating block and hydrogels into one unit.
- Minimize the contact points between the construct and PCR tubes by changing the gel shape to tall cylinders (∅1.5 mm by 3 mm tall) to apply strictly dynamic mechanical strains.

- Characterize photobleaching effects on particle tracking and error introduced to volume strain calculations.
- Calculate the realtime volume strains as defined by equations [11 – 12] using computational algorithms coded in Mathematica.
- Characterize the effect of temperature on the cells by measuring the expression of heat shock proteins using qRT PCR.

This design has the potential for implantation and application of *in vivo* mechanical stimulation with direct application of temperature oscillations. It is possible to tailor the response to temperatures more closely to within physiological ranges to induce dynamic compressive strains in the body without application of external heat. The ability to control response times and volume strain makes this bioreactor-scaffold design optimal for drug loading in cancer treatments in which direct application of heat can be used for directed drug delivery. Any cell type with mechano-sensory properties, for example esophageal smooth muscle cells, could be encapsulated in these hydrogels with tailored crosslinking densities, temperature response, and oscillation frequencies for tissue engineered treatments, such as esophageal cancer.

Appendix A. Figures and Tables

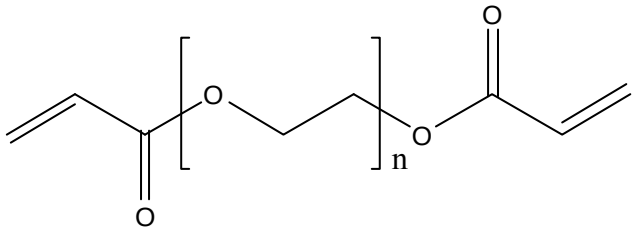

Figure A28. Poly(ethylene glycol) diacrylate. Crosslinker for MO hydrogels (Mw 3400).

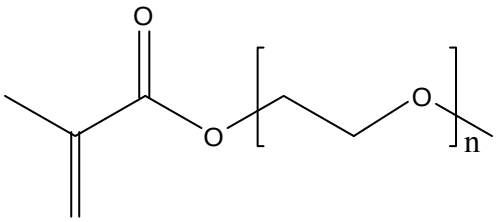

Figure A29. Poly(ethylene glycol) methyl ether methacrylate. For MEO_2MA monomer, n =2 (LCST ~26°C), while OEGMA monomer requires n = 8 or 9 (LCST ~105°C)

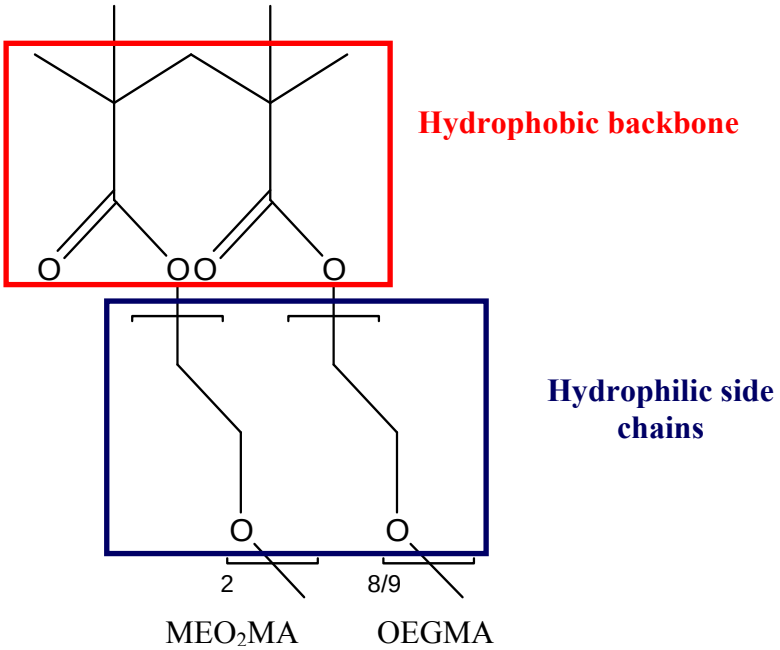

Figure A30. Structure of MEO2MA-OEGMA gels.

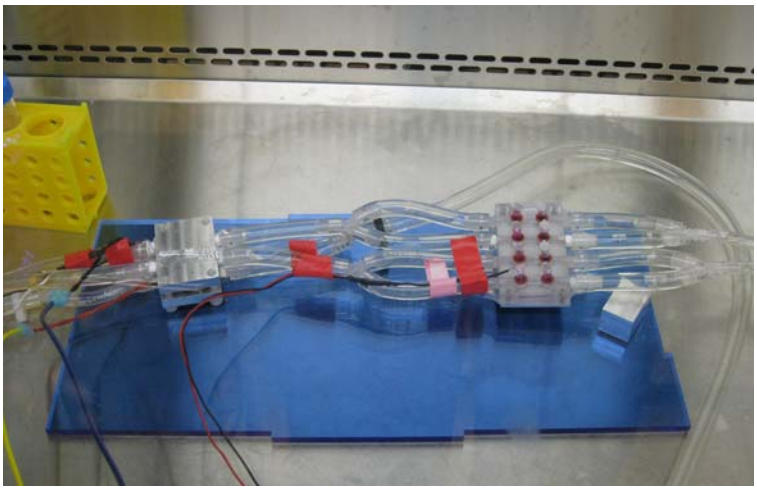

Figure A31. Image of Heating Device. Heating block and gel compartment of heating device were placed in a tissue culture hood.

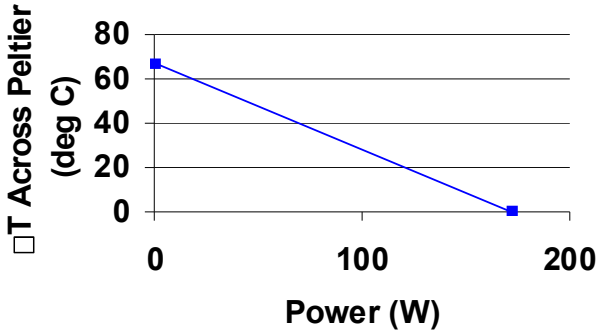

Figure A32. TE Module Performance.

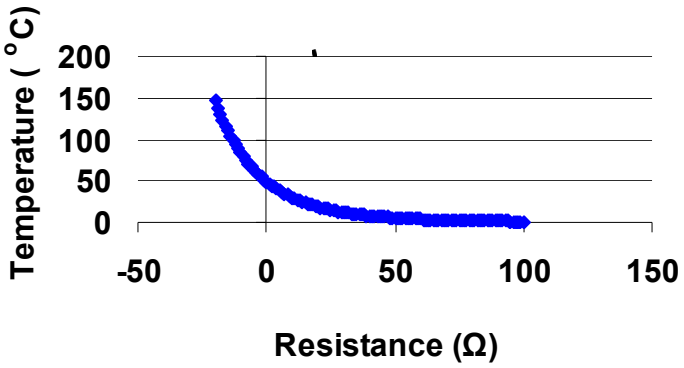

Figure A33. Thermistor Readings. MP-2444 (TE Tech) temperature versus resistance relationship.

Table A5. TE Module and Peristaltic Pump Specifications.

TE module	HP -199-1.4-0.8	TE controller	TC-24-25	Peristaltic Pump	SVP4 H7
I_{max}	11.3 amp(s)	V_{input}	12-28 VDC	Flow rate	87.8 to 1752.3 mL/s
Q_{max}	172 watt(s)	$\Delta T_{control}$	-20 to 100C	Max input signal V	48 VDC
V_{max}	24.6 volt(s)	$T_{max,ambient}$	65°C	Discharge Pressure	1.7-6.9 bar
DT_{max}	67 Th=300K	$T_{max,base}$	80°C	Voltage	120 V 50/60 Hz; 220 V 50/60 Hz
				Motor	12 VDC Gear Motor; 47 rpm; 1/30 HP
				Suction Lift	7.6 m
				Maximum Operating Temperature	52°C

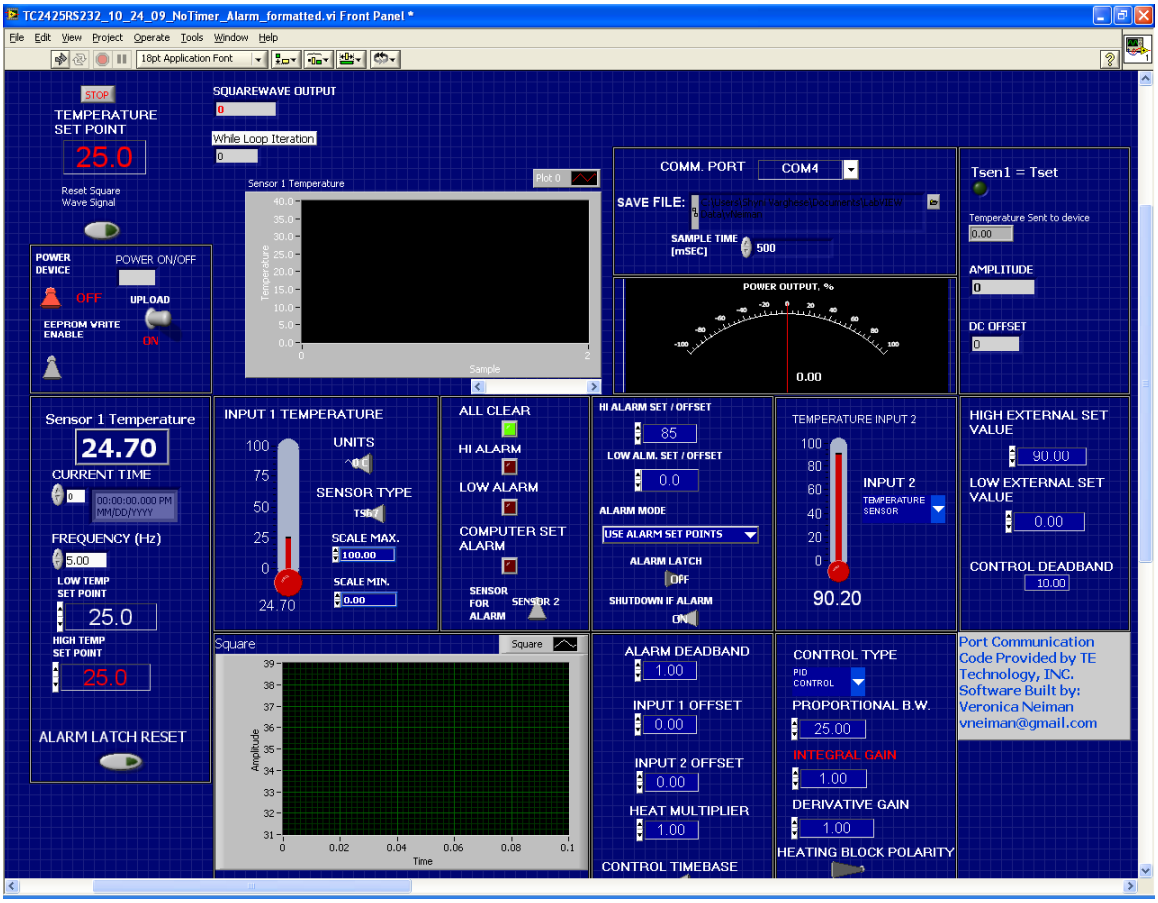

Figure A34. LabVIEW Software for TE Controller Communication.

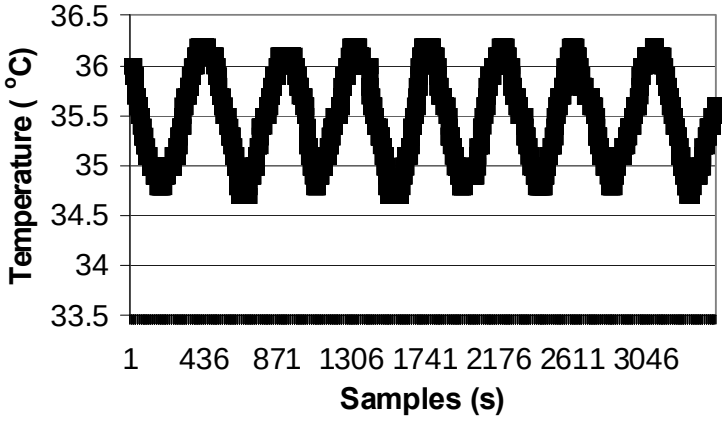

Figure A35. Sample 1 Hour Temperature Profile for Control A and Experimental 1A & 2A.

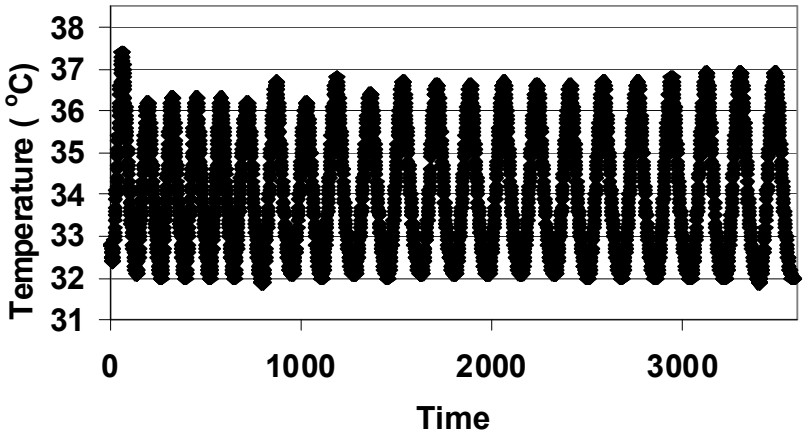

Figure A36. Sample 1 Hour Temperature Profile for Control and Experimental B-D.

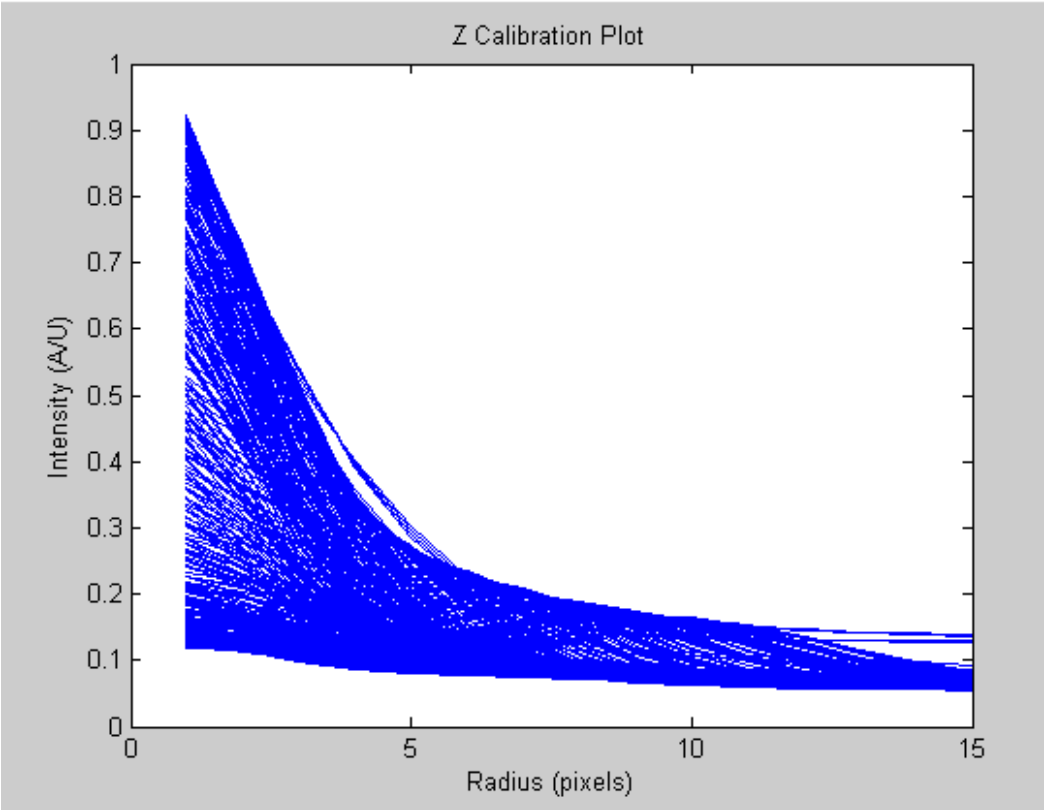

Figure A37. Z Position Calibration Curve. Profile shows half of the symmetric calibration curve. Z coordinate is known for each profile graphed.

Table A6. Average heating oscillation frequencies on each day for MO (10% PEG).

Day	Frequency (Hz)
1	0.0024
2	0.0025
3	0.0025
4	0.0019
5	0.0025
6	0.0024
7	0.0025
8	0.0022
9	0.0022
10	0.0028
11	0.0019
12	0.0021
13	0.0026
14	0.0013
15	0.0014
16	0.0011

Table A7. Average heating oscillation frequencies on each day for MO (20% PEG) and PEGDA (15% PEG).

Day	Frequency (Hz)
1	0.003028
2	0.004861
3	0.001694
4	0.001424
5	0.001667
6	0.0025
7	0.002389
8	0.001844
9	0.001889
10	0.003372
11	0.003333
12	0.006389
13	0.005778
14	0.003722
15	0.005333
16	0.004028

Appendix B. MATLAB Bead Tracking Code (Adapted from Johns Hopkins [87]).

B. Function Definitions

B.1. Z Calibration

B.1.1. Function calibrateCropped = reduce_movCalib(directoryCalib, inputCalibFile, calibOutput,calibFrames);

Function crops calibration images and stores them in an output folder.

Input:

directoryCalib = calibration directory name (same directory as MATLAB files without spaces)
inputCalibFile = filename of calibration images
calibOutput = folder and file name where cropped calibration images are stored.
calibFrames = number of calibration images in one stack

Output:

calibrateCropped = xmin and ymin coordinates of cropped image

B.1.2. Function calibration = calibrate_rpro(directoryCalib, calibOutput, CalibFrames);

Function measures bead intensity and diffraction profile, plotting these profiles as a function of z position.

Input:

Same as A.

Output:

calibration = variable contains the intensity, radial diffraction, and z coordinate profiles of the set of calibration images

B.1.2. Track Beads

B.1.2.1. function reduce_move(directory, inputFile, outputFile, frames)

Function allows cropping a region of interest from a set of images stored in the folder "inputFile" and stores cropped images in "outputFile". The region should include the whole path of one and only one bead. The coordinates of the xmin and ymin are displayed along with the size of the rectangle.

A Window will open with your specified image shown. Using the mouse, a fairly large square is drawn around the bead of interest without overlapping any other beads.

Input:

directory = directory name of images to be analyzed
inputFile = folder and filename template of all images in the stack to be analyzed
outputFile = folder and filename destination of cropped images
frames = number of images in a stack to analyze. Allows analyzing a subset of images in the stack.

B.1.2.2. function pos = measure_pos_bead(calibration, dir, filename, first, last, particle)

This function calls various functions to determine the x,y,z coordinates. The XY coordinates are found as absolute values with respect to the FOV. To get absolute values with respect to the original image, the values of the coordinates of xmin, ymin (displayed when reduce_mov was applied) are added. The Z coordinates are tracked using the calibration curve.

Input:

calibration = Calibrated image stack
dir = directory name of images to be analyzed
filename = output file name of cropped images after reduce_mov() was applied
first = number of first image in stack to be analyzed
last = number of last image in stack to be analyzed
particle = number of particles tracked in FOV

Output:

(X,Y,Z) coordinates of particle tracked in image stack.

Notes:

File naming scheme:

```
if frame <= 9, z = '00'
if frame <= 99, z = '0'
else z = ''
name=[dir filename '\' filename z num2str(frame) '.tif'];
```

B.2. MATLAB Code

B.2.1. Main Class File

```
%{
Author: Veronica Neiman
Date:July 23, 2009.
Description: File reads in a stack of calibration images taken at set
z increments using a motorized stage. Code creates a calibration curve
of the diffraction radius and intensity of one particle as a function of the known z position.
Images to be tracked are loaded into memory. User creates a field of
view (FOV) around the single particle to be tracked by tracing a
rectangle around the particle with sufficient empty space to account for particle movement. This code
tracks a total of 4 particles (A through D). All images in the image stack are cropped with this same FOV
and the particle (x,y,z) coordinates are tracked only within this window.
Output: Displays coordinates of each particle selected in vector form. X coordinate is the first column, Y
coordinate is in the second column, and Z is in the third column.

Instructions:
- Update variables listed above and the coordinates of reduce_movCalib() variable 'rect = [xmin ymin
width height]' which defines the FOV of the calibration images.
- Modify focal plane increment in measure_pos_bead() from images taken for z stack using automated
stage.
```

```
- Update 'first' and 'frames' within reduce_mov().m and measure_pos_bead().m to match variable "first"
and "frames"
%}
%========================================================================

clear all
close all
directoryCalib = 'E:\ImageAnalysis\ImageAnalysisMatLABFiles\'; %Calibration images directory
directory = 'E:\ImageAnalysis\ImageAnalysisMatLABFiles\'; %Analyzed
%image directory
inputCalibFile = 'F01 Tx HYDROGEL_';    %Calibration images
inputFile = '15% PEGDA FPs hMSCs 2_10_2010_heating_'; %Analyzed images
CalibFrames = 329;              %Number of images in calibration stack
calibOutput = 'CalibOutput';     %Cropped calibration images
outputFile = 'CropOuput';        %Cropped analyzed images
first = 43;
frames = 64;
zTicks = [];
%Calibrate particle images for z displacement
calibrateCropped = reduce_movCalib(directoryCalib, inputCalibFile, calibOutput,CalibFrames);
calibrate = calibrate_rpro(directoryCalib, calibOutput,CalibFrames)

%=================================================================
%PARTICLE A:
%===========
%Creates cropped image from mouse selected rectangle
%Display xmin, ymin, width, and height of rectangel selection.
originA = reduce_mov(directory, inputFile, outputFile,first, frames); %store xmin and ymin in origin
%Read in cropped image. Calculate min and max reference coordinates.
%Use xmin and ymin to calculate absolute coordinates
%display('positions in main .m file')
particle = 1
posA = measure_pos_bead(calibrate, directory, outputFile,first, frames,particle);
display('Absolute Position of Center of Bead = highest Intensity')
for i = 1:2
   absPosA(:,i) = posA(:,i) + originA(i)*0.62;
   absPosA(:,3) = posA(:,3);
end

%PARTICLE B:
%===========
originB = reduce_mov(directory, inputFile, outputFile,first, frames); %store xmin and ymin in origin
particle = 2
posB = measure_pos_bead(calibrate, directory, outputFile,first, frames,particle);
display('Absolute Position of Center of Bead = highest Intensity')
for i = 1:2
   absPosB(:,i) = posB(:,i) + originB(i)*0.62;
   absPosB(:,3) = posB(:,3);
end

%PARTICLE C:
%===========
originC = reduce_mov(directory, inputFile, outputFile,first, frames); %store xmin and ymin in origin
```

```
particle = 3
posC = measure_pos_bead(calibrate, directory, outputFile,first, frames,particle);
display('Absolute Position of Center of Bead = highest Intensity')
for i = 1:2
   absPosC(:,i) = posC(:,i) + originC(i)*0.62;
   absPosC(:,3) = posC(:,3);
end

%PARTICLE D:
%==========
%Creates cropped image from mouse selected rectangle
%Display xmin, ymin, width, and height of rectangel selection.
originD = reduce_mov(directory, inputFile, outputFile,first, frames); %store xmin and ymin in origin

%Read in cropped image. Calculate min and max reference coordinates.
%Use xmin and ymin to calculate absolute coordinates
%display('positions in main .m file')
particle = 4
posD = measure_pos_bead(calibrate, directory, outputFile,first, frames,particle);

display('Absolute Position of Center of Bead = highest Intensity')
for i = 1:2
   absPosD(:,i) = posD(:,i) + originD(i)*0.62;
   absPosD(:,3) = posD(:,3);
end
display('PosA')
posA
absPosA
display('PosB')
posB
absPosB
display('PosC')
posC
absPosC
display('PosD')
posD
absPosD
```

B.2.2. Functions

```
%Create cropped images of calibration stack and store in calibOutput
function origin = reduce_movCalib(directoryCalib,inputCalibFile,calibOutput,calibFrames)
%Change these values for each calibration
rect = [586 520 56 44];
input=[dir name_in '\'];
output=[dir name_out '\'];
[status,result]=dos(['mkdir ' dir name_out]);
first=1;

for frame=first:last
   if frame<=9
      z='00';
   elseif frame<=99
      z='0';
```

```
    else
        z='';
    end

    name=[input name_in z num2str(frame) '.tif'];
    pic= imread(name);
    [x, y] = size(pic);

    %Show 1st original image
    if frame == first
    figure; imshow(pic,[])
    title(['Original ',name_in z num2str(frame) '.tif'])
    axis on
    end
    if frame==first
        [crop_pic]=imcrop(pic,rect); %Crop image according to mouse
              %drawn rectangle
        title(['Original ',name_in])
        axis on
        %comment out once have rectangle dimensions
        %rect=floor(rect); %Returns rounded down value to nearest
                %integer of top left coodinates (xmin, ymin), rectangel width
                %and height
        disp(' xmin      ymin      width      height')
        disp(rect)
    end
    crop_pic=imcrop(pic,rect);
    imwrite(crop_pic,[output name_out z num2str(frame) '.tif']);
    origin = rect(1:2);
end
```

```
%Generate calibration profile of bead intensity versus diffraction radius.
function calibration=calibrate_rpro(directoryCalib,calibOutput,CalibFrames)
%Last = number of frames
first=1;    %First frame number
rad_f=15;   %Radius of fluorescent particle in pixels
rad_i=1;    %Radius of initial
calibration=zeros(last-first+1,rad_f-rad_i+1); %Create zero matrix
%#frames X 12

for frame=first:last
    pic=get_pic(dir,filename,frame); %Read image from graphics file
    pic=im2single(pic); %Convert image to single precision
    center=get_center3(pic); %Calculate center coordinate (max
    %intensity) using cross correlation function
    center_list(frame,1:2)=center;
    calibration(frame,:)=get_rpro(pic,center,rad_i,rad_f); % calculate
    %average pixel intensity at radius r from center
end

[frames,rad]= size(calibration)
theta = linspace (0,2*pi,frames)  %length of theta matches number of
%frames
```

```
theta_pol2cart = linspace (0,2*pi,rad)  %Scaled theta to match number
%rad since conversion of pol2cart requires same dimensions
l = size(theta);
radius = 1:rad
[x,y] = pol2cart(theta_pol2cart,radius)
figure(), plot(x,y,'-r')
title('2D plot')
figure(),
for i=1:frames;
   plot(radius,calibration(i,:))
   hold on
end
title('Z Calibration Plot')
xlabel('Radius (pixels)')
ylabel('Intensity (A/U)')

figure (), surf(calibration,'EdgeColor','flat');
title('Calibration Profiles')
xlabel('Pixel distance from center')
ylabel('Intensity of Center')
colormap gray
view(0,90);    %view directly overhead

figure (), surf(calibration,'EdgeColor','interp');
title('Calibration Profiles')
xlabel('Pixel distance from center')
ylabel('Intensity of Center')
colormap gray
view(0,90);    %view directly overhead

figure, plot(center_list(:,1),center_list(:,2))
title('Position of center of bead')
xlabel('x coord')
ylabel('y coord')
```

```
%Create cropped images of images to analyze and store in name_out
function origin=reduce_mov(directory, name_in,name_out,first,last)
input=[dir name_in '\'];
output=[dir name_out '\'];
[status,result]=dos(['mkdir ' dir name_out]);

for frame=first:last
   if frame<=9
      z='00';
   elseif frame<=99
      z='0';
   else
      z='';
   end
   name=[input name_in z num2str(frame) '.tif'];
   pic=imread(name);
   display('size of pic')
   [x, y] = size(pic)
```

```
    %Show original image
    if frame == first
        figure; imshow(pic,[])
        title(['Original ' name_in z num2str(frame)])
        axis on
    end
    if frame==first
        figure
        axis on
        [crop_pic,rect]=imcrop(pic); %Crop image according to mouse
              drawn rectangle
        imshow(crop_pic, [])
        title(['Original ',name_in])

        rect=floor(rect); %Returns rounded down value to nearest
                %integer of top left coodinates (xmin, ymin), rectangel width
                %and height
        disp(' xmin      ymin      width      height');
        disp(rect);
    end
    crop_pic=imcrop(pic,rect);
    imwrite(crop_pic,[output name_out z num2str(frame) '.tif']);
    origin=rect(1:2);
end
```

```
%Assign position of the bead in the set of images of a folder filename
%to a variable pos. The XY measurements are absolute values with
%respect to the images axis. To get absolute values with respect to the
%original image, the values of the coordinates of xmin, ymin (displayed
%when reduce_mov was applied) should be added. The Z measurements are
%made using the variable calibration.
function pos = measure_pos_bead(calibration,dir,filename, first,last,particle)

conversion_pix_nm_z=0.2; %0.2 um/increment between focal planes
conversion_pix_nm_xy=0.62;   %0.62 um/pixel conversion from pixels to
%um in xy plane.
rad_f=30;   %previous value was 15.
rad_i=1;

sc=size(calibration);
center_list=zeros((last-first)+1,2);
z_list=zeros((last-first)+1,1);
count_frame=0;
%z_ref=0;

    for frame = first:last
        pic=0;
    while pic==0
        pic=get_pic(dir,filename,frame);

        if (frame-first >= 0) & (frame-first <=11)
                %Display cropped image enhanced with x and y scale
```

```
            figure(3*particle); subplot(2,6,(frame-first+1)); imshow(pic,[]);
    title(['O_Crop ', num2str(frame)])
            %Enhanced image display without modifying image. For viewing
            %purposes only.
            figure(4*particle); subplot(2,6,(frame-first+1)); image(pic); colormap(gray)
    title(['E_Crop ', num2str(frame)])
    else if (frame-first > 11) & (frame-first <= 23)
          %Display cropped image enhanced with x and y scale
          figure(5*particle); subplot(2,6,(frame-first-11));
          imshow(pic,[]);
          title(['O_Crop ', num2str(frame)])
            %Enhanced image display without modifying image. For viewing
            %purposes only.
            figure(6*particle); subplot(2,6,(frame-first-11)); image(pic);    colormap(gray)
          title(['E_Crop ', num2str(frame)])
    else if (frame-first > 23) & (frame-first <= 35)
          %Display cropped image enhanced with x and y scale
            figure(7*particle); subplot(2,6,(frame-first-23));
            imshow(pic,[]);
    title(['O_Crop ', num2str(frame)])
            %Enhanced image display without modifying image. For viewing
            %purposes only.
            figure(8*particle); subplot(2,6,(frame-first-23)); image(pic);   colormap(gray)
    title(['E_Crop ', num2str(frame)])
    else if (frame-first > 35) & (frame-first <= 47)
          %Display cropped image enhanced with x and y scale
            figure(7*particle); subplot(2,6,(frame-first-35));
            imshow(pic,[]);
    title(['O_Crop ', num2str(frame)])
            %Enhanced image display without modifying image. For viewing
            %purposes only.
            figure(8*particle); subplot(2,6,(frame-first-35)); image(pic); colormap(gray)
    title(['E_Crop ', num2str(frame)])
    else if (frame-first >47) & (frame-first <= 59)
          %Display cropped image enhanced with x and y scale
            figure(7*particle); subplot(2,6,(frame-first-47));
            imshow(pic,[]);
    title(['O_Crop ', num2str(frame)])
            %Enhanced image display without modifying image. For viewing
            %purposes only.
            figure(8*particle); subplot(2,6,(frame-first-47)); image(pic); colormap(gray)
    title(['E_Crop ', num2str(frame)])
       end
       end
       end
       end
    end
end

pic=im2single(pic); %convert image to single precision
count_frame=count_frame+1;
center=get_center3(pic);    %Find center coordinates using cross
correlation function
center_list(count_frame,1:2)=center; %-center_ref;
```

```
display('pro to match: max intensity at center')
pro_to_match=get_rpro(pic,center,rad_i,rad_f);  %get max intensity at center

%Locate Z position
%==================
z = match_pro(calibration,pro_to_match);  %Find matching coord
%intensities between the calibration and center intensity --> e.g. find
%center
z = match_pro(calibration,pro_to_match);  %Find matching coord
%intensities between the calibration and center intensity --> e.g. find
%center
if (z~=1) & (z~=sc(1))
   alpha=interpolate(calibration, z-1,z+1,pro_to_match);%Interpolate 1
   %above and below closest match between calibration and image
   if (alpha<0.5)
      alpha=interpolate(calibration, z-1,z,pro_to_match);
      z_list(count_frame)=z-1+alpha;  % Shift 0.5 units back
   else
      alpha=interpolate(calibration, z,z+1,pro_to_match);
      z_list(count_frame)=z+alpha;    %Shift 0.5 units to the right
   end
end
if z==1
   alpha=interpolate(calibration, z,z+1,pro_to_match);
   z_list(count_frame)=z+alpha;
end
if z==sc(2)
   alpha=interpolate(calibration, z-1,z,pro_to_match);
   z_list(count_frame)=z-1+alpha;
end
z_list(count_frame)=z_list(count_frame); %-z_ref;
end
center_list=center_list.*conversion_pix_nm_xy;
z_list=z_list.*conversion_pix_nm_z;
display('Filename. In measure_pos_bead. Center list (x,y) and z list(z position)')
filename
pos=[center_list,z_list]
```

```
%Read image from graphics file in specified directory and folder
function p=get_pic(dir,filename,frame)
if frame<=9
   z='00';
elseif frame<=99
   z='0';
else
   z='';
end
name=[dir filename '\' filename z num2str(frame) '.tif'];
[status,result]=dos(['dir ' name]);      % Status = 0 means success.

if ~status  % if NOT status
   p=imread(name);
```

```
else
   p=0;
   [name ' was not found']
end
```

```
%Find center coordinate (maximum intensity) using cross correlation
%function. Analyze a box of size region for each iteration
function center=get_center3(pic)
region=200;
scan_range=1;
pic2=pic;
sp=size(pic); %Get picture array dimensions

%x direction
%============
%Floor rounds to minus infinity
pic=imcrop(pic,[1,floor((sp(1)-region)/2),sp(2),region]);
pic=im2single(pic); %Convert image to single precision
base=pic(1,1);      %Define base/start of picture
pic=pic-base;       %Remove start point
%Flip matrix pic left-right. 2D cross-correlation maximum when 2
%matrices are aligned, so their shapes are as similar as possible:
xc2=xcorr2(pic,fliplr(pic));
[im,jm,max]=max_2D(xc2);
%Find max of matrix xc2 (cross correlation)
base_m=xc2(im-scan_range,jm-scan_range);    %Base is the threshold value
pos_sum=[0,0];
vol_sum=0;
count=0;
for i=im-2*scan_range:im+2*scan_range
   for j=jm-2*scan_range:jm+2*scan_range
      if xc2(i,j)>=base_m
         pos_sum=pos_sum+[i,j]*(xc2(i,j)-base_m);
         vol_sum=vol_sum+xc2(i,j)-base_m;
         count=count+1;
      end
   end
end
max_subpixel=pos_sum/vol_sum;
x_center=(max_subpixel(2)+1)/2;

%y direction
%============
pic=imcrop(pic2,[floor((sp(2)-region)/2),1,region,sp(1)]);
pic=im2single(pic);
base=pic(1,1);
pic=pic-base;
xc2=xcorr2(pic,flipud(pic));
[im,jm,max]=max_2D (xc2);
base_m=xc2(im-scan_range,jm-scan_range);
pos_sum=[0,0];
vol_sum=0;
```

```
count=0;
for i=im-2*scan_range:im+2*scan_range
   for j=jm-2*scan_range:jm+2*scan_range
      if xc2(i,j)>=base_m
         pos_sum=pos_sum+[i,j]*(xc2(i,j)-base_m);
         vol_sum=vol_sum+xc2(i,j)-base_m;
         count=count+1;
      end
   end
end
max_subpixel=pos_sum/vol_sum;
count;
y_center=(max_subpixel(1)+1)/2;
center=[x_center,y_center];
```

```
%Return max x and y coordinates
function [x,y,m2]=max_2D(matrix)
[m1,xm]=max(matrix); %Return coordinates of max value of 3D matrix
[m2,y]=max(m1); % Return max coordinates of m1
x=xm(y);
```

```
%Function calculates the RGB values of the bead center and returns the
%Center intensity calculated as a function of radial distance from the centroid.
function pro=get_rpro(pic,center,rad_i,rad_f)
theta_step=0.1;
for r=rad_i:rad_f
   count=0;
%Start at center and move outward in concentric circles CCW stepping
%theta by 0.1 around the center up to a radius of rad_f.
   for theta=theta_step:theta_step:2*pi
      count=count+1;
      row(count)=center(1)+cos(theta)*r;   %Get x coord of center of
               %bead for spec. frame + x component of theta radians CCW from
               %point with magnitude r
               column(count)=center(2)+sin(theta)*r;      %Get y coord of
               %center of bead for spec. frame + y component of theta radians
               %CCW from point with magnitude r
   end
   %Intensity list
   i_list=impixel(pic,row,column); %Determine RGB pixel color values
   %CCW around center point specified by get_center3
   %column and row have coordinates of pixels for RGB values returned
   %in i_list. Column 1 stores red intensity, column 2 is green, and
   %column 3 is blue. kth row of i_list has RGB values for the pixel
   %(row(k),column(k)) where row are x coords, and column are y coords
   %figure();surf(i_list)

   %Fill in from left to right; store average pixel RGB intensity for
   %x component, column 1 of i_list
   pro(r-rad_i+1)=mean(i_list(:,1));    % store only Red intensity
   %(denoted by list(:,1) as a function of distance from center, r
end
```

```
%Locate z coordinate of each image from the calibration profile using squared minimization
function z_pix=match_pro(calibration,profile)
center_cut=1; % independent of the actual profile size
min_inte=1;
range_inte=1;
step_inte=1;
[rc,cc]=size(calibration);
[rp,cp]=size(profile);
columns=min([cc,cp]);
d2_matrix=zeros(columns,floor(range_inte/step_inte));
for i=1:rc
   count_j=0;
   for j=min_inte:step_inte:min_inte+range_inte-step_inte
      count_j=count_j+1;
      %Calculate difference between values
      delta2=sum((calibration(i,center_cut:columns)-
            profile(center_cut:columns)*j).^2);
      d2_matrix(i,count_j)=delta2;
   end
end
%Smallest d2_matrix value indicates a match between the calibration and
%profile
[z_pix,count_j,delta2]=min_2D(d2_matrix);
intensity=(count_j-1)*step_inte+min_inte;
```

```
%Optimize located z coordinate of each image from the calibration profile using interpolation
function alpha=interpolate(calibration,n1,n3,pro)
step_alpha=0.1;
step_inte=.1;
range_inte=.2;
min_inte=.9;
sc=size(calibration);
sp=size(pro);
columns=min([sc(2),sp(1)]);

p1=calibration(n1,1:columns);
p2=pro(1:columns);

p3=calibration(n3,1:columns);
d2_matrix=zeros(1/step_alpha+1,range_inte/step_inte);
count_k=0;
for k=0:step_alpha:1
   count_k=count_k+1;
   profile=p1*(1-k)+p3*k;
   count_j=0;
   for j=min_inte:step_inte:min_inte+range_inte-step_inte
      count_j=count_j+1;
      delta2=sum((p2-profile*j).^2);
      d2_matrix(count_k,count_j)=delta2;
   end
end
[count_k,count_j,delta2]=min_2D(d2_matrix);
```

```
alpha=(count_k-1)*step_alpha;   %(n3-n1)*;
```

```
%{
Author: Veronica Neiman
Calculate R displacement ratio with directionality according to
equation 8.
Input: manually insert x,y,z coordinate matrices of particles analyzed up to 12 particles.
%}
clear all
close all

pos1 = [562.1360091 503.7320748 44.2
562.262131  503.5017992 42
564.1161781 503.5906021 42
565.3919409 503.606919  42
563.6793986 502.777901  42];

pos2 = [560.6063561 503.2684478 42
559.0387053 502.2380535 40.2
559.4540545 502.0287718 40.2
559.8489691 501.5459802 40.2
561.7498856 503.2590748 40.2];

pos3 = [557.4330991 503.9013092 39.8
555.7285911 502.4811988 40.2
563.9388396 503.1421744 39.8
566.8544247 502.6038559 39.8
568.1516178 501.9542211 39.8];

pos4 = [565.8443562 502.962284  39.8
568.0663366 501.8744813 39.8
567.6232635 502.594185  39.8
568.9312416 501.7801358 39.8
571.4788271 499.8964468 39.8];

 [m,n] = size(pos1);
for j = 1   %Manually change j value for corresponding particle to be analyzed.
   if j ==1
      pos = pos1;
   else
      if j == 2
         pos = pos2;
      else
         if j ==3
            pos = pos3;
         else
            if j == 4
               pos = pos4;
            end
         end
      end
   end
```

```
end
   init = pos(1,1:3)

   for q = 1:m-1
      d(q) = sqrt((pos(q+1,1)-pos(q,1))^2 + (pos(q+1,2)-
                  pos(q,2))^2+(pos(q+1,3)-pos(q,3))^2);
      numerator(q) = sqrt((pos(q,1)-init(1,1))^2 + (pos(q,2)-
                  init(1,2))^2 + (pos(q,3)-init(1,3))^2);
      numerator(m) = sqrt((pos(m,1)-init(1,1))^2 + (pos(m,2)-
                  init(1,2))^2 + (pos(m,3)-init(1,3))^2);
      %assign directionality
      if pos(q+1,1) < pos(q,1)||pos(q+1,2) < pos(q,2) ||
                  pos(q+1,3)<pos(q,3)
         numerator(q) = uminus(numerator(q));
      end
      if pos(m,1) < pos(m-1,1)||pos(m,2) < pos(m-1,2) ||
                  pos(m,3)<pos(m-1,3)
         numerator(m) = uminus(numerator(m));
      end

      total = sum(d(:));
   end
end
for k = 1:m-1
   R(k) = (numerator(k)/total);
   R(m) = numerator(m)/total;
end
d
display('numerator')
numerator'
total'
display('R ratio')
R'
```

References

1. Williams, C.G., Kim, T.K., Taboas, A., Malik, A., Manson, P., and Elisseeff, J. In vitro chondrogenesis of bone marrow-derived mesenchymal stem cells in a photopolymerizing hydrogel. Tissue Engineering 9, 679, 2003.

2. Bonaventure, J., Kadhom, N., Cohensolal, L., Ng, K.H., Bourguignon, J., Lasselin, C., and Freisinger, P. Reexpression of cartilage-specific genes by dedifferentiated human articular chondrocytes cultured in alginate beads. Experimental Cell Research 212, 97, 1994.

3. Saadeh, P.B., Brent, B., Mehrara, B.J., Steinbrech, D.S., Ting, V., Gittes, G.K., and Longaker, M.T. Chondrocyte extraction, proliferation, and characterization for construct development. Annals of Plastic Surgery 42, 509, 1999.

4. Stewart, M.C., Saunders, K.M., Burton-Wurster, N., and MacLeod, J.N. Phenotypic stability of articular chondrocytes in vitro: The effects of culture models, bone morphogenetic protein 2, and serum supplementation. Journal of Bone and Mineral Research 15, 166, 2000.

5. Kim, T.K., Park, J.S., Lee, M.C., Seong, S.C., and Kim, H.J. Alternative splicing of type II procollagen gene in the dedifferentiation of rat epiphyseal chondrocytes serially cultured in monolayer. Connective Tissue Research 43, 56, 2002.

6. Elisseeff, J., Puleo, C., Yang, F., and Sharma, B. Advances in skeletal tissue engineering with hydrogels. Orthod Craniofac Res 8, 150, 2005.

7. Cushing, M.C., and Anseth, K.S. Hydrogel cell cultures. Science 316, 1133, 2007.

8. Johnstone, B., Hering, T.M., Caplan, A.I., Goldberg, V.M., and Yoo, J.U. In vitro chondrogenesis of bone marrow-derived mesenchymal progenitor cells. Experimental Cell Research 238, 265, 1998.

9. Mackay, A.M., Beck, S.C., Murphy, J.M., Barry, F.P., Chichester, C.O., and Pittenger, M.F. Chondrogenic differentiation of cultured human mesenchymal stem cells from marrow. Tissue Engineering 4, 415, 1998.

10. Kramer, J., Hegert, C., Guan, K.M., Wobus, A.M., Muller, P.K., and Rohwedel, J. Embryonic stem cell-derived chondrogenic differentiation in vitro: activation by BMP-2 and BMP-4. Mechanisms of Development 92, 193, 2000.

11. Burdick, J.A., and Vunjak-Novakovic, G. Engineered Microenvironments for Controlled Stem Cell Differentiation. Tissue Engineering Part A 15, 205, 2009.

12. Hwang, N.S., Varghese, S., and Elisseeff, J. Derivation of Chondrogenically-Committed Cells from Human Embryonic Cells for Cartilage Tissue Regeneration. Plos One 3, 2008.

13. Hoemann, C.D. Molecular and biochemical assays of cartilage components. Cartilage and Osteoarthritis, Vol 2: Structure and in Vivo Analysis 101, 127, 2004.

14. Terraciano, V., Hwang, N., Moroni, L., Park, H.B., Zhang, Z., Mizrahi, J., Seliktar, D., and Elisseeff, J. Differential response of adult and embryonic mesenchymal progenitor cells to mechanical compression in hydrogels. Stem Cells 25, 2730, 2007.

15. Archer, C.W., McDowell, J., Bayliss, M.T., Stephens, M.D., and Bentley, G. Phenotypic modulation in subpopulations of human articular chondrocytes in vitro. Journal of Cell Science 97, 361, 1990.

16. Hauselmann, H.J., Fernandes, R.J., Mok, S.S., Schmid, T.M., Block, J.A., Aydelotte, M.B., Kuettner, K.E., and Thonar, E. Phenotypic stability of bovine articular chondrocytes after long-term culture in alginate beads. Journal of Cell Science 107, 17, 1994.

17. Reginato, A.M., Iozzo, R.V., and Jimenez, S.A. Formation of nodular structures resembing mature articular-cartilage in long-term primary cultures of ormation of nodular structures resembling mature articular-cartilage in long-term primary cultures of human fetal epiphyseal chondrocytes on a hydrogel substrate. Arthritis and Rheumatism 37, 1338, 1994.

18. Sugiki, T., Uyama, T., Toyoda, M., Morioka, H., Kume, S., Miyado, K., Matsumoto, K., Saito, H., Tsumaki, N., Takahashi, Y., Toyama, Y., and Umezawa, A. Hyaline cartilage formation and enchondral ossification modeled with KUM5 and OP9 chondroblasts. Journal of Cellular Biochemistry 100, 1240, 2007.

19. Heath, C.A., and Magari, S.R. Mini-review: Mechanical factors affecting cartilage regeneration in vitro. Biotechnology and Bioengineering 50, 430, 1996.

20. Mow, V.C., Ratcliffe, A., and Poole, A.R. Cartilage and diarthrodial joints as paradigms for hierarchical materials and structures. Biomaterials 13, 67, 1992.

21. Buckwalter, J.A., Hunziker, E.B., and Rosenberg, L.C. Articular cartilage: Composition and structure. In: Woo, S.-Y., and Buckwalter, J., eds. Injury and Repair of the Musculoskeletal Soft Tissues. Park Ridge: AAOS, 1988, pp. 405-425.

22. Buckwalter, J.A., and Mankin, H.J. Articular cartilage .1. Tissue design and chondrocyte-matrix interactions. Journal of Bone and Joint Surgery-American Volume 79A, 600, 1997.

23. Newman, A.P. Articular cartilage repair. American Journal of Sports Medicine 26, 309, 1998.

24. Buckwalter, J.A., Mow, V.C., and Ratcliffe, A. Restoration of Injured or Degenerated Articular Cartilage. J Am Acad Orthop Surg 2, 192, 1994.

25. Stoop, R., Albrecht, D., Gaissmaier, C., Fritz, J., Felka, T., Rudert, M., and Aicher, W.K. Comparison of marker gene expression in chondrocytes from patients receiving autologous chondrocyte transplantation versus osteoarthritis patients. Arthritis Research & Therapy 9, 2007.

26. Temenoff, J.S., and Mikos, A.G. Review: tissue engineering for regeneration of articular cartilage. Biomaterials 21, 431, 2000.

27. Lee, J., Lee, E., Kim, H.Y., and Son, Y. Comparison of articular cartilage with costal cartilage in initial cell yield, degree of dedifferentiation during expansion and redifferentiation capacity. Biotechnology and Applied Biochemistry 48, 149, 2007.

28. Nair, L.S., and Laurencin, C.T. Biodegradable polymers as biomaterials. Progress in Polymer Science 32, 762, 2007.

29. Nerurkar, N.L., Elliott, D.M., and Mauck, R.L. Mechanics of oriented electrospun nanofibrous scaffolds for annulus fibrosus tissue engineering. Journal of Orthopaedic Research 25, 1018, 2007.

30. Schumann, D., Kujat, R., Nerlich, M., and Angele, P. Mechanobiological conditioning of stem cells for cartilage tissue engineering. Bio-Medical Materials and Engineering 16, S37, 2006.

31. Lee, D.A., and Bader, D.L. The development and characterization of an in vitro system to study strain-induced cell deformation in isolated chondrocytes. In Vitro Cellular & Developmental Biology-Animal 31, 828, 1995.

32. Pelaez, D., Huang, C.Y.C., and Cheung, H.S. Cyclic Compression Maintains Viability and Induces Chondrogenesis of Human Mesenchymal Stem Cells in Fibrin Gel Scaffolds. Stem Cells and Development 18, 93, 2009.

33. Martens, P., and Anseth, K.S. Characterization of hydrogels formed from acrylate modified poly(vinyl alcohol) macromers. Polymer 41, 7715, 2000.

34. Davisson, T., Kunig, S., Chen, A., Sah, R., and Ratcliffe, A. Static and dynamic compression modulate matrix metabolism in tissue engineered cartilage. Journal of Orthopaedic Research 20, 842, 2002.

35. Bryant, S.J., Nuttelman, C.R., and Anseth, K.S. Cytocompatibility of UV and visible light photoinitiating systems on cultured NIH/3T3 fibroblasts in vitro. Journal of Biomaterials Science-Polymer Edition 11, 439, 2000.

36. Burtonwurster, N., Verniersinger, M., Farquhar, T., and Lust, G. Effect of comprehensive loading and unloading on the synthesis of total protein, proteoglycan, and fibronectin by canine cartilage explants. Journal of Orthopaedic Research 11, 717, 1993.

37. Bryant, S.J., Chowdhury, T.T., Lee, D.A., Bader, D.L., and Anseth, K.S. Crosslinking density influences chondrocyte metabolism in dynamically loaded photocrosslinked poly(ethylene glycol) hydrogels. Annals of Biomedical Engineering 32, 407, 2004.

38. Appelman, T.P., Mizrahi, J., Elisseeff, J.H., and Seliktar, D. The differential effect of scaffold composition and architecture on chondrocyte response to mechanical stimulation. Biomaterials 30, 518, 2009.

39. Schmidt, O., Mizrahi, J., Elisseeff, J., and Seliktar, D. Immobilized fibrinogen in PEG hydrogels does not improve chondrocyte-mediated matrix deposition in response to mechanical stimulation. Biotechnology and Bioengineering 95, 1061, 2006.

40. Hu, Z.B., Zhang, X.M., and Li, Y. Synthesis and application of modulated polymer gels. Science 269, 525, 1995.

41. Beebe, D.J., Moore, J.S., Bauer, J.M., Yu, Q., Liu, R.H., Devadoss, C., and Jo, B.H. Functional hydrogel structures for autonomous flow control inside microfluidic channels. Nature 404, 588, 2000.

42. Leong, T.G., Randall, C.L., Benson, B.R., Bassik, N., Stern, G.M., and Gracias, D.H. Tetherless thermobiochemically actuated microgrippers. Proceedings of the National Academy of Sciences of the United States of America 106, 703, 2009.

43. Osada, Y., Okuzaki, H., and Hori, H. A polymer gel with electrically driven motility. Nature 355, 242, 1992.

44. Frimpong, R., Fraser, S., and Hilt, J.Z. Synthesis and temperature response analysis of magnetic-hydrogel nanocomposites. Journal of Biomedical Materials Research Part A 10, 1, 2006.

45. Irie, M., Yoshifumi, M., Tusuyoshi, T. Stimuli-responsive polymers – chemical-induced reversible phase-separation of an aqueous-solution of poly(N-isopropylacrylamide) with pendent crown-ether groups. Polymer 34, 4531, 1993.

46. Collett, J., Crawford, A., Hatton, P.V., Geoghegan, M., and Rimmer, S. Thermally responsive polymeric hydrogel brushes: synthesis, physical properties and use for the culture of chondrocytes. Journal of the Royal Society Interface 4, 117, 2007.

47. Huang, X., Zhang, Y., Donahue, H.J., and Lowe, T.L. Porous thermoresponsive-co-biodegradable hydrogels as tissue-engineering scaffolds for 3-dimensional in vitro culture of Chondrocytes. Tissue Engineering 13, 2645, 2007.

48. Colter, D.C., Sekiya, I., and Prockop, D.J. Identification of a subpopulation of rapidly self-renewing and multipotential adult stem cells in colonies of human marrow stromal cells. Proceedings of the National Academy of Sciences of the United States of America 98, 7841, 2001.

49. Shake, J.G., Gruber, P.J., Baumgartner, W.A., Senechal, G., Meyers, J., Redmond, J.M., Pittenger, M.F., and Martin, B.J. Mesenchymal stem cell implantation in a swine myocardial infarct model: Engraftment and functional effects. Annals of Thoracic Surgery 73, 1919, 2002.

50. Jiang, Y.H., Jahagirdar, B.N., Reinhardt, R.L., Schwartz, R.E., Keene, C.D., Ortiz-Gonzalez, X.R., Reyes, M., Lenvik, T., Lund, T., Blackstad, M., Du, J.B., Aldrich, S., Lisberg, A., Low, W.C., Largaespada, D.A., and Verfaillie, C.M. Pluripotency of mesenchymal stem cells derived from adult marrow. Nature 418, 41, 2002.

51. Martin, I., Shastri, V.P., Padera, R.F., Yang, J., Mackay, A.J., Langer, R., Vunjak-Novakovic, G., and Freed, L.E. Selective differentiation of mammalian bone marrow stromal cells cultured on three-dimensional polymer foams. Journal of Biomedical Materials Research 55, 229, 2001.

52. Pittenger, M.F., Mackay, A.M., Beck, S.C., Jaiswal, R.K., Douglas, R., Mosca, J.D., Moorman, M.A., Simonetti, D.W., Craig, S., and Marshak, D.R. Multilineage potential of adult human mesenchymal stem cells. Science 284, 143, 1999.

53. Calvert, J.W., Marra, K.G., Cook, L., Kumta, P.N., DiMilla, P.A., and Weiss, L.E. Characterization of osteoblast- like behavior of cultured bone marrow stromal cells on various polymer surfaces. Journal of Biomedical Materials Research 52, 279, 2000.

54. Huang, A.H., Farrell, M.J., and Mauck, R.L. Mechanics and mechanobiology of mesenchymal stem cell-based engineered cartilage. Journal of Biomechanics 43, 128, 2010.

55. Rosen, V., Nove, J., Song, J.J., Thies, R.S., Cox, K., and Wozney, J.M. Responsiveness of clonal limb bud cell-lines to bone morphogenetic protein-2 reveals a sequential relationship between cartilage and bone cell phenotypes. Journal of Bone and Mineral Research 9, 1759, 1994.

56. Majumdar, M.K., Wang, E., and Morris, E.A. BMP-2 and BMP-9 promote chondrogenic differentiation of human multipotential mesenchymal cells and overcome the inhibitory effect of IL-1. Journal of Cellular Physiology 189, 275, 2001.

57. Sekiya, I., Colter, D.C., and Prockop, D.J. BMP-6 enhances chondrogenesis in a subpopulation of human marrow stromal cells. Biochemical and Biophysical Research Communications 284, 411, 2001.

58. Alliston, T.N., Derynck, R., and Canalis, E. Transforming growth factor-beta in skeletal development and maintenance. Skeletal growth factors, 233, 2000.

59. Tae, S.K., Lee, S.H., Park, J.S., and Im, G.I. Mesenchymal stem cells for tissue engineering and regenerative medicine. Biomedical Materials 1, 63, 2006.

60. Kuo, C.K., and Tuan, R.S. Tissue engineering with mesenchymal stem cells. Ieee Engineering in Medicine and Biology Magazine 22, 51, 2003.

61. Hui, T.Y., Cheung, K.M.C., Cheung, W.L., Chan, D., and Chan, B.P. In vitro chondrogenic differentiation of human mesenchymal stem cells in collagen microspheres: Influence of cell seeding density and collagen concentration. Biomaterials 29, 3201, 2008.

62. Kavalkovich, K.W., Boynton, R.E., Murphy, J.M., and Barry, F. Chondrogenic differentiation of human mesenchymal stem cells within an alginate layer culture system. In Vitro Cellular & Developmental Biology-Animal 38, 457, 2002.

63. Huang, A.H., Stein, A., Tuan, R.S., and Mauck, R.L. Transient Exposure to Transforming Growth Factor Beta 3 Improves the Mechanical Properties of Mesenchymal Stem Cell-Laden Cartilage Constructs in a Density-Dependent Manner. Tissue Engineering Part A 15, 3461, 2009.

64. Jurvelin, J., Helminen, H.J., Lauritsalo, S., Kiviranta, I., Saamanen, A.M., Paukkonen, K., and Tammi, M. Influences of joint immobilization and running exercise on articular-cartilage surfaces of young-rabbits - a semiquantitative stereomiscroscopic and scanning electron-microscopic study. Acta Anatomica 122, 62, 1985.

65. Muir, H., , Carney, S.L. Pathological and biochemical changes in cartilage and other tissues of the canine knee resulting from induced joint instability. In: H. J. Helminen, I.K., and M. Tammi, ed. Joint Loading: Biology and Health of Articular Structures. Briston Norfolk: John Writh, 1987, pp. 47-63.

66. Saamanen, A.M., Tammi, M., Kiviranta, I., Jurvelin, J., and Helminen, H.J. Maturation of proteoglycan matrix in articularcartilage under increased and decreased joint loading—A study in young-rabbits. Connective Tissue Research 16, 163, 1987.

67. Kim, Y.J., Sah, R.L.Y., Grodzinsky, A.J., Plaas, A.H.K., and Sandy, J.D. Mechanical regulation of cartilage biosynthetic behavior-physical stimuli. Archives of Biochemistry and Biophysics 311, 1, 1994.

68. Sah, R.L.Y., Kim, Y.J., Doong, J.Y.H., Grodzinsky, A.J., Plaas, A.H.K., and Sandy, J.D. Biosynthetic response of cartilage explants to dynamic compression. Journal of Orthopaedic Research 7, 619, 1989.

69. Angele, P., Kujat, R., Nerlich, M., Yoo, J., Goldberg, V., and Johnstone, B. Engineering of osteochondral tissue with bone marrow mesenchymal progenitor: Cells in a derivatized hyaluronan-gelatin composite sponge. Tissue Engineering 5, 545, 1999.

70. Miyanishi, K., Trindade, M.C.D., Lindsey, D.P., Beaupre, G.S., Carter, D.R., Goodman, S.B., Schurman, D.J., and Smith, R.L. Dose- and time-dependent effects of cyclic hydrostatic pressure on transforming growth factor-beta 3-induced chondrogenesis by adult human mesenchymal stem cells in vitro. Tissue Engineering 12, 2253, 2006.

71. Broom, N.D., and Myers, D.B. A study of the structural response of wet hyaline cartilage to various loading situations. Connective Tissue Research 7, 227, 1980.

72. Grodzinsky, A.J., Levenston, M.E., Jin, M., and Frank, E.H. Cartilage tissue remodeling in response to mechanical forces. Annual Review of Biomedical Engineering 2, 691, 2000.

73. Millward-Sadler, S.J., and Salter, D.M. Integrin-dependent signal cascades in chondrocyte mechanotransduction. Annals of Biomedical Engineering 32, 435, 2004.

74. Hiroki, A., Maekawa, Y., Yoshida, M., Kubota, K., and Katakai, R. Volume phase transitions of poly(acryloyl-L-proline methyl ester) gels in response to water-alcohol composition. Polymer 42, 1863, 2001.

75. Varghese, S., and Elisseeff, J.H. Hydrogels for musculoskeletal tissue engineering. Polymers for Regenerative Medicine, 95, 2006.

76. Brock, D. Review of artificial muscle based on contractile polymers. MIT Artificial Intelligence Laboratory, 1, 1991.

77. Carver, S.E., and Heath, C.A. Semi-continuous perfusion system for delivering intermittent physiological pressure to regenerating cartilage. Tissue Engineering 5, 1, 1999.

78. Ikehara, T., Nishi, T., and Hayashi, T. Volume phase transition process and spin diffusion in heterogeneous structure of acrylamide gels studied by pulsed NMR. Polymer Journal 28, 169, 1996.

79. Schlick, S., Pilar, J., Kweon, S.C., Vacik, J., Gao, Z., and Labsky, J. Measurements of diffusion-processes in hema-degma hydrogels by ESR imaging. Macromolecules 28, 5780, 1995.

80. Olsen, M.G., Bauer, J.M., and Beebe, D.J. Particle imaging technique for measuring the deformation rate of hydrogel microstructures. Applied Physics Letters 76, 3310, 2000.

81. Roy, P., Petroll, W.M., Cavanagh, H.D., Chuong, C.J., and Jester, J.V. An in vitro force measurement assay to study the early mechanical interaction between corneal fibroblasts and collagen matrix. Experimental Cell Research 232, 106, 1997.

82. Roy, P., Petroll, W.M., Cavanagh, H.D., and Jester, J.V. Exertion of tractional force requires the coordinated up-regulation of cell contractility and adhesion. Cell Motility and the Cytoskeleton 43, 23, 1999.

83. Tamariz, E., and Grinnell, F. Modulation of fibroblast morphology and adhesion during collagen matrix remodeling. Molecular Biology of the Cell 13, 3915, 2002.

84. Harley, B.A., Freyman, T.M., Wong, M.Q., and Gibsony, L.J. A new technique for calculating individual dermal fibroblast contractile forces generated within collagen-GAG scaffolds. Biophysical Journal 93, 2911, 2007.

85. Petroll, W.M., Ma, L., and Jester, J.V. Direct correlation of collagen matrix deformation with focal adhesion dynamics in living corneal fibroblasts. Journal of Cell Science 116, 1481, 2003.

86. Vanni, S., Lagerholm, B.C., Otey, C., Taylor, D.L., and Lanni, F. Internet-Based image analysis quantifies contractile behavior of individual fibroblasts inside model tissue. Biophysical Journal 84, 2715, 2003.

87. Bloom, R.J., George, J.P., Celedon, A., Sun, S.X., and Wirtz, D. Mapping local matrix remodeling induced by a migrating tumor cell using three-dimensional multiple-particle tracking. Biophysical Journal 95, 4077, 2008.

88. Toprak, E., Balci, H., Blehm, B.H., and Selvin, P.R. Three-dimensional particle tracking via bifocal imaging. Nano Letters, 2041, 2007.

89. Speidel, M., Jona, S., and Florin, E. Three-dimensional tracking of fluorescent nanoparticles with subnanometer precision by use of off-focus imaging. Optical Letters 69, 69, 2003.

90. Levi, V., Ruan, Q.Q., and Gratton, E. 3-D particle tracking in a two-photon microscope: Application to the study of molecular dynamics in cells. Biophysical Journal 88, 2919, 2005.

91. Correlation and Covariance. MathWorks, 2010.

92. Gelles, J., Schnapp, B.J., and Sheetz, M.P. Tracking kinesin-driven movements with nanometre-scale precision. Nature 331, 450, 1988.

93. Zhou, J., Huang, G., Li, M., Soh, A.K. Stress Evolution in a phase-separating polymeric gel. Modelling and Simulation in Materials Science and Engineering 18, 1, 2010.

94. Zhang, C., Aung, A., Liao, L.Q., and Varghese, S. A novel single precursor-based biodegradable hydrogel with enhanced mechanical properties. Soft Matter 5, 3831, 2009.

95. Keane, R.D., and Adrian, R.J. Theory of cross-correlation analysis of PIV images. Applied Scientific Research 49, 191, 1992.

96. Live/Dead (R) Viability/Cytotoxicity Kit for Mammalian cells. Invitrogen, 2005.

97. Livak, K.J., and Schmittgen, T.D. Analysis of relative gene expression data using real-time quantitative PCR and the 2(T)(-Delta Delta C) method. Methods 25, 402, 2001.

98. Kim, M.S., Hwang, N.S., Lee, J., Kim, T.K., Leong, K., Shamblott, M.J., Gearhart, J., and Elisseeff, J. Musculoskeletal differentiation of cells derived from human embryonic germ cells. Stem Cells 23, 113, 2005.

99. Quant-iT™ PicoGreen ® dsDNA Reagent and Kits. Invitrogen, 2008.

100. Baeurle, S.A., Kiselev, M.G., Makarova, E.S., and Nogovitsin, E.A. Effect of the counterion behavior on the frictional-compressive properties of chondroitin sulfate solutions. Polymer 50, 1805, 2009.